Technische Universität München

Fakultät für Medizin

Klinik und Poliklinik für Frauenheilkunde (Prof. Dr. Marion B. Kiechle)

The functional role of CXCL9 and CX3CL1 in breast cancer biology

Tobias Fabian Dreyer

Vollständiger Abdruck der von der Fakultät für Medizin der Technischen Universität München zur Erlangung des akademischen Grades eines

Doktors der Naturwissenschaften (Dr. rer. nat.)

genehmigten Dissertation

Vorsitzender: Prof. Dr. Carsten Schmidt-Weber

Prüfer der Dissertation: 1. Priv.-Doz. Dr. Holger Bronger

2. Prof. Dr. Michael Groll

3. Prof. Dr. Marcus Schmidt

Die Dissertation wurde am 23.06.2020 bei der Technischen Universität München eingereicht und durch die Fakultät für Medizin am 29.12.2020 angenommen

For my beloved wife Anna

TABLE OF CONTENT

AChE *Acetyl Cholin Esterase*
ADAM17 *a disintegrin and metalloproteinase 17*
ADCC *antibody dependent cellular cytotoxicity*
ASS *Acetylsalicylic acid*
ATCC *American Type Culture Collection*
ATM *ataxia-telangiectasia mutated*
BRCA1 *breast cancer 1*
BRCA2 *breast cancer 2*
BSA *bovine serum albumine*
Ca^{2+} *Calcium*
CD 25 *cluster of differentiation 25*
CD11b *cluster of differentiation 11b*
CD19 *cluster of differentiation 19*
CD3 *cluster of differantiation*
CD4 *cluster of differentiation*
CD56 *cluster of differentiation*
CD8 *cluster of differentiation 8*
CD86 *cluster of differentiation 86*
CHEK2 *checkpoint kinase 2*
CO_2 *carbon dioxide*
COX *cyclooxygenase*
CTC *circulating tumor cells*
CX3CL1 *CX3C motif ligand 1*
CX3CR1 *CX3C motif receptor 1*
CXCL9 *CXC motif ligand 9*
CXCR3 *CXC motif receptor 3*
DCIS *ductal carcinoma in situ*
DFS *disease free survival*
DMEM *Dulbecco modified eagle medium*
DMSO *Dimethyl sulfoxide*
DNA *Desoxy Ribonucleic acid*
ELISA *enzyme linked immuno sorbent assay*
ELR *glucine leucine arginine*
ER *estrogen receptor*
EU Assay *Europium Assay*
FCS *fetal calf serum*
FMO *fluorescence minus one*
FoxP3 *Forkhead box protein P3*
GAPDH *glycerine aldehyde 3 phosphate dehydrogenase*
H_2SO_4 *sulfuric acid*
HBSS *hanks buffered saline solution*
HE *hematoxylin Eosin*
HEPES 4-(2-hydroxyethyl)-1-piperazineethanesulfonic acid
HER2 *human epidermal growth factor receptor 2*
HR *hormone receptor*
HRP *horseradish peroxidase*
IFN-γ *Interferon gamma*
IFN-α *interferon α*
IgG *Immunoglobulin G*
IHC *immuno histo chemistry*
IL-2 *interleukin 2*
LCIS *lobular carcinoma in situ*
MACS *magnetic assissted cell sorting*
MAPK *mitogen-activated protein kinase*
mRNA *messenger RNA*
NGS *next generation sequencing*
NK *natural killer*
OS *overall surviva*
PALB2 *partner and localizer of BRCA2*
PARP *ADP-ribose polymerase*
PBS *phosphate buffered saline*
PD-L1 *programmed cell death ligand 1*
PGE2 *prostaglandin E2*
PI3K *phosphoinositide-3-kinase*
RAD51 *RAD51 protein*
rcf *relative centrifugal force*
RIPA *Radioimmunoprecipitation assay buffer*
RNA *ribonucleic acid*
RORγT *RAR related orphan receptor gamma*
rpm *rounds per minute*
RPMI *medium from the Roswell Park Memorial Institute*
RT-qPCR *real time quantitative polymerase chain reaction*
SCID *severe combined immunodeficiency*
SDS-PAGE *sodium dodecyl sulfate polyacrylamide gel electrophoresis*
STAT *signal transducer and activator of transcription*
STK11 *serin/threonine kinase 11*
T-bet *T box protein expressed in T cells*
TBS-T *tris buffered saline with Tween*
TEMED *N,N,N',N'-Tetramethylethylenediamine*
TH2 *T helper 2*
TILs *tumor-infiltrating lymphocytes*
TNBC *triple-negative breast cancer*
TNF-α *tumor necrosis factor α*

TNM *tumor lymphnode metastasis (classification system of solid tumors)*
TP53 *tumor protein 53*
Tr1 *T regulatory 1*
w/v *weight per unit volume*

List of Tables

List of Figures

I. ABSTRACT

Monoclonal antibodies, like the HER2-directed antibody trastuzumab, are a crucial part of modern breast cancer therapy. The mode of action consists, besides the modulation of anti-proliferative signal transduction pathways, of the labeling of tumor cells for further recognition by cytotoxic lymphocytes like natural killer (NK) cells, also known as antibody-dependent cellular cytotoxicity (ADCC). The chemokines CXCL9, a ligand of CXCR3, and CX3CL1, the ligand of CX3CR1, are capable of recruiting immune cells, including NK cells, into the tumor. Besides, CX3CL1 is expressed as a transmembrane protein and shows adhesive capacity towards cells expressing its receptor. In this thesis, the effects of CXCL9 and CX3CL1 on the anti-tumor response in breast cancer were analyzed *in vitro* and *in vivo* with the ultimate aim to exploit those chemokines to improve the future targeted breast cancer therapies.

The syngenic 4T1 breast cancer mouse model was used to analyze the effects of Cxcl9 modulation showing tumor-suppressive effects upon *Cxcl9* overexpression. Furthermore, cyclooxygenase (COX) inhibition was identified as a positive modulator of *Cxcl9* expression in murine 4T1 cells and human SKBR3 and MDA-MB 231 breast cancer cells *in vitro*. Treatment with indomethacin, a non-selective COX-inhibitor, in mice showed a reduction of tumor growth and lung metastasis as well as an increase of lymphocytic influx into the tumor, including NK cells. Moreover, the amount of CXCL9 was determined immunohistochemically in breast cancer specimens as well as its protein concentration in blood samples of breast cancer patients. The expression patterns showed differential expression among all breast cancer subtypes.

The regulation of CX3CL1 in four human HER2-positive cancer cell lines was analyzed, especially the generation of the soluble isoform of CX3CL1. The inflammatory cytokine TNF-α was identified as a strong inducer of CX3CL1, and the protease ADAM17 as a potent shedding protease for the generation of the soluble isoform. The impact of CX3CL1 on the NK cell-mediated cell lysis of cancer cells was also determined and indicated that

forced *CX3CL1* overexpression induced NK cell-mediated tumor cell lysis. The same was shown for inhibition of ADAM17. A combination of *CX3CL1* overexpression in tumor cells and trastuzumab treatment showed enhanced killing compared to either monotherapy. In the 4T1 breast cancer mouse model, *Cx3cl1* overexpression led to decreased tumor growth and lung metastasis, together with an increased influx of immune cells, including NK cells. In a HER2 positive orthotopic mouse model, artificial increase reduced the tumor burden *in vivo* and could compensate for GM-1 antibody based NK-cell depletion. In the HER2-low expressing, intrinsically trastuzumab-resistant HT29 cancer model, Cx3cl1 enabled trastuzumab therapy, resulting in reduced tumor burden and increased overall survival. CX3CL1, its corresponding receptor CX3CR1 and the shedding proteases ADAM10 and ADAM17 were quantified immunohistochemically and were linked to clinical parameters, revealing a good prognostic impact of CX3CL1 as well.

In summary, both chemokines, CXCL9 and CX3CL1, show tumor-suppressive properties *in vivo.* These effects can be linked to modulation of the immune cell infiltration and increase of NK cell activity. Moreover, *Cx3cl1* overexpression was sufficient to improve anti-HER2 treatment with trastuzumab *in vitro* and *in vivo.* Differential expression of both chemokines was detected in human breast cancer specimen and blood samples. All these findings indicate an important functional role of CXCL9 and CX3CL1 in anti-tumor immunity and make both chemokines a potential therapeutic target for the improvement of immunotherapies of breast cancer.

II. INTRODUCTION

1. Breast cancer

1.1. Epidemiology of breast cancer

Breast cancer is the most common malignant tumor entity of women worldwide. With over a million new cases every year, almost half a million women die of breast cancer annually, making it the most common cause of cancer-related deaths (Stewart and Wild 2014; Akram et al. 2017). In Germany, breast cancer accounts for 30.7% of all female cancer-related diseases, with tumor-related mortality of 17.8% (Robert Koch-Institut 2015). The average age of breast cancer patients at first diagnosis is 63.5 years. Early detection enables good therapeutic opportunities. However, the clinical course and aggressiveness of the disease are highly dependent on the time of diagnosis as well as the subtype of the tumor, making a successful therapy still challenging.

1.2. Histological breast cancer subtypes and staging

Breast cancer can be histologically classified into several subgroups (Mayr 2019). First, a difference must be made between invasive carcinomas and invasive precancerous tumors: ductal carcinoma *in situ* (DCIS) and lobular carcinoma *in situ* (LCIS), which indicate a non-invasive carcinoma *in situ*. Those are lesions that can eventually progress to invasive cancer (Page et al. 1985). The most common type of invasive carcinomas of the breast is the invasive ductal subtype, with an incidence of 40-75%. The second most common entity with a frequency of 5-15% is the invasive lobular carcinoma. The other cases comprise invasive medullary, tubular, mucinous, and papillary subtypes (WHO Classification of Tumours Editorial Board., International Agency for Research on Cancer., and World Health Organization).

All invasive mammary carcinomas are graded following different histological and cytological parameters, including tubules formation, nucleus pleomorphism, and mitosis rate (Elston and Ellis 1991). Thereby they can be separated into three grades, G1: well-differentiated, G2: moderately

differentiated, and G3: poorly differentiated.

The pathological staging of the tumor is based on the TNM system of the Union for International Cancer Control (UICC) (Brierley, Gospodarowicz, and Wittekind 2017). The TNM-system describes the overall status of a tumor by using the descriptive parameters tumor size (T), lymph node status (N), and the presence of distant metastases (M), (Table 1). In the last decades, the TNM system was extended by additional information such as tumor rest after surgery (Harris et al. 2003) or tumor cell invasion of lymph vessels (Mohammed et al. 2011).

Table 1: Extended TNM classification of mammary carcinomas adapted by the UICC with additional information about lymph node invasion and residual tumor.

pT - primary Tumor	
pTX	primary tumor cannot be evaluated
pT0	no indication for primary tumor
pT1	primary tumor ≤ 2 cm
pT2	primary tumor ≥ 2 cm but ≤ 5 cm
pT3	primary tumor ≥ 5 cm
pT4	primary tumor with contact to skin or nipple
pN – lymph Node status	
pNX	lymph nodes cannot be staged
pN0	no regional lymph node
pN1	metastases in 1 – 3 lymph nodes
pN2	metastases in 4 – 9 lymph nodes
pN3	metastases in ≥ 10 lymphnodes
pM - distant Metastasis	
pMX	the occurrence of distant metastasis cannot be evaluated or is unknown
pM0	no distant metastasis
pM1	presence of distant metastasis

1.3. Molecular classification of breast cancer subtypes

Expression profiles and genetic signatures led to the definition of molecular subtypes of breast cancer. The immunohistochemical differentiation of intrinsic breast cancers is defined as abstracted in Table 2: (Goldhirsch et al. 2011).

Table 2: Molecular subtypes of mammary carcinomas based on the classical receptor expressions

	ER	PR	Ki-67	HER2
Triple-negative	negative	negative	50-60%	negative
HER2-positive	negative	positive		positive
Luminal-A	positive	positive	<14%	negative
Luminal-B	positive	negative	>14%	positive/negative

Receptor expression

All mammary carcinomas are tested for the expression of progesterone (PR) and estrogen receptor-α (ER). Together, both are well-established predictive markers for the efficacy of endocrine therapy. The evaluation is carried out by immunohistochemical analysis, already 1% receptor-positive cells are sufficient to render the tumor hormone-sensitive, but most of the tumors show expression between 60 – 70% (Early Breast Cancer Trialists' Collaborative Group (EBCTCG) 2005). Another important predictive biomarker is the human epidermal growth factor receptor 2 (HER2). 12% to 32% of all mammary carcinomas are tested positive for HER2 overexpression (Holbro and Hynes 2003). The expression is also determined by immunohistochemical analysis, and in case of unclear expression levels, the HER2 status can be further determined by *in situ* hybridization analysis. HER2-positive tumors can be efficiently treated with targeted molecules such as the monoclonal antibody trastuzumab directed against the HER2 antigen. The development of new anti-HER2 compounds has been promoted during the last years and increased the variety of therapeutics, e.g., pertuzumab, an anti-HER2 antibody abolishing the HER2 dimerization, or antibody-drug conjugates like T-DM1, but also small-molecule tyrosine kinase inhibitors like lapatinib or neratinib which also target HER2 and other EGF receptor family members (Waks and Winer 2019).

Cell proliferation

Ki67 is a molecule that is only expressed during cell division, one of the mechanisms that are directly targeted by most of the chemotherapies. Ki67 is easy to detect with immunohistochemical analysis. Thereby, Ki67 evaluation gives additional information about therapy responsiveness in advance (Duffy et al. 2017). However, there is great variability in Ki67 analysis among different laboratories.

Circulating tumor cells

Another prognostic factor that has gained much attention in recent years are circulating tumor cells (CTC). These are easy to acquire from patient's blood and have been shown to have prognostic relevance in patients with primary mammary carcinoma (Rack et al. 2010; Pachmann et al. 2008; Pierga et al. 2008; Lucci et al. 2012). Nevertheless, the consequences for clinical applications have to be further evaluated, and questions concerning consistent methodology remain unclear. So far, no clinical therapy decisions are recommended based solely on the CTC status (Sundling and Lowe 2019).

Genetic signatures

Molecular features of tumors can also be assessed on real-time quantitative PCR (RT-qPCR) basis using tests like Oncotype DX (Paik et al. 2004), MammaPrint (van 't Veer et al. 2002), PAM50 (Sestak et al. 2015) or Endopredict (Martin et al. 2014). These tests can provide additional prognostic or predictive information. Especially in intermediate-risk cases such as several HR+/HER2- cancers, these tools allow clinicians to decide about the necessity for adjuvant or neoadjuvant chemotherapy. Nevertheless, the match between the different tests is only about 40% (Bartlett et al. 2016), so the combination of different tests might be needed.

In addition to the PCR-based evaluation of expression profiles, as mentioned above, it is also possible to get access to further genetic information by next-generation sequencing (NGS). Especially in terms of

immunotherapies, the number of neoantigens, tumor-associated genes as well as the tumor mutational burden can contribute to a thorough prognostic decision. For this purpose, multi-gene panels have been developed to be integrated into the clinical routine, such as Oncomine (Maruvka et al. 2019).

Immune checkpoints

Another predictive marker for effective immune therapy, such as checkpoint inhibitors, is the quantification of the expression of programmed cell death ligand 1 (PD-L1) in the tumor tissue. The use of checkpoint inhibitors can be another therapy option, especially for breast cancer subtypes, which are thought to be more immunogenic, such as triple-negative breast cancer (TNBC) (Planes-Laine et al. 2019; Barrett et al. 2018).

A summary of the prognostic markers mentioned above and other therapy relevant factors are summarized in Table 3.

Table 3: Prognostic and predictive markers for breast cancer (Degenhardt et al. 2019)

Parameter	Prognostic	Predictive	Therapy
Age (< 35 years, unfavorable)	X		Chemotherapy
Menopause	X	X	Endocrine therapy
Tumor size	X		
Nodal status	X		Chemotherapy
Histological subtype	X		
Grading	X		
Hormone receptor status	X	X	Endocrine therapy
HER2	X	X	HER2-directed therapy
Ki-67	X	X	Chemotherapy
Gene expression	X	X	Chemotherapy
Pathological complete response (pCR) after neoadjuvant therapy	X	X	

1.4. Hereditary breast cancers

15 to 20% of all breast cancer cases occur because of genetic or epigenetic factors. The genetic predisposition is caused by high penetrance genes in 50% of all of these cases (Turnbull and Rahman 2008). The major genes being responsible for the increased risk are breast cancer 1 (*BRCA1*) and breast cancer 2 (*BRCA2*); both of them are tumor suppressors as their gene products participate in the DNA repair machinery (Ripperger et al. 2009). Other high penetrance genes have been identified as well, but the percentages of cases are very low, such as tumor protein 53 (*TP53*), which is mutated in 2.5% of all hereditary breast cancer cases (Turnbull and Rahman 2008).

All the cases that cannot be classified as “related to high penetrance genes” build a group of complex mutations in different genes including high penetrance genes or moderate to low penetrance genes, such as checkpoint kinase 2 (*CHEK2*), partner and localizer of BRCA2 (*PALB2*) or ataxia-telangiectasia mutated (*ATM*) (Hunter et al. 2007; Easton et al. 2007)

Patients diagnosed early with mutations in risk genes can benefit from different clinical options ranging from intensified screening to prophylactic surgery. In cases of BRCA mutations, new therapeutic approaches such as poly ADP-ribose polymerase (PARP) inhibitors complement the existing therapeutic options (Bryant et al. 2005; Zimmer et al. 2018).

1.5. Carcinogenesis of breast cancer

In most cases, the initiation of breast cancer starts with the hyperproliferation of ductal cells, which leads to the formation of benign tumors or invasive carcinomas. There are two hypothetical theories for breast cancer initiation and progression (Polyak et al. 2007):

1. The cancer stem cell theory suggests that all cancer subtypes originate from the same type of stem or progenitor cell. The different subtypes are acquired via different genetic mutations or epigenetic modifications.

2. The stochastic theory suggests that each tumor subtype originates from a single cell and that random mutations can accumulate in literally every

epithelial breast cell. This mutational burden can, in the end, lead to the transformation into tumor cells.

Histopathological observations and genetic studies provide a base model of breast cancer progression. The earliest neoplastic lesions give rise to low-grade DCIS, which can progress into high-grade DCIS and can eventually proceed to invasive carcinoma. This progression is accompanied by multistep genetic and gene expression changes in early and late stages of progression (Moulis and Sgroi 2008).

Those genetic alterations include gain-of-function mutations in proto-oncogenes and loss-of-function mutations in tumor suppressor genes. Genes, which are mutated with high penetrance in the population, include *BRCA1, BRCA2*, and *TP53*. Nevertheless, many other mutations, which are less frequently mutated, have been suggested to play a significant role in the initiation and progression of breast cancer such as cadherin-11 (*CDH11*), serine/threonine kinase 11 (*STK11*), *RAD51* and *HER2* (Sheikh et al. 2015). Furthermore, the initiation of genetic alterations can be further enhanced by epigenetic changes such as DNA-methylation and histone modifications (Byler et al. 2014).

Although there are many different genetic and non-genetic alterations possible (Cairns et al. 1975), there are several histopathological features that define neoplastic and invasive stages of breast cancer. The breast consists of adipose tissue supplied by a network of nerves, blood vessels, lymph vessels, and lymph nodes, all surrounded by fibrous connective tissue and ligaments. Lobes are embedded in the adipose tissue and are further divided into smaller lobules, which are connected via the milk ducts (Akram et al. 2017). A normal duct contains a basement membrane and a bilayer of epithelial cells, which combines luminal epithelial cells and surrounding myoepithelial cells (Polyak et al. 2007). During the early stages of malignant breast disease, this lumen is filled with non-invasive cells. Those are considered to be the precursor stages of DCIS. Those DCIS lesions already contain proliferative cells that still confine in the basement membrane and show no invasion into the neighboring tissue and positive expression of basal cytokeratin markers (Harris et al. 2003). Derived from those DCIS lesions, invasive breast cancer cells may arise (Burstein et al.

2004). This process involves the loss of the basal membrane barrier and myoepithelial cells. This depletion of the natural boundary enables the invasion of cancer cells into the surrounding tissue and, in the end, might lead to the formation of metastases in the liver, the lung, the bones, or distant organs such as the brain.

The accumulation of mutations in distinct cells and the expansion of particular high proliferative cell clones together with the ongoing stimulation by the microenvironment (e.g., the stroma) leads to the formation of solid tumors in the breast. If not diagnosed early, tumor cells can detach from the solid tumor and migrate to distant organs.

1.6. Treatment of breast cancer

The utmost goal of successful breast cancer treatment is the increase in life expectancy and the conservation of the quality of life. In non-metastatic (early) breast cancer, surgery with the aim to completely remove the tumor remains a fundamental cornerstone of therapy. Besides the primary tumor, the tumor-closest (axillary) lymph nodes, so-called sentinel lymph nodes, are dissected and pathologically checked for malignant transformation. In the case of tumor-positive axillary lymph nodes, at least 10 of them (and all macroscopically suspicious ones) have to be surgically removed. This clinical readout provides further information about the stage and prognosis of the disease and can be important for further therapy decisions. After successful (breast-conserving) surgery, patients are treated with radiotherapy in order to significantly reduce the recurrence rate (Wöckel et al. 2010).

Aggressive subtypes such as triple-negative breast cancer (TNBC), HER2-positive breast cancer, or locally advanced breast cancers require chemotherapy. Usually given after surgery, in recent years, the concept of neoadjuvant chemotherapy has been established. The standard chemotherapy regimen comprises an anthracycline (doxorubicin or epirubicin) in combination with cyclophosphamide and a taxane (paclitaxel or docetaxel). Hormone receptor-positive, HER2-negative patients can be alternatively treated with endocrine therapy (Early Breast Cancer Trialists'

Collaborative Group (EBCTCG) 2011). In the case of *HER2* overexpression, the therapy with the HER2-targeted agents such as the monoclonal antibody trastuzumab has been shown to be very effective (Perez et al. 2011). There have been different mechanisms of action suggested for successful trastuzumab treatment. Direct binding of the antibody to HER2 leads to an internalization of the receptor and, thereby, the degradation of available receptors on the cell surface for active growth signaling (Klapper et al. 2000). Usually, this activity includes receptor dimerization followed by phosphorylation of several downstream signaling molecules. This leads to inhibition of the mitogen-activated protein kinase (MAPK) and phosphoinositide-3-kinase (PI3K)/Akt pathway and eventually to increased cell cycle arrest (Junttila et al. 2009). Another major mechanism of trastuzumab is the labeling of tumor cells for further immune cell recognition via the Fc-fragment/Fc receptor interaction. This proximity-based connection activates the natural cytolytic ability of cytotoxic immune cells such as NK cells, a mechanism called antibody-dependent cellular cytotoxicity (Arnould et al. 2006).

In recent years, additional HER2-directed agents have been approved, particularly for the therapy of metastatic breast cancer: pertuzumab, a monoclonal antibody inhibiting HER2 heterodimerization, T-DM1, a trastuzumab molecule bound to a chemotherapeutic, and Lapatinib, a small molecule tyrosine kinase inhibitor. The former two antibodies also function at least in part via an ADCC (Pondé et al. 2018; Barok, Joensuu, and Isola 2014). However, this kind of efficient treatment remains suitable only for patients with *HER2* overexpression. Till now, patients with *HER2* intermediate or low expression cannot benefit from this therapeutic approach (Meric-Bernstam et al. 2019)

1.7. Breast cancer as an immunogenic disease

Breast cancer entities are characterized by a variety of antigens, which can be recognized by the immune system. These tumor-associated antigens consist of cancer germline antigens, which are present during the whole disease and neoantigens, which can be acquired during cancer

progression. This accumulation of mutations is indicated by studies suggesting that the mutational load in the tumor cells is increased during cancer progression, making it more likely that new antigens evolve (Budczies et al. 2015). This newly provided variety of antigens leads to increased infiltration of immune cells during the disease progression (Hussein and Hassan 2006). Those tumor-infiltrating lymphocytes (TILs) are proven to be higher in malignancies compared to healthy tissue and thereby have been suggested as independent prognostic factors (Carsten Denkert et al. 2010). Changes in immune cell infiltration can also be detected in correlation to therapy (García-Martínez et al. 2014). Especially in breast cancer, TILs play an essential role in the matter of progression and therapy response (Dushyanthen et al. 2015). It has been shown that especially the aggressive subtypes of breast cancer, HER2-positive, and triple-negative, show increased amounts of TILs (Nagalla et al. 2013). Altogether, breast cancers seem to be immunogenic tumors, and the evaluation of TILs seems feasible as a prognostic marker in all subtypes (Salgado et al. 2015; Dieci et al. 2018; Miyoshi et al. 2019; Denkert et al. 2018).

However, high expression of tumor-associated antigens does not necessarily correlate with the amount of tumor-infiltrating lymphocytes (TIL) in breast cancer (Kotoula et al. 2016). The tumors can protect themselves from efficient detection and eradication by several immune evasion mechanisms. Such evasive mechanisms include the downregulation of antigen presentation, lack of immune effector cells, enrichment of immune suppressor cells, and the upregulation of checkpoint molecules (Angelova et al. 2015). Since these bypass strategies can accumulate during the course of the disease, it becomes more and more important that the immune cell infiltration into the tumor can be guaranteed.

There is evidence that in the tumor tissue, the amount of infiltrating lymphocytes correlates with the concentration of chemotactic agents. Classifications of genetic phenotypes of breast cancer have revealed a highly immunogenic phenotype. This phenotype shows high amounts of chemokines and also high numbers of tumor-infiltrating lymphocytes (Hendrickx et al. 2017). Furthermore, in ER-negative tumors, high amounts of T and B cells were associated with elevated levels of the chemokine C-

X-C motif ligand 9 (CXCL9) (Nagalla et al. 2013; Denkert et al. 2010). The same was described for NK cells and the chemokine C-X3-C motif ligand 1 (CX3CL1) in ER-positive breast cancer entities (Verma et al. 2015).

2. Chemokines

Chemokines are a group of small homologous molecules, whose name is derived as a short version of chemotactic cytokines. Up till now, there are 47 different human chemokines known (Table 4, page 15). However, several more have been shown in other species, e.g., in mice (Zlotnik and Yoshie 2012).

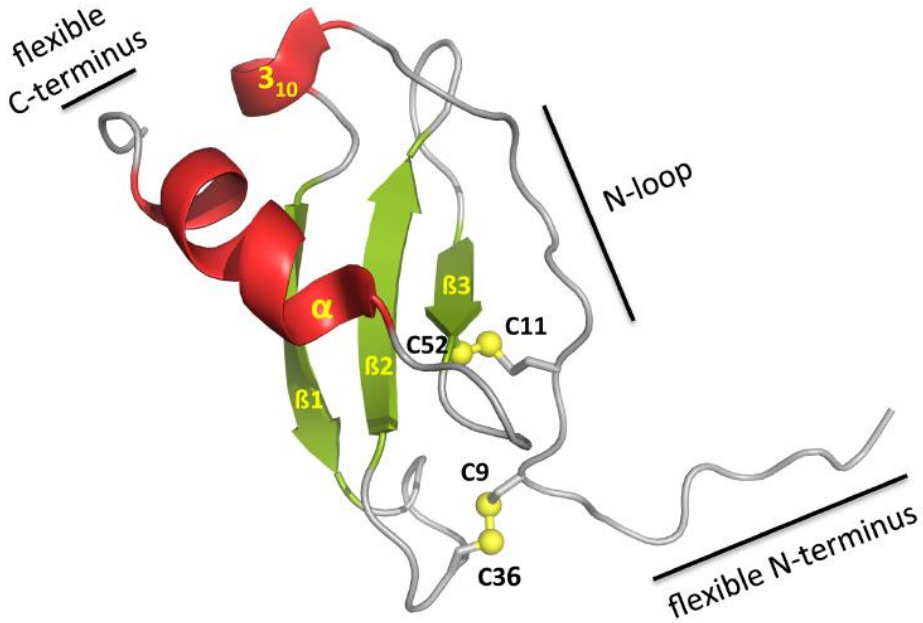

Figure 1: 3D structure of a CXC chemokine. Marked in yellow are the two disulfide bridges. An α-helix and a short loop are marked in red. The main β-sheet is marked in green (Bronger et al. 2019).

The molecular structure (Figure 1) of chemokines includes four conserved cysteine residues, which divide the chemokines into four different groups based on the arrangement of the N-terminal cysteine residues: CXC, CC, (X)C and CX3C (X being an arbitrary amino acid). The main structure of the chemokine is a three-stranded β-sheet terminated by a C-terminal α-helix and interrupted by a short loop. The N-terminus is composed of a flexible end, which is most notably necessary for the ligand and receptor interaction, followed by a rigid N-loop, which mainly contributes to the very stable structure of the chemokine domain (Bronger et al. 2019). Besides their chemical classification, chemokines can be categorized into several functional groups. The first includes inflammatory chemokines, which orchestrate different functions under inflammation-related conditions and

are upregulated by various agents (Vandercappellen et al. 2008). Their primary function is the recruitment of lymphocytes to inflamed tissue. Some of those chemokines are also angiogenic and have an ELR (Glu-Leu-Arg) motif before the first cysteine residues. Non-ELR motif chemokines are considered to be angiostatic. Another group of chemokines has homeostatic properties and regulates the migration and homing of various cells, including lymphocytes. These chemokines are expressed constitutively, e.g., in lymphoid tissue. Overlaps between both groups are possible, and the classification is continuously changing. Chemokine receptors are a class of G-protein coupled transmembrane receptors and are, corresponding to their ligands, separated into the four subgroups mentioned above. So far, 18 chemokine receptors have been identified, and five atypical receptors are known (Zlotnik and Yoshie 2012) Table 4, page 15.

Table 4: Summary of human chemokines and their corresponding receptors. The chemokines are further classified by the existence of the ELR motif if applicable and by their physiological function.

	CXC Chemokines	
name	**receptor**	**category**
CXCL1	CXCR2	inflammatory, ELR
CXCL2	CXCR2	inflammatory, ELR
CXCL3	CXCR2	inflammatory, ELR
CXCL4	CXCR3-B	platelet, non-ELR
CXCL4L1	CXCR3-B	platelet, non-ELR
CXCL5	CXCR2	inflammatory, ELR
CXCL6	CXCR1, CXCR2	inflammatory, ELR
CXCL7	CXCR1, CXCR2	platelet, inflammatory, ELR
CXCL8	CXCR1, CXCR2	inflammatory, ELR
CXCL9	CXCR3, CCR3	inflammatory, non-ELR
CXCL10	CXCR3, CCR3	inflammatory, non-ELR
CXCL11	CXCR3, CXCR7, CCR3, CCR5	inflammatory, non-ELR
CXCL12	CXCR4, CXCR7	homeostatic, non-ELR
CXCL13	CXCR5, CXCR3	homeostatic, non-ELR
CXCL14	unknown	homeostatic, non-ELR
CXCL16	CXCR6	inflammatory
CXCL17	unknown	unknown
	CC chemokines	
name	**receptor**	**category**
CCL1	CCR8	inflammatory
CCL2	CCR2	inflammatory
CCL3	CCR1, CCR5	inflammatory
CCL3L1	CCR1, CCR3, CCR5	inflammatory

CCL3L3		inflammatory
CCL4	CCR5	inflammatory
CCL4L1		inflammatory
CCL4L2		inflammatory
CCL5	CCR1, CCR3, CCR5	inflammatory, platelet
CCL7	CCR1, CCR2, CCR3, CCR5	inflammatory
CCL8	CCR1, CCR2, CCR5	inflammatory
CCL11	CCR3, CCR5, CXCR3, CCR2	dual
CCL13	CCR2, CCR3	inflammatory
CCL14	CCR1, CCR3, CCR5	platelete
CCL15	CCR1, CCR3	platelete
CCL16	CCR1, CCR2, CCR5, CCR8	unknown
CCL17	CCR4	dual
CCL18	CCR3	homeostatic
CCL19	CCR7	homeostatic
CCL20	CCR6	dual
CCL21	CCR7	homeostatic
CCL22	CCR4	dual
CCL23	CCR1	platelet
CCL24	CCR3	homeostatic
CCL25	CCR9	homeostatic
CCL26	CCR3, CX3CR1, CCR1, CCR2, CCR5	inflammatory
CCL27	CCR10	homeostatic
CCL28	CCR10, CCR3	homeostatic

XC chemokines

name	receptor	category
XCL1	XCR1	dual
XCL2	XCR1	dual

CX3C chemokines

name	receptor	category
CX3CL1	CX3CR1	dual

2.1. CXCR3 chemokine system

The CXC chemokine family comprises 17 members (Table 4, page 15). They can be further classified by the existence of a highly conserved ELR motif (Glu-Leu-Arg). This motif is shared by the chemokines CXCL1-3 and CXCL5-8 (Zlotnik and Yoshie 2012). The other chemokines lack the ELR motif (CXCL4, CXCL4L1, and CXCL9-16). The presence of the ELR motif in CXCL17 has not been described so far. Most of the non-ELR motif chemokines bind to the receptor CXCR3.

The CXCR3 ligands CXCL9-11 can be expressed by immune cells like T cells and monocytes, especially peripheral blood monocytes and macrophages. Also, endothelial cells, keratinocytes, and fibroblasts have been detected to express CXCR3 ligands (Metzemaekers et al. 2018).

The CXCR3 receptor is expressed on a wide variety of immune cells, including regulatory T cells, dendritic cells, NK and NKT cells, as well as CD4 and CD8-positive T cells (Chen and Mellman 2013; Wendel et al. 2008).

The initially identified variant of CXCR3 was called CXCR-A and is a 368 amino acid long, seven-transmembrane G-protein coupled receptor capable of binding the ligands CXCL9, CXCL10 and CXCL11. After ligand/receptor interaction, the receptor provides intracellular signaling leading to proliferation, invasion, chemotaxis, and cell survival (Billottet et al. 2013). A splice variant of CXCR3 was identified and named CXCR3-B. In addition to the “classical ligands”, this isoform can also interact with CXCL4 and CXCL4L1 (Mueller et al. 2008). However, the activation lacks the induction of chemotaxis and instead promotes apoptosis, angiostasis, and growth suppression. There is another splice isoform called CXCR3-alt, which only accepts CXCL11 as an agonist (Ehlert et al. 2004). The function of CXCR3-alt is not defined yet.

CXCL9, CXCL10, and CXCL11 are strongly induced by interferon-γ (INF-γ). CXCL10 and CXCL11 can also be induced by IFN-α (Vanguri and Farber 1990; Groom and Luster 2011). All of the CXCR3 ligands are susceptible to post-translational modification, such as proteolytic cleavage (Bronger et al. 2019). The binding affinities of the three CXCR3 ligands sharply differ, and

a hierarchical binding is described. CXCL11 shows the highest binding affinity, followed by CXCL10 with intermediate affinity. CXCL9 has the lowest binding affinity to the receptor (Murphy et al. 2000). Interestingly, CXCL11 is the only ligand that can also bind to the inactivated, G-protein uncoupled, receptor. There are differential effects described after the binding of the different CXCR3 ligands. CXCL9 and CXCL10 tend to induce mainly chemotaxis and Ca^{2+} influx, whereas CXCL11 is the most potent inducer of receptor internalization (Colvin et al. 2004).

The interaction of ligand and receptor induces, besides migration and Ca^{2+} influx, phosphorylation-dependent signaling. The downstream phosphorylation can activate target proteins like transcription factors such as members of the STAT family. CXCL11 binding can induce the phosphorylation of STAT3 and STAT6, which leads to a regulatory phenotype of CD4 positive T-cells (TH2 or Tr1) (Zohar et al. 2014). Conversely, CXCL9 and CXCL10 activate STAT1, STAT4, and STAT5, which leads to a stepwise polarization of CD4-positive T cells via T-bet and RORyT towards an effector lineage (Th1 and Th17). (Groom et al. 2012; Groom and Luster 2011; Karin and Wildbaum 2015).

Taken altogether, the interaction between the three ligands CXCL9, CXCL10, and CXCL11 and their receptor CXCR3 orchestrates a complex regulatory network that plays a major role in immune-modulation during inflammation and associated diseases like cancer.

2.1.1. *CXCL9* expression and cancer

The progression and development of cancer are dependent on the cross-talk between carcinoma tissue and the surrounding microenvironment. Chemokines and their receptors are known to play an essential role in this context. CXCL9 is secreted by various cell types in this compartment including T lymphocytes, NK cells (Smit et al. 2003), dendritic cells (Muthuswamy et al. 2008), macrophages (Ikeda et al. 2014) and non-immune cells, like endothelial cells, tumor cells and fibroblasts (Vandercappellen et al. 2008).

The role of CXCL9 in tumor progression is quite controversial and indicates tumor-suppressing and tumor-promoting properties. High concentrations of

CXCL9 in tumor tissue have been associated with a good prognosis in ovarian cancer, lung cancer, colorectal cancer and melanoma (Bronger et al. 2016; Addison et al. 2000; Bedognetti et al. 2013; Kryczek et al. 2009; Z. Wu et al. 2016; Zhang et al. 2003). This favorable prognostic value was also demonstrated for breast cancer and was suggested to be dependent on the influence of CXCL9 and associated T cell-related markers, which caused a significantly increased pathological complete response rate after neoadjuvant therapy (Denkert et al. 2010). It was also shown that in a murine breast cancer model using the parental tumor cell line 66.1 in Balb/c mice, *CXCL9* overexpressing tumor cells lead to reduced local tumor growth and lung metastasis. The reduced tumor burden was associated with high numbers of CXCR3-positive, CD4- and CD8-positive T cells. The protective potential of CXCL9 could be abolished by T cell depletion but not by NK cell depletion (Walser et al. 2007). On the other hand, the anti-tumor activity could be reduced by depletion of endogenous CXCL9 and thereby, the reduction of infiltrating T cells (Andersson et al. 2011). Similar effects have been shown after the epigenetic silencing of CXCL9, which led to a weak immune cell infiltration (Peng et al. 2015)

However, there is evidence that CXLC9 can be connected to poor prognosis in other cancer entities, such as hepatocellular carcinoma, cervical cancer, prostate cancer and glioblastoma (Liu et al. 2015; Zhi et al. 2014; S. Hu et al. 2015; Sreekanthreddy et al. 2010). For breast cancer, high levels of CXCL9 protein have been shown in sera of patients with HR-positive metastatic breast cancer compared to HR-negative patients and healthy controls (Ejaeidi et al. 2015).

2.1.2. CXCL9 in cancer therapy

Modulating the microenvironment of breast cancer, including the chemokine CXCL9, has been shown to have beneficial effects on therapy outcome. There is a strong association of COX-2 (cyclooxygenase-2) and its immunomodulatory products, prostaglandin E_2 (PGE_2) and CXCL9, in a lymphocyte-dependent manner shown in different cancer entities, including breast cancer (Howe et al 2007). This interaction could be further supported

in breast cancer patients demonstrating that COX-2 expression correlates inversely with the CXCL9 expression (Bronger et al. 2012). Similar effects were also observed in transgenic HER2-overexpressing mice with COX-2-deficient mammary epithelial cells. Here, the intra-tumoral CXCL9 influx was increased, resulting in enhanced recruitment of $CD4^+$ Th cells and $CD8^+$ CTLs (Markosyan et al. 2013). Furthermore, it was shown that similar effects in various breast cancer models could be achieved with both COX inhibition and PGE_2 receptor antagonism. The treatment suppressed local tumor growth and metastasis spread in an IFN-γ and T-cell- or NK cell-dependent manner (Kundu et al. 2009; Ma et al. 2006; Kundu et al. 2005).

Not only the interaction between COX-2 and CXCL9 seems to affect tumor progression. There are also some implications between CXCL9 and standard chemotherapy. The CXCL9 expression is increased in human melanoma cell lines after cisplatin or dacarbazine treatment (Hong et al. 2011). On the other hand, the antitumor effects of cisplatin therapy were enhanced after CXCL9 gene therapy in lewis lung carcinoma and colon carcinoma (Zhang et al. 2006). Increased CXCL9 concentrations have also been detected after treatment with other chemotherapeutics like 5-fluorouracil (Lu et al. 2012) and lapatinib plus doxorubicin (Hannesdóttir et al. 2013). All these findings suggest that there is a link between CXCL9 expression and therapy response. Specht and colleagues also indicated that breast cancer patients showed a better response to cyclophosphamide/methotrexate/5-fluoruracil therapy when the tumors contained a high expression of *CXCL9* mRNA (Specht et al. 2009).

Due to the potential increased recruitment of different immune cell populations, CXCL9 is more and more discussed as a potent partner for immunotherapies such as the PD-L1 blockade (Zou et al. 2016). Especially the PD-L1/PD-1 axis seems to be affected by CXCL9 regulation; Zhang and colleagues (Zhang et al. 2018) have shown that CXCL9 can upregulate PD-L1 in gastric cancer. Furthermore, the general mechanism of angiogenesis conducted by CXCL9 might generally support therapies in cancer entities being highly dependent on robust angiogenesis (Romagnani et al. 2001).

2.2. CX3CL1

CX3CL1 is so far the only member of the CX3C chemokines and is defined by additional three amino acids in between the characteristic cysteine residues of the chemokine domain. The protein is expressed as a transmembrane protein with an N-terminal extracellular chemokine domain after a highly glycosylated mucin-like stalk. The C-terminus is located inside the cell (Bazan et al. 1997). The basal expression of CX3CL1 conducts homeostatic processes like the recruitment of tissue-resident immune cells. It is also involved in inflammatory processes (Ludwig and Weber 2007). Thereby, strong expression patterns can be found after exposure to inflammatory modulators, including tumor necrosis factor-α (TNF-α) and NF-κB (Chandrasekar et al. 2003). As a transmembrane protein, CX3CL1 is capable of providing excellent adhesive properties to its receptor CX3CR1 (Harrison et al. 2001). Good adhesion is supported by the kinetics of the receptor and ligand interaction. A very slow receptor off rate has been shown, supporting the functional adhesive capacity (Haskell et al. 2000). The chemotactic phenomena are very likely to be provided by a soluble isoform of CX3CL1. This isoform can be generated by proteolytic cleavage of the chemokine domain. Many different proteases have been suggested to contribute to the shedding process. The disintegrin and metalloproteinase (ADAM) 17 and 10 shed an active form of CX3CL1 (Garton et al. 2001; Hundhausen et al. 2003). Also, active cathepsin S- and MMP9-mediated cleavage of CX3CL1 are discussed to contribute to inflammatory evens in the liver (Fonović et al. 2013; Bourd-Boittin et al. 2009).

CX3CL1 has been connected to the recruitment of tumor-suppressive NK cells, T cells, and dendritic cells augmenting anti-tumor immunity (Guo et al. 2003). These effects were also found in breast cancer, although there have been contradictory findings suggested concerning the influence on patients' prognosis. Tsang et al. stated an association between CX3CL1 and lymphocyte infiltration but a poor prognosis for breast cancer patients (Tsang et al. 2013). Other researchers suggested similar results with a focus on the attraction of $CD8^+$ T cells, NK cells, and dendritic cells associated with a good prognosis for breast cancer patients (Park et al. 2012).

The association between high intratumoral CX3CL1 expression and good prognosis has also been demonstrated in other cancer entities, such as colon cancer, glioma and prostate cancer (Mlecnik et al. 2010; Sciumè et al. 2010; Blum et al. 2008)

The anti-tumor activity mediated by CX3CL1 is already applied in several experimental therapy approaches that undergo preclinical studies at the moment, demonstrating that CX3CL1 gene therapy leads to tumor suppression in colon cancer (Kanagawa et al. 2007; Kim et al. 2015). A sub-analysis of the differential effects of the soluble and the membrane-bound form showed that both isoforms contribute to the tumor-suppressive effect in this cancer entity (Vitale et al. 2007). The promising effects of a CX3CL1 therapy could also be shown in different cancer entities such as colon cancer and osteosarcoma. Treatment with a CX3CL1 encoding nanosphere via aerosolization was sufficient to decrease the amount of lung metastasis in the CT26 (colon) and K7M2 (osteosarcoma) mouse tumor models (Richard-Fiardo et al. 2011) as well as in hepatocellular carcinoma (Tang et al. 2007). The results are further promoted by *CX3CL1* RNA knockdown, which shows tumor-promoting effects in melanoma (Siddiqui et al. 2016)

III. AIMS OF THE THESIS

This thesis aimed to identify the influence of CXCL9 and CX3CL1 on the anti-tumor response against breast cancer *in vitro* and *in vivo.* Especially the potential use as a therapeutic target for the enhancement of anti-HER2 therapy was investigated, as this treatment depends on the presence of immune cells and their close interaction with the tumor cells. The project can be divided into the following subprojects:

CXCL9 is a regulator of immune cell migration and angiogenesis. These effects have been linked to anti-tumor activity in several tumor entities. Is CXCL9 a mediator of anti-tumor response in breast cancer, and is there a way to pharmacologically increase its concentration in the tumor?

The expression of CXCL9 in breast cancer patients has been connected to improved therapy response. How is the expression pattern of CXCL9 in human breast cancer tissue and blood samples, and is there a link between chemotherapy and CXCL9 expression in breast cancer cells?

CX3CL1 is expressed in two isoforms and thereby combines adhesive and chemotactic properties. How are both isoforms regulated in breast cancer cells *in vitro*?

The CX3CR1 receptor is expressed on different tumor-suppressive lymphocytes, including NK cells. Does CX3CL1 affect the cytotoxic capability of NK cells? Is there an effect on cell lysis *in vitro,* and can this effect be exploited therapeutically? Furthermore, has CX3CL1 an effect on the anti-tumor response *in vivo*, and is there an influence on the tumor microenvironment? Do CX3CL1-dependent effects enhance immunotherapy with trastuzumab *in vivo*?

The expression of CX3CL1 and its receptor CX3CR1 has been analyzed for its prognostic value in other cancer entities. How is the expression of CX3CL1, its receptor, and the major shedding proteases in breast cancer patients?

IV. MATERIAL AND METHODS

1. Material

1.1. Tissue samples for immunohistochemical analysis and patient cohort

For immunohistochemical studies, a cohort of breast cancer patients (n=347) was compiled (Table 5). Tissue was formalin-fixed and paraffin-embedded. All patients were treated at the Department of Gynecology and Obstetrics, Klinikum rechts der Isar, Technische Universität München between 1988 and 2012, and had given written informed consent.

Table 5: Composition of the breast cancer cohort used for immunohistochemical analyses

Age median [years] (range)	63 (23-97)
stage	
I	42 (12.1%)
II	170 (48.9%)
III	135 (38.8%)
pT (tumor size)	
1	174 (50%)
2	145 (41.7%)
3	13 (3.7%)
4	15 (4.3%)
pN (lymph node involvement)	
pN0	215 (61.8%)
pN+	132 (37.9%)
subtype	
HR+/HER2-	283 (81.3%)
HER2+	38 (10.9%)
Triple-negative	27 (7.8%)

1.2. Human blood samples

Blood samples were taken prospectively from 161 therapy-naive patients diagnosed with breast cancer (Table 6). Blood samples were stored for 30 min at room temperature and afterwards centrifuged for 15 min at 1000 rcf. The sera were then pipetted into cryotubes and stored for further analysis at -20 °C. All patients were treated at the Department for Gynecology and Obstetrics, Klinikum rechts der Isar der Technischen Universität München between 2012 and 2019. Written informed consent was obtained from all patients.

Table 6: Patient characteristics of the breast cancer cohort used for determination of chemokines in blood samples (n=161)

Age median [years] (range)	58 (22-91)
stage	
I	22 (13.7%)
II	86 (53.4%)
III	43 (26.7%)
pT (tumor size)	
is	1 (0.6%)
1	74 (46%)
2	60 (37.3%)
3	12 (7.5%)
4	11 (6.8%)
pN (lymph node involvement)	
pN0	110 (68.3%)
pN+	49 (30.4%)
subtype	
HR+/HER2-	118 (73.3%)
HER2+	23 (14.3%)
Triple-negative	13 (8.1%)

1.3. Eukaryotic cell lines

All the cell lines used were provided by the American Type Culture Collection (ATCC), Manassas, VA, USA.

Table 7: Cell lines used

Cell line	ATCC number	Tissue	Origin	Disease
SKBR3	HTB-30	breast cancer	human	adenocarcinoma
BT474	HTB-20	breast cancer	human	ductal carcinoma
MDA-MB 453	HTB-131	breast cancer	human	metastatic carcinoma
MDA-MB 231	HTB-26	breast cancer	human	adenocarcinoma
HT29	HTB-38	colon cancer	human	adenocarcinoma
4T1	CRL-2539	breast cancer	murine	stage IV breast cancer
4T1-COX-2$^{(-/-)}$	Kindly provided by Prof. William Schieman	breast cancer	murine	stage IV breast cancer

1.3.1. Cell culture media

Table 8: Cell culture medium used

Medium	Company	Cell lines/Assay
RPMI	Life Technologies, Carlsbad, CA, USA	4T1, MDA-MB 231
RPMI indicator	Life Technologies, Carlsbad, CA, USA	EU Assay
Mc-Coy Medium	Life Technologies, Carlsbad, CA, USA	SK-BR-3, HT29
Leibovitz Medium	Life Technologies, Carlsbad, CA, USA	MDA-MB 453

Table 9: Supplements for cell culture used

Cell culture supplements	
fetal calf serum (heat-inactivated at 57 °C for 30 min)	10% (w/v)
HEPES buffer solution	10 mM
L-Arginine	0.550 mM
L-Asparagine	0.272 mM
Sodium Pyruvate	1 mM
Penicillin/Streptomycin	100 U/ml
Neomycin (G418)	1 g/l
Puromycin	5 ng/m

1.4. Antibodies

1.4.1. Primary antibodies used for IHC and western blot analyses

Table 10: Antibodies used for IHC and western blot

Antibodies	Reactivity	Host	Clonality	Number	Company
Anti-CXCL9	human	mouse IgG	monoclonal	MAB392	R&D Systems
Anit-CXCR3	human	mouse IgG	monoclonal	MAB160	R&D Systems
Anti-CX3CL1	human	goat IgG	polyclonal	AF365	R&D Systems
Anti-CX3CR1	human	goat IgG	polyclonal	AF5285	R&D Systems
Anti-ADAM10	human	mouse IgG	monoclonal	MAB1427	R&D Systems
Anti-ADAM17	human	mouse IgG	monoclonal	MAB9301	R&D Systems
Anti-HER2	human	rabbit IgG	polyclonal	A0485	Dako
Anti-GAPDH	human	Mouse IgG	monoclonal	MAB374	Merck
IgG Isotype		mouse IgG		AB-108-C	R&D Systems
IgG Isotype		goat IgG		MAB002	R&D Systems

1.4.2. Antibodies used for FACS

Table 11: Antibodies used for FACS analysis

Antibodies	Reactivity	Dye	Clone	Number	Company
CD3	mouse	PE-Cy7	17A2	100220	Biolegend
CD4	mouse	efluor450	RM4-5	48-0042-82	ebioscience
CD8 a	mouse	APC-Cy7	[53-7.3]	47-0081-82	ebioscience
DX5	mouse	APC	DX5	17-5971-82	ebioscience
CD 25	mouse	pe	PC61.5	12-0251-8	ebioscience
FoxP3	mouse/ rat	FITC	FJK-16s	11-5773-8	ebioscience
CD11b	mouse	PE-Cy7	M1/70	25-0112-82	ebioscience
CD11c	mouse	efluor450	N418	48-0114-80	ebioscience
MHCII	mouse	APC	M5/114.15.2	17-5321-82	ebioscience
Ly6C	mouse	APC-Cy7	HK1.4	128026	Biolegend
Ly6G	mouse	FITC	1A8	127606	Biolegend
F4/80	mouse	PE-Cy7	BM8	25-4801-8	ebioscience
CD86	mouse	PE-Cy5	GL1	15-0862-82	ebioscience

1.4.3. Secondary antibodies

Table 12: Secondary antibodies used

Antibodies	Reactivity	Host	Clonality	Number	Company
anti-mouse HRP	Mouse	goat IgG (H+L)	Polyclonal	115-035-003	Jackson
anti-rabbit HRP	Rabbit	goat IgG (H+L)	Polyclonal	G-21234	Invitrogen
anti-goat HRP	Goat	donkey IgG (H+L)	Polyclonal	A15999	Life Technologies
AlexaFluor 488	Mouse	Goat	Polyclonal	A11001	Life Technologies
AlexaFluor 488	Goat	Rabbit	Polyclonal	A-11078	Life Technologies

1.5. Technical devices

Table 13: Technical devices and machines

Device	Company	Equipment/ Application
Bandelin Sonopuls	Bandelin electronic, Berlin, Germany	Ultrasonic homogenizer
Cawomat 2000 IR	Cawo, Schrobenhausen, Germany	X-ray film processor
Centrifuge 54 24 R	Eppendorf AG, Hamburg, Germany	Centrifuge
EV231	Consort bvba, Turnhour, Belgium	Electrophoresis power supply
FACS Calibur	Becton Dickinson, Franklin Lakes, NJ, USA	FACS
FACS Canto	Becton Dickinson, Franklin Lakes, NJ, USA	FACS
Blotting chamber	Bio-Rad Laboratories GmbH, Munich, Germany	western blot
HERACELL 150i	Thermo Fisher Scientific, Waltham, MA, USA	Cell incubator
Herasafe	Thermo Fisher Scientific, Waltham, MA, USA	Laminar flow
IKA MAG REO	IKA Labortechnik, Staufen, Germany	Stirring Plate
Mini-Protein 3 Cell	Bio-Rad Laboratories GmbH, Munich, Germany	SDS-PAGE chamber
MS1 Minishaker	Carl Roth, Karlsruhe, Germany	Vortex Mixer
Multiskan FC	Thermo Fisher Scientific, Waltham, MA, USA	ELISA Reader
Wallac Victor 3	Perkin Elmer, Waltham, MA, USA	Fluorescence photometer (EU assay)
LSM 800	Zeiss, Oberkochen, Switzerland	Confocal laser microscope
NanoZoomer Digital Pathology RS	Hamamatsu, Hamamatsu, Japan	Slide Scanner
pH-Meter Lab 850	Schott, Mainz, Germany	pH Meter
Polymax 2014	Heidolph Instruments GmbH. Schwabach, Germany	

Olympus CK30	Olympus, Tokyo, Japan	Light microscope
Gel Doc XR+	Bio-Rad Laboratories GmbH, Munich, Germany	Geldoc and westernblot
Centrifuge 4K15C	Sigma	Centrifuge
Lightcycler MX3005	Agilent	q-RT-PCR
Power Pac 300	Bio-Rad Laboratories GmbH, Munich, Germany	Electrophoresis power supply
Purelab classic	Elga GmbH, Wein, Austria	high purity water
Rotina 48 R	Hettich Zentrifugen, Tuttlingen, Germany	Centrifuge
Sartorius basic	Sartorius AG, Göttingen, Germany	Scale
Sartorius BP 1200	Sartorius AG, Göttingen, Germany	Scale
Vortex Genie 2	Bender und Hobein AG, Zürich, Switzerland	vortex mixer
WMF Schnellkochtopf PERFECT	WMF, Geislingen an der Steige, Germany	pressure cooker

1.6. Consumables

Table 14: Consumables used

Consumable	Company
Blotting paper MN 8273	Macherey-Nage, Düren, Germany
Cell culture flasks	Greiner bio-one, Kremsmünster, Austria
cell culture plates	Becton Dickinson Labware, Franklin Lakes, NJ, USA
Cell strainer 70 γM	Corning, NY, USA
Combitips plus 2.5ml/5ml	Eppendorf AG, Hamburg, Germany
Cryogenic vials	NALGENE Labware, Thermo Fisher Scientific, Roskilde, Denmark
96-well ELISA Microplates, PS, F-bottom Microcolon 200, med binding	Greiner bio-one, Kremsmünster, Austria
FASC vials conical	Greiner bio-one, Kremsmünster, Austria
Feather Disposable Scalpel	Feather Safety Razor Co. LTD, Osaka, Japan
Microscope slides	R. Langenbrinck, Emmendingen, Germany
Minisart sterile filter 0.1/0.2 γm	Sartorius AG, Göttingen, Germany
Nitrocellulose Transfer Membrane Protran BA 85, pore size 0.45 γm	Schleicher und Schuell, Dassel, Germany
Neubauer countig chamber	LO Laboroptik. Lancing, UK

NUNC Immuno 86-well plates	Nunc, Thermo Fisher Scientific, Roskilde, Denmark
Pasteuer pipettes glass	Hirschmann Laborgeräte, Berestadt, Germany
Pipette tips	Sarstedt, Nümbrecht, Germany
Reaction tubes	Sarstedt, Nümbrecht, Germany
Serological pipettes	Greiner bio-one, Kremsmünster, Austria
Sterile Syringes	Braun, Melsungen, Germany
Falcon Tubes	Greiner bio-one, Kremsmünster, Austria
X-Ray films CEA RP-new	Agfa healthcare NV, Mortsel, Belgium

1.7. Chemicals

Table 15: Chemicals used

Chemical	Company
7AAD Viability staining solution	eBioscience, San Diego, CA, USA
Acetylsalicylic acid	Sigma, St. Louis, MN, USA
Ammonium persulfate (APS)	Carl Roth, Karlsruhe, Germany
Antibody diluent	Zytomed Systems GmbH, Berlin, Germany
Bovine Serum Albumin (BSA)	Sigma, St. Louis, MN, USA
Bromophenol blue	Serva, Heidelber, Germany
Celecoxib	Sigma, St. Louis, MN, USA
Citric acid monohydrate	Sigma, St. Louis, MN, USA
Complete + EDTA Protease Inhibitor Cocktail	Roche Diagnostics gmbH, Mannheim, Germany
Cyclophosphamide	provided by the pharmacy, Technical University of Munich
Dimethyl sulfoxide (DMSO)	Sigma, St. Louis, MN, USA
Dulbeccos's Phosphate-buffered Saline (PBS)	Life Technologies, Carlsbad, CA, USA
EC-Fixierer F 1000	Ernst Christiansen G,bH, Planegg, Germany
Epirubicin	provided by the pharmacy, Technical University of Munich
Ethylenediaminetetraacetic acid	Biochrom AG, Berlin, Germany
Ethanol	provided by the Department of Pathology, Technical University of Munich
Fetal Calf serum	Life Technologies, Carlsbad, CA, USA

Geneticin G418 Sulfate	Life Technologies, Carlsbad, CA, USA
HEPES buffer solution 1M	Life Technologies, Carlsbad, CA, USA
Hydrogen chloride	Carl Roth, Karlsruhe, Germany
Hydrogen chlride fuming 37%	Merck, Darmstadt, Germany
Hydrogen Peroxide 30%	Merck, Darmstadt, Germany
IL-2	PeproTech, London, UK
Indomethacin	Sigma, St. Louis, MN, USA
Interferon-γ	PeproTech, London, UK
Lapatinib	provided by the pharmacy, Technical University of Munich
L-Arginine	Sigma, St. Louis, MN, USA
L-Asparagine	Sigma, St. Louis, MN, USA
Mayer's hematoxylin solution	Carl Roth, Karlsruhe, Germany
Methanol	Carl Roth, Karsruhe, Germany
Paclitaxel	provided by the pharmacy, Technical University of Munich
PageRuler Prestained Protein Ladder	Pierce Biotechnology Thermo Fisher Scientific, Rockford, IL, USA
Penicillin-Streptomycin	Sigma, St. Louis, MN, USA
Pertex mounting medium	Medite GmbH, Burgdorf, Germany
Ponceau S	AppliChemo, Darmstadt, Germany
Polybrene	Satna Curz Biotechnology, Dallas, TX, USA
Potassium chloride	RdH Labrchemikalien, Seelze, Germany
Potassium dihydrogen phosphate	Merck, Darmstadt, Germany
Puromycin 10 mg/ml	Life Technologies, Carlsbad, CA, USA
Rotiphorese 40 /Acrylamid)	Carl Roth, Karlsruhe, Germany
RPMI Medium 1640	Life Technologies, Carlsbad, CA, USA
Roche Universal Probe	Roche, Basel, Switzerland
Roche Universal Probe	Roche, Basel, Switzerland
Roche Universal Probe	Roche, Basel, Switzerland
Skimmed Milk powder	Sigma, St. Louis, MN, USA

Sodium chloride	Carl Roth, Karlsruhe, Germany
Sodium dodecyl sulfate (SDS) Pellets	Carl Roth, Karlsruhe, Germany
Sodium fluoride (NaF)	Carl Roth, Karlsruhe, Germany
Sodium hydroxide solutions	Merck, Darmstadt, Germany
Sodium orthovanadate	Sigma, St. Louis, MN, USA
Sodium pyrophosphate	Sigma, St. Louis, MN, USA
Sodium pyruvate	Sigma, St. Louis, MN, USA
Tapi-2	Sigma, St. Louis, MN, USA
N,N,N',N'-Tetramethylethylenediamine (TEMED)	AppliChem, Darmstadt, Germany
Tumor necrosis factor-α	PeproTech, London, UK
Trastuzumab	provided by the pharmacy, Technical University of Munich
Tris (Ultra Pure)	Carl Roth, Karlsruhe, Germany
Tris hydrochloride	Carl Roth, Karlsruhe, Germany
Triton X-100	Sigma, St. Louis, MN, USA
TRIZMA Base	Sigma, St. Louis, MN, USA
Trypan blue solution 0.4%	Biochrom AG, Berlin, Germany
Trypsin/EDTA solution (10x)	Biochrom AG, Berlin, Germany
Tween 20	Sigma, St. Louis, MN, USA
qPCR Mastermix, low ROX	Agilent, Santa Clara, USA
Xylene	Department of Pathology, Technical University of Munich

1.8. KITS

Table 16: Commercially available kits used

Kit	Company	Method
Pierce BCA Protein Assay Kit	Pierce Biotechnology Thermo Fisher Scientific, Rockford, IL, USA	western blot
DAB substrate kit high contrast	Zytomed Systems GmbH, Berlin, Germany	IHC
Duo Set ELISA Cxcl9	R&D Systems, MN, USA	ELISA
Duo Set ELISA CXCL9	R&D Systems, MN, USA	ELISA
Duo Set ELISA hCXCL10	R&D Systems, MN, USA	ELISA
Duo Set ELISA Cx3cl1	R&D Systems, MN, USA	ELISA
Duo Set ELISA hCX3CL1	R&D Systems, MN, USA	ELISA
Pierce ECL western Blotting Substrate	Pierce Biotechnology Thermo Fisher Scientific, Rockford, IL, USA	western blot
TMB Microwell Peroxidase Substrate System	KPL, Gaithersburg MD, USA	ELISA
ZytoChem Plus HRP Broad Spectrum Bulk Kit	Zytomed Systems GmbH, Berlin, Germany	IHC
NucleoBond Xtra Midi	Machery-Nagel, Düren, Germany	Plasmid preparation
RNeasy Plus Kit	Qiagen, Hilden, Germany	qPCR
Foxp3 staining Kit	eBioscience, San Diego, USA	FACS

1.9. Plasmids

Table 17: Plasmids used

Plasmid	Company
pCMV6-Cxcl9	OriGene Technologies, Rockville, USA
pCMV6-Cx3cl1	OriGene Technologies, Rockville, USA
pRS-SCXCL9	OriGene Technologies, Rockville, USA
pCMV6-Kan/Neo	OriGene Technologies, Rockville, USA
pCMV6-Entry	OriGene Technologies, Rockville, USA
pRS-scrambled	OriGene Technologies, Rockville, USA

1.10. Primer

Table 18: Primer used

Target	Nucleotide sequence of forward primers in 5'→3' direction	Nucleotide sequence of reverse primers in 5'→3' direction
Cxcl9	CTT TTC CTC TTG GGC ATC AT	GCA TCG TGC ATT CCT TAT CA
Cx3cl1	GGC TTT GCT CAT CCG CTA T	CAG AAG CGT CTG TGC TGT GT
Hprt	CCT CCT CAG ACC GCT TTT T	AAC CTG GTT CAT CAT CGC TAA

2. Methods

2.1. Cell culture

2.1.1. Cultivation of cells

All cells were incubated in a cell incubator (HERACELL 150i) at 37 °C and 5% CO_2 in a water-saturated atmosphere. The appropriate cell culture medium was changed every three to four days (Table 19). Cells were cultured until a maximum confluence of 70% was reached. For splitting, the medium was removed, and the cells were washed with PBS (Dulbecco's PBS). Cells were incubated with a cell-specific splitting solution (

Table 20. Page 35) for 5 min at 37 °C in the incubator. Afterwards, the detached cells were washed off with cell culture medium, transferred into a 15 ml tube and centrifuged at 1000 rcf for 3 min. The supernatant was discarded, and the cell pellet was resuspended in fresh cell culture medium and passed into a fresh cell culture flask.

Table 19: Cell line-specific cell culture media

Cell line	Medium	supplement
4T1, MDA-MB 231	RPMI	10% FCS 10 mM HEPES 0.550 mM L-Arginine 0.272 mM L-Asparagine
SK-BR-3, HT29	Mc Coy's	10% FCS 10 mM HEPES 0.550 mM L-Arginine 0.272 mM L-Asparagine
BT474	DMEM	10% FCS 10 mM HEPES 0.550 mM L-Arginine 0.272 mM L-Asparagine

MDA-MB 453	Leibovitz's	10% FCS 10 mM HEPES 0.550 mM L-Arginine 0.272 mM L-Asparagine
NK cells	RPMI	10% (v/v) FCS 0.550 mM L-Arginine 0.272 mM L-Asparagine 1% (v/v)Sodium Pyruvat 1% (v/v)Penecillin/Streptomycin

Table 20: Splitting solutions

Cell line	Splitting solution
RPMI, MDA-MB 231	5% (v/v) EDTA in PBS
SK-BR-3, BT474, MDA-MB 453	0.05% (v/v) Trypsin 0.02% (v/v) EDTA in PBS

2.1.2. Storage of cell culture cells

Cells were frozen in liquid nitrogen for longtime storage. Therefore, the cells were detached with a splitting solution (

Table 20), washed off with PBS, transferred to a 15 ml tube and centrifuged for 3 min at 1000 rcf. The supernatant was discarded, and the cell pellet was resuspended in freezing medium (10^6 cells/ml in 5% DMSO and 95% FCS) and transferred to sterile cryogenic tubes. The cells were cooled down with a constant gradient of 1 °C/min until -80 °C was reached. Afterwards, the tubes were transferred to liquid nitrogen at -196 °C. Frozen cells were thawed on demand for reuse in cell culture. After removing the cells from liquid nitrogen, the frozen pellet was washed with cold cell culture medium (Table 19, page 34) until it was resuspended and moved to a fresh 15 ml tube containing 8 ml cold cell culture medium. The cells were centrifuged at 1000 rcf for 3 min, and the supernatant, including the cell-toxic DMSO, was discarded. The cell pellet was resuspended in cell culture medium and transferred to an FCS-precoated cell culture flask. After 24 hours, the

medium was replaced by fresh medium, and the cells were cultivated as previously described.

2.1.3. *In vitro* stimulation experiments

Murine and human breast cancer cells were removed from cell culture flasks and resuspended with 10 ml cell culture medium (Table 19, page 34). Cells were counted and seeded at fixed concentrations in cell culture plates overnight (1.4 * 10^5 cells/well for 12-well-plates and 2.5 * 10^5 cells/well for 6-well-plates). The next day, the cell culture medium was removed, and cells were starved in serum-free medium without FCS. After 24 hours, the serum-free medium was renewed, and different stimuli (Table 21) were added to the cells together with the corresponding controls. 24 hours later, the supernatant was removed and stored at -20 °C, the cells were detached, and the cell pellets were stored at -20 °C.

Table 21: Substances for *in vitro* stimulation cell culture experiments

Reagent	Stock	Dilution	Control
TNF-α	5 ng/µl in 0.1% BSA/PBS	10 ng/ml	0.1% BSA/PBS
IFN-γ	100 ng/µl	10 ng/ml	0.1% BSA/PBS
Tapi-2	12 mM in aqua dest.	7.5 µM	aqua dest.
Indomethacin	10 mg/ml in ethanol	10 µM	ethanol
Ibuprofen	10 mg/ml in ethanol	50 µM	ethanol
ASS	10 mg/ml in ethanol	10 µM	ethanol
Paclitaxel	6 mg/ml in aqua dest.	12.5 nM	aqua dest.
Epirubicin	2 mg/ml in aqua dest.	1.6 nM	aqua dest.
Cyclophosphamid	20 mg/ml in aqua dest.	250 µM	aqua dest.

2.1.4. NK cell isolation

NK cells were freshly isolated from a leukapheresis product of a volunteer donor. The $CD19^+$ B cells and $CD3^+$ T cells were separated from the NK cells in a negative selection. The leukapheresis product was diluted with RPMI 1:3. Afterwards, a density gradient separation was prepared by

transferring 10 ml density gradient separation medium (LSM1077) into a fresh 50 ml tube. The diluted cell suspension was added carefully, and the whole suspension was centrifuged at 300 rpm for 20 min. The lymphocytes accumulated in the interphase between medium und LSM1077 were collected by pipetting and transferred to a new 50 ml tube. The cells were washed with RPMI and centrifuged again. The cell pellet was then resuspended with 10 ml NK cell medium, and the cells were counted with a Neubauer counting chamber. Cell density was adjusted to a concentration of 20 * 10^6 cells/ml and incubated overnight at 37 °C. The next day, the cell suspension was removed from the flask and centrifuged at 300 rpm for 5 min. The supernatant was discarded, and the cell pellet was resuspended in 50 ml MACS buffer. 100 ml were taken for FACS analysis and mixed with 1 ml of FACS buffer. The antibody incubation was performed for 30 min on ice and protected from light. The antigens tested are listed in (Table 22):

Table 22: Antibody panels for determination of NK cell purity

Antibody	Amount of antibody in FACS staining
Panel 1	
IgG1-FITC	5 µl
IgG1-PE	5 µl
IgG1-PerCP	5 µl
IgG1-APC	1 µl
Panel 2	
CD56-FITC	5 µl
CD19-PE	20 µl
CD3-PerCp	10 µl
CD45-APC	1 µl

The rest of the cell suspension in MACS buffer was centrifuged at 300 rpm for 5 min, and the supernatant was discarded. The cells were resuspended in MACS buffer at a concentration of 2 * 10^8 cells/ml. Afterwards, CliniMCAS

microbeads were added to the cell suspension (1 ml CD3 microbeads for $2*10^9$ cells and 1 ml CD19 microbeads for $0.666 * 10^9$ cells). The solution was incubated in a head-over-head rotator at room temperature for 30 min. Gentle MACS XS columns were equilibrated with 50 ml MACS buffer by washing three times. The magnetic field was activated, and the incubated cell suspension was filtered through a 100 µm mesh and applied to the columns. The columns were washed three times with MACS buffer, and selected cells were eluted by deactivating the magnetic field and rewashing them with MACS buffer. NK cell enrichment was determined with a FACS analysis of the eluted cells. Afterwards, cells were centrifuged and resuspended in freezing medium and frozen as previously described for longtime storage. The purity of $CD56^+$ cells was above 83%.

2.1.5. NK cell cultivation

NK cells were thawed as previously described and resuspended in 8 ml NK cell medium and transferred to a suspension cell culture flask. The cells were then incubated overnight at 37 °C. The next day, the cells were counted and adjusted to a concentration of $5 * 10^6$/ml. The suspension was then seeded into 6-well plates and stimulated with 100 U IL-2 for at least three days.

2.1.6. Stable overexpression of breast cancer cell lines

Cells were seeded in 6-well plates, as previously described IV.2.1.3. On the next day, the medium was replaced by 1 ml of fresh serum-free medium. The transfection reagent was prepared by adding 6 µl of Lipofectin reagent to 100 µl serum-free medium in a sterile polystyrene round-bottom tube and 3 µg of the desired overexpression plasmid (Table 17, page 33) in 100 µl hunger medium in another tube. Both solutions were incubated for 45 min

at room temperature. After incubation, the DNA-containing solution was added to the Lipofectin solution, and the mixture was incubated for another 15 min at room temperature. The transfection solution was then added to the adherent cells and incubated for 6 hours. After that, the supernatant was discarded, and 3 ml of fresh cell culture medium were added. The cells were incubated until the 6 well plate was at a confluence of 80%. Then the cells were split into two 10 cm Petri-dishes and cultured until 80% confluence again. Dependent on the plasmid, the appropriate selection medium was added to the cells. The surviving clones were slightly detached with a splitting solution (Table 20, page 35)and single-cell clones were expanded for analysis of the transfection efficiency with Enzyme-linked immunosorbent assay (ELISA).

2.1.7. Stable shRNA-mediated knockdown of breast cancer cell lines

For stable knockdown, a retrovirus packaging cell line was used (Phoenix-ECO). The cells were seeded in a 6-well plate as previously described and cultured overnight to a confluence of 70% (IV.2.1.3). The cells were then transfected with lipofection, as previously described using an shRNA-containing plasmid IV.2.1.6. After six hours, the supernatant was removed, and fresh culture medium was added. The medium was then changed every morning and evening for the next two days. The whole retroviral phage-containing supernatant was collected, and 10 µg/ml polybrene was added. Target cells were seeded as previously described and were covered with retrovirus-containing solution. The solution was renewed after 12 hours and replaced by cell culture medium the next day. The cells were then grown to a confluence of 80% and split into two 10 cm dishes. The selection was then

performed as previously described (IV 2.1.6).

2.1.8. Proliferation assay

Different 4T1 transfectants and wildtype cells were seeded in 24-well plates, as previously described (2 * 10^4 cells/well). Cells were detached with increasing amounts of splitting solution and counted by using a Neubauer counting chamber after 3 hours (200 µl splitting solution), 24 hours (300 µl splitting solution), 48 hours (400 µl splitting solution) and 72 hours (500 µl splitting solution). The proliferation rate was measured by normalization to the initial cell count.

2.2. Flow cytometry of cultured cells

Cells were removed from cell culture flask with splitting solution, centrifuged at 1000 rcf for 3 min, and the supernatant was discarded and resuspended in 1 to 5 ml FACS buffer (Table 23).

Table 23: Preparation of FACS buffer

FACS buffer	
fetal calf serum	1%
EDTA	0.1 mM
sodium azide	0.1%
PBS	ad 1l

Samples were counted afterwards, and 1 * 10^6 cells were used for one sample. Cells were washed in 500 µl FACS-buffer, centrifuged, and resuspended in another 50 µl FACS buffer. 8 µl of antibody (200 µg/ml) was added to the sample and incubated for two hours on ice and resuspended every 20 min. Samples were centrifuged and washed in 500 µl FACS buffer. After another centrifugation, the cells were resuspended in 700 µl FACS buffer, and 2 µl of the fluorophore-conjugated secondary antibody (Alexa

488 goat anti-mouse) were added. The incubation was done for 30 min on ice and protected from light. After the incubation, cells were washed with 500 µl FACS buffer, centrifuged, and resuspended in 700 µl of FACS buffer. 4 µl of the viability staining (7AAD) was added, and samples were ready to be measured after 10 min incubation in the dark. Centrifugation at 1000 rpm for 3 min and washing with 500 µl FACS buffer was performed between each step.

2.2.1. Flow cytometry of murine tissue

Five million dissociated tumor or spleen cells were used for each sample. Cells were stained with live/dead fixable dye 506 in 100 µl FACS-buffer (1:200, Table 23, page 40) for 15 min at room temperature. Afterwards, free Fc-fragments were blocked with 2.4G 2 antibody in 100 µl FACS-buffer (1:300) for 10 min at 4 °C without further washing, and the surface labeling was performed with different antibodies (Table 24, page 42) for 15 min on ice. In preparation for Foxp3 detection, the eBioscience Foxp3 staining kit was used. Cells were now resuspended in 200 µl freshly prepared fix/perm solution for 60 min at 4 °C. Afterwards, cells were washed three times with perm buffer. Foxp3 detection was performed in 100 µl perm buffer for 60 min at room temperature. Cells were washed in 200 µl perm buffer after 15 min incubation. For measurement, cells were resuspended in 500 µ l of FACS buffer. If not mentioned otherwise, there was a washing step with 500 µl FACS buffer between each step, followed by centrifugation at 1000 rcf for 3 min. For each sample, fluorescence minus one (FMO), unstained control, and live/dead only controls were prepared and measured.

Table 24: Antibody panels for lymphocyte determination in murine tumors

Antigen	Channel/Fluorophore	Dilution
CD3	PE-Cy7	1:200
CD4	eFluor 450	1:400
CD8a	APC-Cy7	1:200
DX5	APC	1:200
CD 25	PE	1:300
FoxP3	FITC	1:200
CD11b	PE-Cy7	1:600
CD11c	eFluor 450	1:300
MHCII	APC	1:600
Ly6C	APC-Cy7	1:400
Ly6G	FITC	1:300
F4/80	PE-Cy7	1:400
CD86	PE-Cy5	1:400

2.3. *In vivo* experiments

2.3.1. Mouse strains

The mouse strains Balb/c and Balb/c SCID were obtained from Charles River Laboratories. Mice were maintained at the helicobacter-free mouse room 4 in the animal facilities of the Zentrum für Präklinische Forschung of the Technical University of Munich. All experiments were performed according to standards and approved by the government of Upper Bavaria.

2.3.2. Subcutaneous tumor inoculation

Mice at the age of eight weeks were taken for the tumor implantation experiments. Two different models were used following the same procedure. A syngeneic mouse model was achieved by transplanting 10^4 4T1 murine breast cancer cells into the 4th fat pad of female Balb/c wild type mice. The same model was used in a xenogenic context by transplanting $2 * 10^6$ human HT29 or MDA-MB 453 cells into the 4th fat pad of immunocompromised female Balb/c SCID mice (CBySmn.Cg-*Prkdc*^{scid}/J). In addition, transfected cell lines were used for the *in vivo* experiments. The

animals were sedated with isoflurane before inoculation, and cells were then injected with a sterile syringe in a volume of 50 µl PBS. The mice were closely followed up every 48 hours, and the tumor size was measured using a caliper. The mice were sacrificed after a total tumor diameter of 1.5 cm had been reached or if any other predefined critical status was observed. Those included losses of weight, unnatural social behavior, or injuries.

2.3.3. Indomethacin treatment

The mice were treated by oral gavage every day for 14 days. For this, 50 µg of Indomethacin were dissolved in 100 µl 20% ethanol in water and fed afterwards. Control mice were fed with 20% ethanol in water only. Animals were sacrificed after a total of 21 days.

2.3.4. Trastuzumab treatment

The mice were treated by intraperitoneal injection twice a week. To this end, the appropriate dose of 5 mg/kg was diluted in water of injectable grade, and animals were treated afterwards. Control mice were injected with water only. Animals were sacrificed when a critical status, as described above, was observed, and the animals were further analyzed.

2.3.5. Tissue generation

The mice were anesthetized with isoflurane and blood samples were taken from the *v. fasciales*. Afterwards, the mice were sacrificed by cervical dislocation. The tumor and spleen were removed, weighed, measured, and photo-documented. Kidneys, liver, lungs, and lymph nodes were also dissected. The tissue was either freshly frozen with liquid nitrogen or moved to fixation with 4% paraformaldehyde overnight at 4 °C. Pieces of tumor and spleen, as well as the lungs, were used for immediate dissociation.

2.3.6. Dissociation of mouse tissue

Tumor and spleen were removed from the mouse right after sacrifice. Tissue weight was measured on a scale, and half of the tissue was stored in 2 ml HBSS in a 24-well plate on ice. The other half of the tissue was stored for IHC analysis and fresh frozen. For dissociation, the tumor was cut into small pieces with a fresh scalpel and 1 ml of digestions solution (RPMI medium containing 0.5 mg/mL Liberase TL and 0.25 mg/mL Dnase I) was added. Solution and tissue pieces were blown through a 3 ml syringe for optimal homogenization. Afterwards, the samples were incubated for 45 min at 37 °C. The reaction was stopped by adding 20 µl EDTA solution (0.5 M). All the samples were strained through a new 70 µm cell strainer into a 50 ml Falcon. Samples were washed with 4 ml of FACS buffer. Cells were centrifuged at 250 rpm or 10 min at 4°C, resuspended in FACS buffer. The cell solution was then processed to FACS analysis.

2.3.7. Lung metastasis colony formation assay

Lungs were digested in the same way as tumors and spleens. The cell suspension was washed three times with 10 ml of HBSS. Cells were afterwards resuspended in selection medium (Table 25). Three dilutions were prepared (1:10, 1:100, 1:1000), and all of them were plated in 10 cm cell culture dishes. After two weeks of incubation at 37 °C, the medium was removed, and colonies were fixed with ice-cold methanol. Colonies were counted for every dilution and every sample.

Table 25: Selection medium for selection of positively transfected cell clones

Selection medium	
FCS	10% (v/v)
Penicillin/Streptomycin	1% (v/v)
6-Thioguanine	5 µg/ml
RPMI	ad 500 ml

2.4. Enzyme-Linked ImmunoSorbent Assay (ELISA)

A precise and sensitive way of measuring protein concentrations in solutions or tissue lysates is ELISA. In this project, only commercially available and validated ELISA assays were used (R&D Systems, CXCL9, CXCL10, CX3CL1, Prostaglandin IV.1.8). The following procedure is adapted from the distributor's manual (R&D Systems).

2.4.1. Sandwich ELISA

This technique is based on a two-step reaction with two antibodies being used for the detection. The first antibody captures the analyte out of a solution or lysate. The second antibody is conjugated to a reporter enzyme and links this specifically to the analyte.

Uncoated NUNC microtiter plates were incubated with 1% BSA/PBS solution for one hour at room temperature to block unspecific background signals. After the blocking steps, the wells were incubated with the corresponding dilutions of the capture antibody for one hour (Table 26):

Table 26: Capture antibodies for chemokine detection via ELISA

Antigen	Species	Concentration
CXCL9	mouse	1:180
CXCL10	mouse	1:180
CX3CL1	mouse	1:180
CXCL9	human	1:180
CXCL10	human	1:180
CX3CL1	human	1:180

The supernatant was discarded, and all wells were washed three times with PBS-T (PBS with 0.5% Tween 20). Doublets of 100 µl of sample and standard (dilution series) were loaded in each well and incubated for two hours at room temperature. The supernatant was discarded, and the wells

were washed with PBS-T. Now the HRP-conjugated detection antibody was added to each well and incubated for two hours at room temperature.

Table 27: Detection antibodies for chemokine detection via ELISA

Antigen	Species	Concentration
CXCL9	mouse	1:180
CXCL10	mouse	1:180
CX3CL1	mouse	1:180
CXCL9	human	1:180
CXCL10	human	1:180
CX3CL1	human	1:180

The final reporter reaction was performed by the addition of hydrogen peroxide and HRP substrate for 20 min and stopped by the addition of H_2SO_4. Signal accumulation was detected at 450 nm.

2.4.2. Competitive ELISA

In some cases, the analyte is too small to provide two epitopes for two potentially binding antibodies. Therefore, a competitive PGE_2 ELISA Kit (Cayman) was used. The plates were precoated with an anti-mouse IgG. The wells were incubated with a tracer (AChE linked to PGE_2), the specific PGE_2 antibody, and either sample or standard. The measurement was performed in triplets. All unbound reagents were removed by repeated washing steps with PBS-T. The wells were then incubated with ELLmanns reagent, which can be catalytically cleaved by the AChE.

2.5. Europium NK cell lysis assay

NK cells were thawed by the addition of 8 ml NK cell medium (Table page 34). The solution was then transferred to a T-25 suspension cell culture flask and was incubated overnight. The next day, the NK cells were counted and adjusted to a concentration of $5 * 10^6$ cells/ml in 6-well plates. Afterwards,

the cells were stimulated with IL-2 (final concentration 500 U/ml) for three days. Tumor cells were prepared by seeding 5 * 10^5 cells/well in a 6-well plate. The next day, the cells were stimulated or transfected, as previously described (IV.2.1.6). The cell lysis assay was performed by labeling 5 * 10^5 tumor cells with 0.5% DELFIABATDA reagent in 200 ml Europium medium for 30 min at 37 °C. After that, the cells were resuspended in 10 ml Europium medium (RPMI Medium w/o Phenol red, 10% FCS), and 100 µl were used for each well in the assay. The NK cells were resuspended in 5 ml Europium medium and counted. 1.4 * 10^6 cells were then resuspended in 28 ml Europium medium, and a 6-fold 1:1 dilution series was prepared. 100 µl of each NK cell dilution was added to the prepared tumor cell solution. Each sample was prepared in triplicates, and altogether different tumor cell/NK cell ratios were measured (1:10; 1:5; 1:2.5). For determination of specific cell lysis, a blank value with medium only, maximum lysis with 0.5% Triton and spontaneous lysis with tumor cells only, was also prepared. NK cells and tumor cells were centrifuged and incubated for 4 hours at 37 °C. After the incubation, 25 µl from each well were transferred to 200 µl of Europium solution (Perkin Elmer), and the fluorescence was measured with a time-resolved fluorometer. The specific cell lysis was calculated after subtraction of the blank value (medium only) and spontaneous lysis related to the maximum lysis.

2.6. Protein isolation

2.6.1. Isolation of tissue

For the protein isolation, small pieces of fresh frozen tissue (0.5 cm^3) from human or murine samples were placed into frozen cryotubes together with a freshly autoclaved steel ball. The samples were homogenized for 2 * 10 seconds in a tissue lyser. The dissociated tissue was resuspended in 250 µl lysis buffer (Table 28). The probe was centrifuged at maximum speed for 5 minutes, and the supernatant was transferred to a fresh tube and used for concentration determination and gel-electrophoreses.

Table 28: RIPA buffer

Triton X100	1%
protease inhibitors	1x
Vanadate	1 mM
glycerol phosphate	1 mM
sodium flouride	50 mM
sodium pyrophosphate	10 mM
TBS (pH7.4)	ad 100 ml

2.6.2. Isolation of cells

10^6 Cells were removed from the flasks with splitting solution (

Table 20, page 35) and washed with PBS. After centrifugation at 1000 rcf for 3 minutes, the supernatant was discarded and resuspended with 250 µl of lysis buffer. Samples were incubated on ice for 20 minutes, and afterwards, the cells were sonicated for 10 seconds. The supernatant was used for concentration determination or gel electrophoreses after a final centrifugation step for 5 min at maximum speed.

2.6.3. Protein concentration.

The Pierce BCA Protein Assay KIT (Thermo scientific) was used. All reagents were prepared according to the supplier's protocol. The BCA assay Kit is based on a copper reduction reaction, which leads to intense purple color, stoichiometrically equal to the concentration of protein in the solution. A good quantification is possible by preparing a calibration row of bovine serum albumin within every experiment (2 mg, 1.5 mg, 0.75 mg, 0.5 mg, 0.25 mg, 0.125 mg, 0.025 mg). 10 µl of protein solution was mixed with 200 µl of working solution, prepared according to the manual. Samples were prepared in doublet. Afterwards, the reaction was incubated at 37 °C for 30 min. Absorption was quantified at 569 nm.

2.7. SDS-Polyacrylamide Gel electrophoresis (SDS-PAGE)

Gels containing 7% to 12% polyacrylamide were prepared as followed in glass plates with a distance of 1.5 mm (Table 29). Gels were moved to a protean tetra chamber (Biorad, München). All lysates were diluted to 30 µg of protein per slot with protein lysis buffer, and 6 µl of reducing Lämmli buffer with mercaptoethanol was added to a total volume of 30 µl. The samples were denatured at 95 °C for 5 min before being loaded onto the polyacrylamide- gel.

Table 29: Stacking and separation gel for SDS-PAGE

stacking gel		**separation gel**	
aqua dest	4.1 µl	aqua dest	3 ml
Tris HCl 1.5 M pH 8.8	2.6 µl	Tris HCl 1 M pH 6.8	1.3 ml
Polyacrylamid	3.3 µl	Polyacrylamid	750 µl
10%SDS	100 µl	10%SDS	50 µl
TEMED	50 µl	TEMED	25 µl
APS 10%	15 µl	APS 10%	10 µl
total	10 ml	total	5 ml

The chamber was filled with electrophoresis buffer (Table 30), and two gels could be processed in parallel. The samples were run for one hour at 120 V or until the loading front was close to the end of the gel.

Table 30: Electrophoresis buffer

Electrophoresis buffer	
Tris Base	25 mM
Glycin	190 mM
SDS	0.10%
aqua dest	Ad 1 l

2.8. Western Blot analysis

The blot was performed in the same protean tetra chambers using a procedure for wet protein transfer. When the SDS-PAGE was finished, the gel was removed from the glass plates, and the stacking gel was discarded. A nitrocellulose membrane with a pore size of 0.45 µm was moved onto the separation gel. Since constant pressure, in order to guarantee sufficient contact, is necessary for a successful protein transfer, three layers of filter paper and sponges were applied to each side of the gel/membrane stack. The whole staple was then moved into a blotting cassette and placed into the blotting chamber. All steps were performed under wet conditions. The chamber was filled with blotting buffer (Table 31), and the full aperture was placed in sufficient amounts of ice. The electroblotting was done for 1.5 hours at 250 mA.

Table 31: Wet blotting buffer

Blotting buffer	
Tris Base	25 mM
Glycin	190 mM
Methanol	20%
aqua dest	ad 1 l

After successful blotting, the membrane was removed and blocked with 5% (w/v) skimmed milk powder in TBS-T for one hour at room temperature. Afterwards, following short washing, the blocking solution was discarded, and the primary antibody in 2.5% (w/v) skimmed milk powder in TBS-T was added to the membrane and incubated for one hour at room temperature or 4 °C overnight (Table 32).

Table 32: Primary antibodies for western blot. For further detail see (Table 10 page27)

Primary antibody	Isotype	Final concentration
CX3CL1	monoclonal mouse IgG	1 µg/ml
ADAM10	polyclonal goat IgG	2 µg/ml
ADAM17	monoclonal mouse IgG	1 µg/ml
CX3CR1	polyclonal goat IgG	1 µg/ml
GAPDH	monoclonal mouse IgG	0.5 µg/ml

The membrane was washed three times with TBS-T for 5 min. Then, the secondary HRP-conjugated antibodies in 2.5% skimmed milk powder TBS-T were added to the membrane and were incubated for 1 hour at room temperature.

Table 33: Secondary antibodies for western blot

Secondary antibody	Isotype	Final concentration
Goat anti-mouse HRP	Polyclonal IgG (H+L)	1:10000
Donkey anti-goat HRP	Polyclonal IgG (H+L)	1:1000

After another washing step with TBS-T, the membranes were incubated with ECL western blot detection reagent and detected in an automatic X-ray film processing machine. Afterwards, the antibodies were removed by incubating the membrane in stripping buffer at 80 °C for 20 min. After stripping, the membrane was blocked and incubated with antibodies as described above. This procedure was performed at maximum for two times

Table 34: Stripping buffer

Stripping buffer	
Glycin	200 mM
NaCl	280 mM
pH	2.5
aqua dest.	Ad 1 l

2.9. Paraffin embedded tissue analysis

2.9.1. Hematoxylin and Eosin (HE) staining

Samples were deparaffinized with xylol 10 minutes two times, followed by a descending alcohol series, starting at 96% to 50% for 3 min each. After that, the sections were put into tap water and were then incubated in a haemalaun solution for 3 min. Blueing was performed for at least 5 min in tap water. Eosin staining was conducted in prepared eosin solution (1.5 g eosin in 1% acidic acid in 300 ml 96% ethanol). Slides were stained in the solution for 1 min and then washed again in tap water. Slides were dehydrated using an ascending alcohol series to 96% for 3 min each and two times xylol for 5 minutes each. Sections were mounted with Pertex (Medite) afterwards.

2.9.2. Immunohistochemical analysis (IHC)

Several IHC protocols have been established depending on the used antibody and tissues. In general, all the sections were deparaffinized with xylol tow times for 10 minutes each and a descending alcohol series for 5 minutes each. Afterwards, the slides were washed two times with TBS buffer followed by antigen retrieval using an appropriate buffer and pressure cooking for four minutes. Slides were cooled down slowly with aqua dest. and washed with TBS-T two times for 5 minutes. Endogenous peroxidase activity was blocked with 3% peroxide solution for 20 min. Different blocking

steps were applied to get rid of endogenous biotin, avidin, and FC fragments. The primary antibody was diluted to the proper concentration in the antibody dilution solution (Table 10, page 27). Sections were incubated with 120 µl of antibody dilution for 1 hour at room temperature or 4 °C overnight. Signal detection was achieved using a two-step labeled streptavidin-biotin (LSAB, Dako) system. A species-specific biotin-conjugated secondary antibody was incubated for 20 min. A streptavidin-conjugated HRP was incubated for another 20 min. Detection was acquired using DAB substrate for 20 min. Afterwards, the reaction was stopped with aqua dest. For better contrast, the slides were counterstained with haemalaun for 3 min, and the blueing was performed for at least 5 min. In between every step, there was a washing step performed with TBS for 5 min. Finally, the slides were dehydrated with an ascending alcohol series for 3 min each and two times xylol for 10 min. Slides were mounted with Pertex afterwards.

2.10. Reverse transcription-quantitative polymerase chain reaction (RT-qPCR)

2.10.1. RNA Isolation

The isolation of total RNA was carried out according to the manufacture's protocol. Deep frozen tissue pieces (0.5 cm^3) were homogenized and resuspended in RLT buffer (Qiagen). The RNeasy mini kit (Qiagen) is based on a step by step purification of RNA. In the first step, unwanted gDNA is removed, and, in a second step, the RNA is isolated and purified.

2.10.2. Evaluation of RNA quality

The concentration of the freshly isolated mRNA was measured by using 1 µl of a sample in the nanodrop spectrophotometer (Thermo scientific). Potential contamination of DNA and protein was calculated by building the proportion between 260 nm and 280 nm, as well as 230 and 260 nm. Samples with a ratio of 1.8 were accepted as good quality and stored at -80 °C. 100 ng of the spectrophotometrically approved samples were put in a 1% agarose gel to check for the proper integrity of the ribosomal RNA bands. Samples showing two bands at 28S and 18S ribosomal RNA were accepted and put into further analysis.

2.10.3. cDNA synthesis

For cDNA synthesis, 1 µg of RNA was reversely transcribed using the cAMV reverse transcription kit (Thermo Fisher). The reaction mix was prepared according to the manufacturer's protocol and filled up with aqua dest. to a total of 20 µl (Table 35). The mixture was incubated for 10 min at 23 °C, and the synthesis was performed for 10 min at 55 °C, followed by an inactivation step for 10 min at 80 °C. The cDNA concentration was measured and adjusted to a total concentration of 70 ng/µl with aqua dest. and stored at -20°C for further use.

Table 35: Pipetting scheme for cDNA synthesis

cDNA synthesis	
5x cDNA synthesis buffer	4 µl
dNTP mix	2 µl
RNA Primer (Random hexameres)	1 µl
Reverse transcriptase enhancer	1 µl
Template RNA	x µl = 1 µg RNA
Water PCR Grad (Rnase free)	12 - x µl
total	20 µl

2.10.4. q-RT-PCR

This technique makes use of the PCR-dependent amplification of DNA and allows a quantitative analysis by adding a quenched fluorescent, amplicon-specific probe (Roche Universal Probe Library) to the reaction. After polymerase readout, the quencher is lost, and the fluorescent signal can be detected. The mass equivalent fluorescence makes it possible to measure the amount of amplified target DNA accurately in a time-dependent manner.

Table 36: Roche universal probes used for qRT-OCR

target gene	Roche probe #
Cx3cl1	80
Cxcl9	91
Hprt	95

210 ng of cDNA was used for the qPCR analysis. After an initial denaturation step at 95 °C for 3 min, 40 cycles each 15 s at 95 °C followed by 1 min at 60 °C were used for the measurement.

Table 37: qPCR pipetting scheme

qPCR	
aqua dest	5.8 µl
forward primer 20 µM	0.4 µl
reverse primer 20 mM	0.4 µl
Roche UPL	0.4 µl
Brilliant III Master Mix	10 µl
cDNA 70 ng/µl	3 µl
total	20 µl

2.11. Transformation of bacterial cells

For plasmid amplification, the target plasmids were transformed into competent DH5α bacteria. 0.5 µg of plasmid DNA was added to 50 µl DH5 α bacterial cells. The mixture was incubated for 20 min on ice, and

afterwards, a heat shock was applied for 45 s at 42 °C. The samples were then incubated on ice for at least 2 min and then transferred to a pre-culture in 1 ml of LB medium (Table 38) for one hour at 37 °C. The pre-culture was then added into 100 ml LB medium containing the corresponding selection antibiotic for overnight culture at 37 °C. After a maximum of 16 hours, the cells were centrifuged at 5000 rcf for 10 min and pellets were stored at -20 °C.

Table 38: LB Medium

LB Medium	
tryptone	1 g
yeast extract	0.5 g
NaCl	1 g
aqua dest.	ad 100 ml

2.12. Plasmid preparation

The plasmid preparation was performed using the Midi Prep Protocol and the NucleoBond Xtra Midi Kit. The cell pellets of transformed DH5 α cells were resuspended in the provided buffer, and the protocol was conducted according to the manufacturer’s instructions. After purification, the concentration of plasmid DNA was measured, and the solutions were stored at -20 °C for further use.

V. RESULTS

1. Induction of Cxcl9 by inflammatory cytokines in murine 4T1 breast cancer cells

The release of Cxcl9 by the murine breast cancer cell line 4T1 was measured in the cell supernatants by ELISA after the stimulation with the inflammatory cytokine IFN-γ *in vitro*.

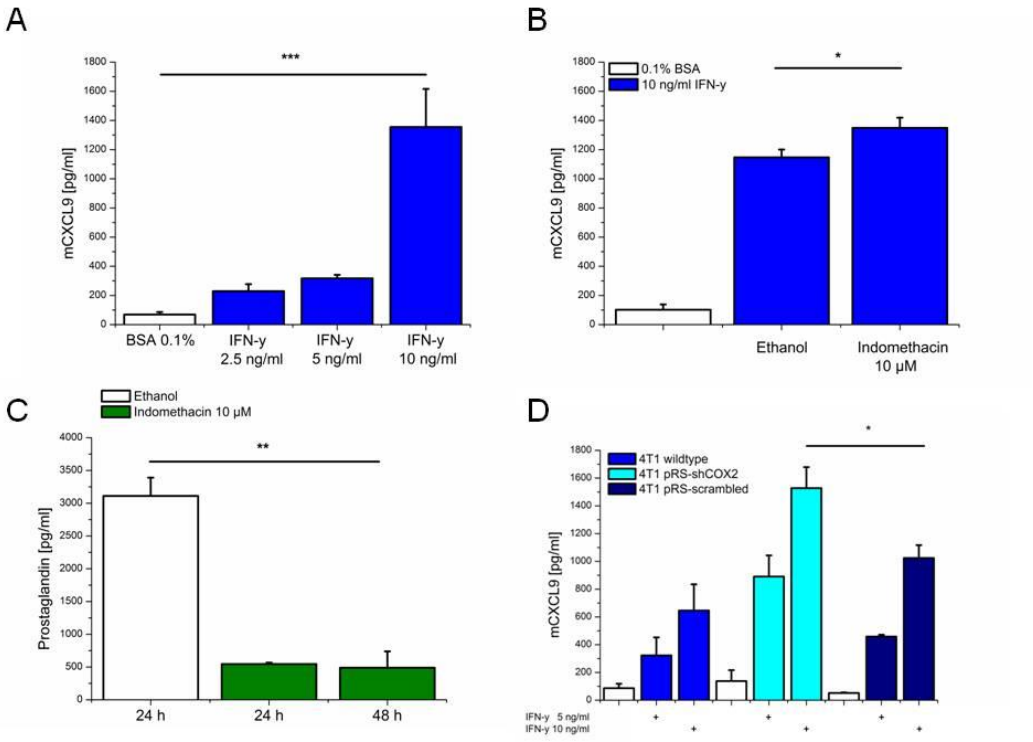

Figure 2: Induced Cxcl9 secretion in the murine 4T1 breast cancer cell line.

The secretion of Cxcl9 in 4T1 breast cancer cells could be significantly increased by inflammatory stimulus and COX inhibition (A), Dose-dependent stimulation with the inflammatory cytokine IFN-γ (2.5;5;10 ng/ml) (B) Non-selective COX inhibition by indomethacin (10 µM) together with an IFN-γ stimulation (10 ng/ml). (C) The COX inhibition led to reduced prostaglandin PGE_2 synthesis. (D) Stable COX-2 knockdown (4T1pRS-shCOX-2) and dose-dependent IFN-γ stimulation led to differential secretion of Cxcl9. Data from three independent experiments; *$p < 0.05$, **$p < 0.005$, ***$p < 0.001$.

Under baseline conditions in our experimental setting, the secretion of Cxcl9 by 4T1 cells was at a concentration of 68.7 pg/ml. The accumulation of Cxcl9 in the cell culture supernatant could be increased in a dose-dependent manner by raising the IFN-γ concentration. The amount of secreted Cxcl9 was tripled after stimulation with 2.5 ng/ml IFN-γ to a concentration of 229 pg/ml (<0.001, Figure 2A, page 57). Further stimulation with 5 ng/ml IFN-γ increased the secretion to 317 pg/ml (p<0.001, Figure 2A, page 57). A final concentration of 10 ng/ml IFN-γ is sufficient to increase Cxcl9 by the factor of 14 compared with baseline secretion to a concentration of 1.35 ng/ml (p<0.0001, Figure 2A, page 57).

2. Induction of Cxcl9 by non-selective COX inhibition

A study analyzing the effect of COX inhibition in human breast cancer cells revealed an increased CXCL9 secretion after treatment with non-selective COX inhibitors (Bronger et al. 2012). Additionally, an increased COX expression in breast cancer specimens was associated with a decreased amount of TILs in the tumor tissue. Following the regulation of Cxcl9 in 4T1 cells via IFN-γ, the effects of unselective COX inhibition (indomethacin) together with IFN-γ stimulation in the same experimental set up were analyzed.

Combined treatment of 4T1 cells with 10 µM indomethacin and 10 ng/ml IFN-γ showed 17% increased Cxcl9 secretion (1350 ng/ml) compared to IFN-γ only (1150 ng/ml; p=0.039, Figure 2B, page 57). The synthesis of PGE_2 was significantly impaired by indomethacin-induced COX inhibition. The absolute concentrations decreased from 3090 pg/ml to 545 and 488

pg/ml after 24 h and 48 h (p=0.010 and p=0.002, Figure 2C, page 57). To further validate the effect of COX inhibition, COX-2 was knocked down in 4T1 cells via short hairpin RNA (shRNA) (cells were kindly provided by Prof. William Schieman, Institute of Cancer Research, Case Western Reserve University). The COX-2-depleted cells and the corresponding scrambled control cells showed no increased Cxcl9 secretion compared to wildtype 4T1 cells under normal cell culture conditions (Figure 2D, page 57). After stimulation with IFN-γ, the COX-2-depleted cells showed increased Cxcl9 secretion compared to the scrambled control and wildtype cells, in a dose-dependent manner (Figure 2D page 57). Stimulation with 1 ng/ml IFN-γ doubled Cxcl9 concentration compared to non-stimulated control cells, the effect was stronger with a concentration of 5 ng/ml IFN-γ and increased Cxcl9 secretion by a factor of 1.5 (p=0.023, Figure 2D, page 57).

3. Overexpression or depletion of Cxcl9 does not affect cell growth *in vitro* in murine 4T1 breast cancer cells

In order to further analyze the effects of Cxcl9 in a murine model of breast cancer, 4T1 cells were stably transfected with Cxcl9 (pCMV6-Cxcl9) and shRNA against Cxcl9 (pRS-sCXCL9).

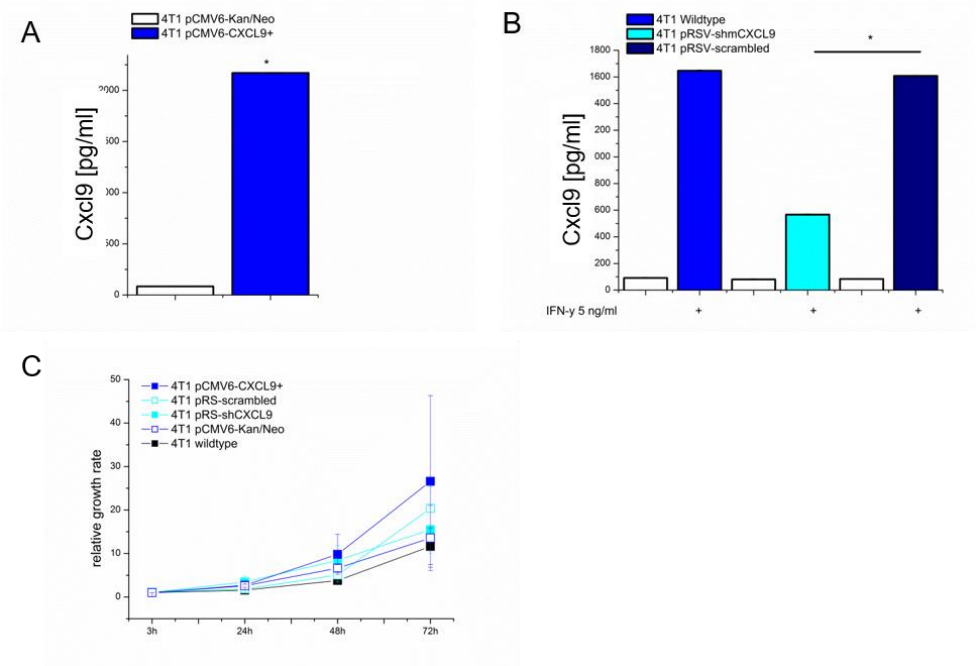

Figure 3: Generation of stably *Cxcl9*-overexpressing and *Cxcl9*-depleted 4T1 murine breast cancer cells.

(A) Cxcl9-depleted cells (pRS-shCxcl9) showed significantly decreased Cxcl9 secretion upon IFN-γ stimulation. Data was generated by ELISA of three different experiments (*p<0.05).(B) Cxcl9-overexpressing (pCMV6-Cxcl9+) 4T1 cells showed approx. 200-fold increased Cxcl9 secretion compared to control vector-transfected cells (pCMV6-Kan/Neo).(C) Relative growth curves of Cxcl9-transfected (pCMV6-Cxcl9+) or Cxcl9-depleted (pRS-sCXCL9) cells and of control cells (pCMV6-Kan/Neo, pRS-scrambled) were determined by cell counting in three independent experiments. The quantification of growing cells was set in relation to the initial cell count at three hours after seeding.

ELISA for Cxcl9 showed a significant chemokine secretion in the stably *Cxcl9*-transfected cells under unstimulated conditions (2230 pg/ml) as compared to the control vector cells (105 pg/ml, p<0.001, Figure 3A). On the other hand, knockdown of *Cxcl9* by shRNA impaired Cxcl9 secretion upon IFN-γ stimulation compared to wild-type or scrambled-control cells by

approx. 60% ($p<0.001$, Figure 3B, page 60). The *Cxcl9*-overexpressing cells, as well as the *Cxcl9* depleted cells, showed no significant change in growth rates compared to control cells (Figure 3C, page 60).

4. *Cxcl9* overexpression improves the anti-tumor response in the 4T1 syngenic mouse breast cancer model

Stably *Cxcl9*-overexpressing 4T1 cells and the corresponding control cells were subcutaneously injected into female Balb/c mice. The tumor diameter was measured regularly, and the mice were sacrificed after 21 days. Blood was taken for determination of the chemokine concentration, and the tumor was dissected and documented as described in the Materials section (Figure 4, page 62).

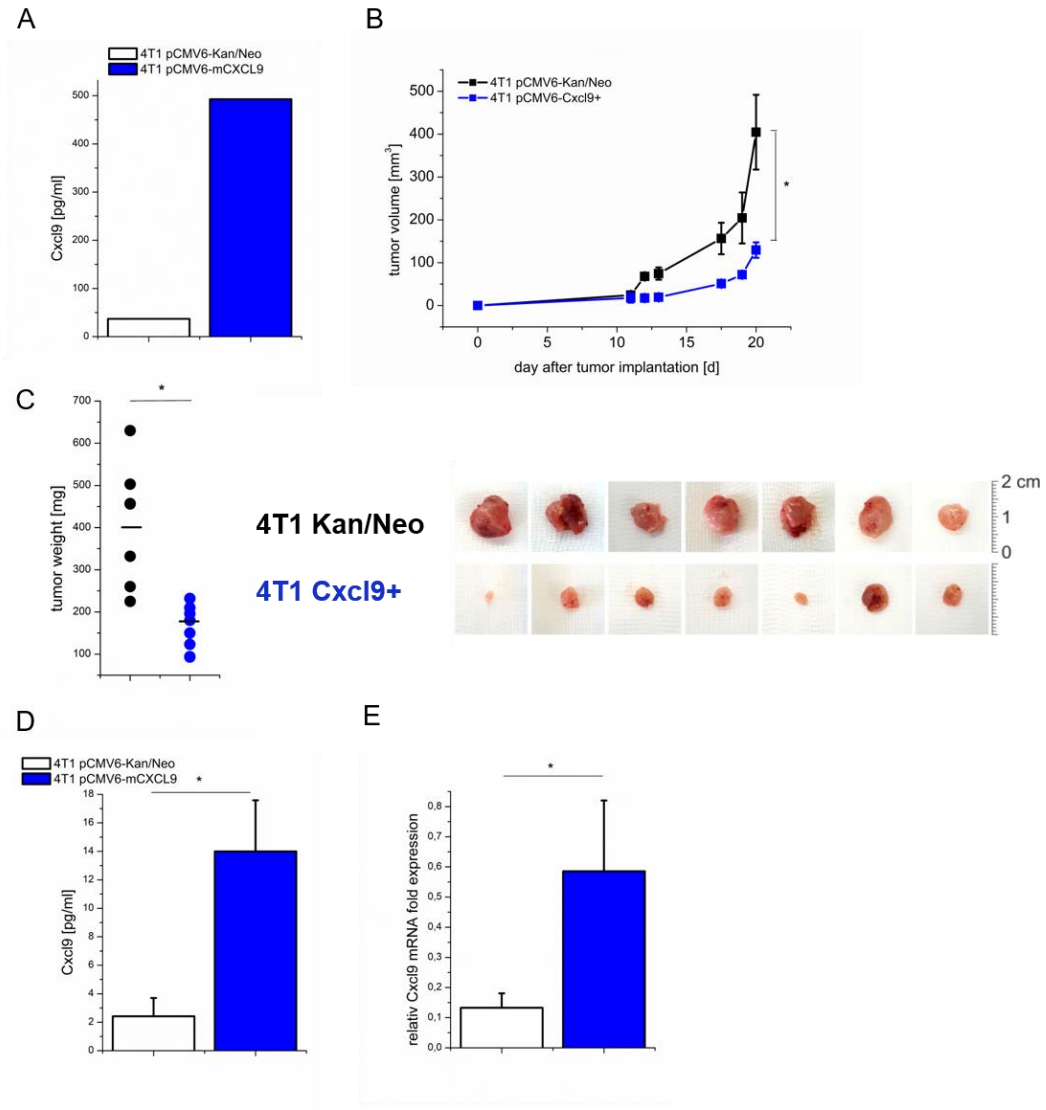

Figure 4: High *Cxcl9* expression of tumor cells led reduced tumor burden in the syngenic 4T1 mouse model.

(A) Cxcl9 secretion was significantly increased in Cxcl9-overexpressing cells (pCMV6-Cxcl9) compared to control cells (pCMV6-Kan/Neo). Unstimulated cell supernatants were tested by ELISA right before tumor injection (n=3). $1x10^4$ tumor cells were injected in the fat pad of female Balb/c mice and tumor growth was documented for 21 days. 7 mice were used per group. Tumor volume (B) and tumor mass (C) were significantly decreased in Cxcl9-overexpressing cells (pCMV6-Cxcl9) compared to control cells (pCMV6-Kan/Neo) (D) increased Cxcl9 levels of blood samples in mice with Cxcl9-overexpressing tumors as determined by ELISA (n=7) and (E) increased Cxcl9-mRNA levels in tumor tissue of mice with Cxcl9-overexpressing tumors as determined by RT-qPCR normalized to HPRT expression (n=7).*p>0.05

A highly *Cxcl9*-overexpressing 4T1 cell clone was used for the *in vivo* experiment with a secretion of 0.50 ng/ml Cxcl9 in the supernatant compared to 0.07 ng/ml in the control cells (Figure 4A). The tumor volume

of mice bearing *Cxcl9*-overexpressing tumors differed significantly from the control group after 12 days (pCMV6-Cxcl9: 17.7 ± 8.6 mm^3 and pCMV6-Kan/Neo: 67.9 ± 7.5 mm^3; p=0.002, Figure 4B, page 62). The difference in tumor size increased after 17 days by a factor of 3 (pCMV6-Cxcl9: 51 ± 6.5 mm^3 and pCMV6-Kan/Neo: 156.4 ± 36.8 mm^3 p=0.035, Figure 4, page 62). The discrepancy in tumor volume persisted till the end of the experiment at day 21 with a final mean tumor volume of 129.3 ± 18.1 mm^3 for Cxcl9-overexpressing tumors and 404.4 ± 87.2 mm^3 for control tumors (p=0.003, Figure 4, page 62). The 4T1 wild type tumors showed a mean weight of 456 mg ± 133 mg in comparison to 165 mg ± 50 mg for Cxcl9-overexpressing tumors (p<0001, Figure 4C, page 62). The analysis of Cxcl9 in blood samples showed elevated Cxcl9 concentrations in plasma of mice bearing *Cxcl9*-overexpressing tumors suggestive of its secretion into the circulation by the tumor cells (2 pg/ml vs. 14 pg/ml p=0.013, Figure 4D, page 62). Analysis of *Cxcl9* mRNA expression in the tumors after 21 days revealed stably increased chemokine mRNA levels in tumor tissue of *Cxcl9*-overexpressing 4T1 cells by a factor of 6 compared to control tumors (0.13 ± 0.05 vs. 0.58 ± 0.23, p=0.024, Figure 4E, page 62).

5. *CXCL9* knockdown does not affect tumor growth in the 4T1 syngeneic breast cancer mouse model

Cxcl9-depleted 4T1 cells and scrambled RNA control cells were injected into the fat pad of female Balb/c mice. The tumor volume was measured for 21 days. On day 21, the mice were sacrificed, blood samples were taken, and tumor tissue was dissected and documented (Figure 5, page 65). The *Cxcl9*-depleted 4T1 cells showed a significantly reduced secretion of Cxcl9 compared to the scrambled control cells ($p<0.001$, Figure 5A, page 65).

There was no significant difference in tumor volume during the whole experiment and, in the end, resulted in a mean tumor volume of 140 ± 89 mm^3 for *Cxcl9* depleted 4T1 cells and 163.8 ± 55 mm^3 for scrambled control cells (Figure 5C, page 65).

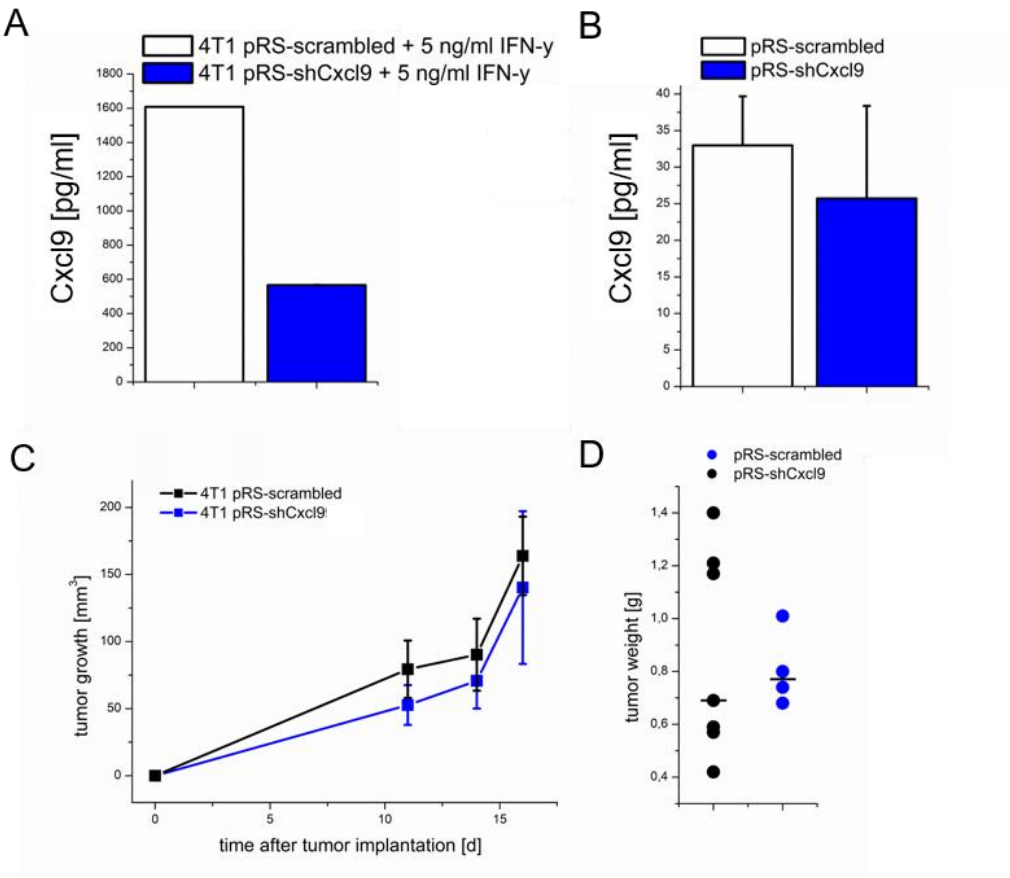

Figure 5: *Cxcl9* knockdown showed no significant effect on tumor growth in the syngenic 4T1 mouse model.

1x10^4 tumor cells were injected in the fat pad of female Balb/c mice, and tumor growth was assessed for 21 days in 7 animals per group. (A) Successful knockdown showed significantly decreased Cxcl9 secretion after stimulation with 5 ng/ml IFN-γ detected with ELISA (n=3). (B) Plasma levels of Cxcl9 after 21 days showed no significant difference between Cxcl9-depleted samples and controls, measured by ELISA (n=7). (C) No significant difference in tumor growth was detected between *Cxcl9*-depleted tumors (pRS-sCxcl9) and controls (pRS-scrambled). (D) There was no difference in tumor weight detected after 21 days (n=7).

The evaluation of Cxcl9 concentration in plasma samples showed no difference between the *Cxcl9* depleted cells and scrambled controls with a mean expression of approx. 30 pg/ml (Figure 5B). The determination of tumor mass after dissection showed no difference between Cxcl9-depleted tumors and the control group (pRS-sCXCL9: 0.69 ± 0.36 g, pRS-scrambled: 0.77 ± 0.12 g, Figure 5D).

6. Non-selective COX inhibition with indomethacin suppresses tumor growth in the 4T1 breast cancer model *in vivo*

4T1 wild type cells were subcutaneously injected into the 4th fat pad of female Balb/c mice. Seven days after tumor inoculation, the mice were randomized and treated with 50 µg/kg/d of indomethacin or ethanol as control by oral gavage every day for two weeks. Tumor diameters were measured, and the mice were sacrificed after 21 days. Tumor and spleen were freshly dissected and documented (Figure 6, page 67). Blood samples were taken for Cxcl9 concentration determination. The dissected tissues were homogenized and used for fluorescence assisted cell sorting (FACS) analysis of different immune cell surface markers (Figure 7 page 68).

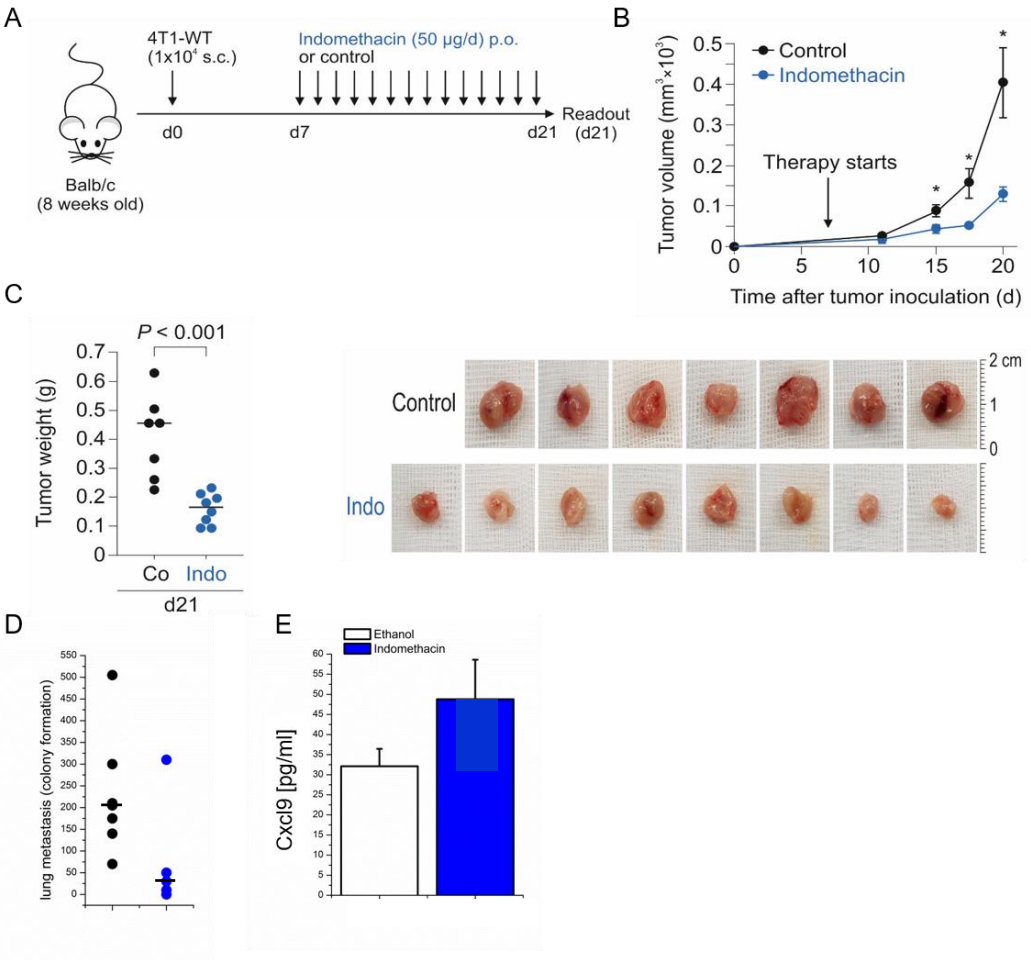

Figure 6: Non-selective COX inhibition by indomethacin promotes tumor-suppressive effects in the 4T1 breast cancer model *in vivo*.

(A) Eight weeks old female Balb/c mice were inoculated subcutaneously (s.c) with $1x10^4$ 4T1 wildtype cells (4T1-WT). Indomethacin or vehicle control treatment was started 7 days after tumor inoculation (Indomethacin per os 50 µg/d/kg and equivalent ethanol control, n=7).(B) After treatment, the tumor volume was significantly lower in the indomethacin-treated group compared to the ethanol control group. (C) Tumor weight was significantly lower in the indomethacin-treated animals at the end of the experiment on day 21. (D) Formation of lung metastases was significantly decreased in indomethacin-treated mice compared to the control group (p=0.05). (E) The plasma level of Cxcl9 assessed by ELISA was showed higher chemokineconcentration after 14 days of indomethacin treatment compared to the control group (n=7; p=0.14). *p < 0.05; **p < 0.005, ***p<0.001.

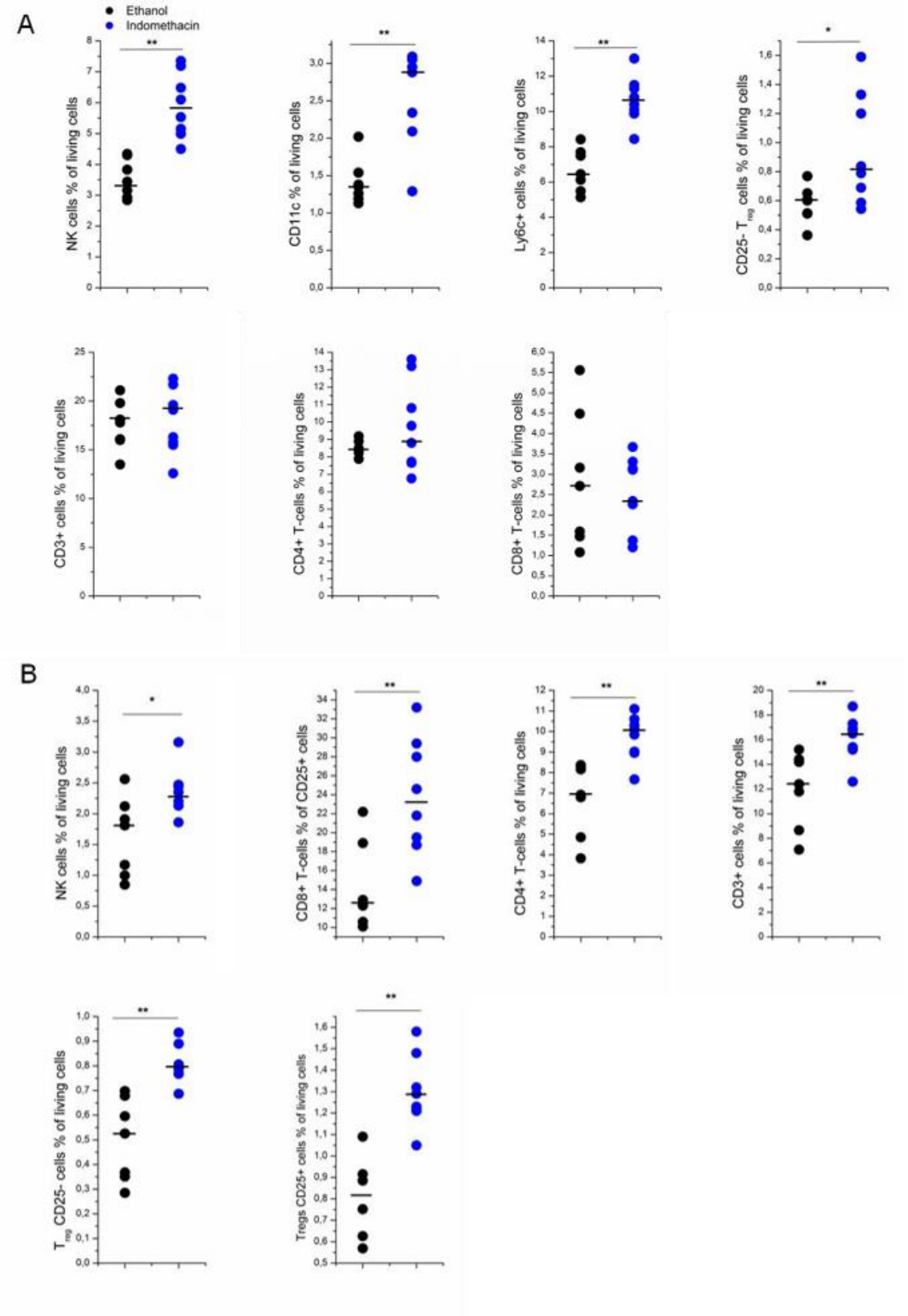

Figure 7: Indomethacin modulates tumor immune cell infiltration in the 4T1 breast cancer model *in vivo*.

(A) Increased populations of NK cells, Ly6C$^+$ and CD11$^+$ dendritic cells and regulatory as well as CD3$^+$, CD4$^+$ and CD8$^+$ T cells were detected in tumors of indomethacin-treated mice compared to the control group (n=7 per group). (B) NK cells, CD8$^+$ and CD4$^+$ T cells, regulatory T cells and total CD3+ immune cells were increased in spleens of indomethacin-treated mice compared to the control. *$p < 0.05$; **$p < 0.005$

The indomethacin treatment of 4T1 cell-derived tumors induced a significant reduction of tumor growth (tumor volume) during the whole experiment. The tumor volume was significantly different 12 days after tumor inoculation by the factor of three in indomethacin-treated mice (17 ± 3 mm^3) compared to ethanol-treated animals (67 ± 2 mm^3, $p<0.001$, Figure 6B, page 67). After 15 days, the tumor volume of indomethacin-treated tumors increased to a mean volume of 44 ± 3 mm^3, whereas the tumor volume of ethanol-treated mice was significantly increased (100 mm^3, $p=0.04$, Figure 6B, page 67). After 21 days, the volumes of untreated tumors raised to a median size of 400 ± 87 mm^3, and the indomethacin-treated tumors remained at a three-time lower median volume of 120 ± 18 mm^3 ($p=0.006$, Figure 6B, page 67). The mean tumor weight of the indomethacin-treated samples was at 159 mg ± 49 mg in comparison to 409 ± 133 mg of ethanol-treated animals ($p=0.0005$, Figure 6C, page 67). The formation of lung metastases was also decreased after indomethacin treatment (mean colony count: 20) compared to ethanol control (median colony count: 205, $p=0.048$, Figure 6D, page 67). The quantification of Cxcl9 serum levels showed a trend towards an elevated Cxcl9 concentration in the indomethacin-treated animals (32.1 vs. 54.3 pg/ml; $p=0.143$; Figure 6E, page 67).

The evaluation of different immune cell populations in the tumor showed significant elevations of $DX5^+$ cell populations (3.5% vs. 5.9%; $p<0.001$), $CD25^-$ $Foxp3^+$ cells (0.6% vs. 0.9%; $p<0.001$), $Ly6c^+$ cells (6.7% vs. 10.7%; $p<0.001$) and $CD11^+$ cells (1.4% vs. 2.6%; $p<0.001$) in indomethacin-treated mice (Figure 7A, page 68). Other T-cell subsets were not changed by the treatment with indomethacin, especially $CD3^+$ (17.5% vs. 17.9%), $CD4^+$ (8.5% vs. 9.7%) and $CD8^+$ (2.8% vs. 2.6%). Additional effects on immune

cell populations were detected in the spleens of the corresponding animals. Increased populations of $CD3^+$ (12% vs. 16.2%; p=0.0058), $CD4^+$ (6.7% vs. 9.7%; p=0.002) and $CD8^+$ T-cells (0.01% vs. 0.02%; p=0.005) as well as $DX5^+$ cells (1.6% vs. 2.4%; p=0.014) were detected in the spleens of indomethacin-treated mice compared to the control group (Figure 7B, page 68). Also, the number of $CD25^-$ and $CD25^+$ $Foxp3^+$ cells (0.8% vs. 1.3%; p=0.0015) was found to be increased in spleen samples of animals fed with indomethacin (Figure 7B, page 68).

7. Induction of CXCL9 in human breast cancer cell lines upon cytokine stimulation

The human breast cancer cell lines SKBR3 and MDA-MB 231 were treated with different concentrations of IFN-γ and different COX inhibitors (indomethacin, acetylsalicylic acid (ASS), and celecoxib) to determine the effects of cytokine stimulation and COX inhibition on the secretion of CXCL9.

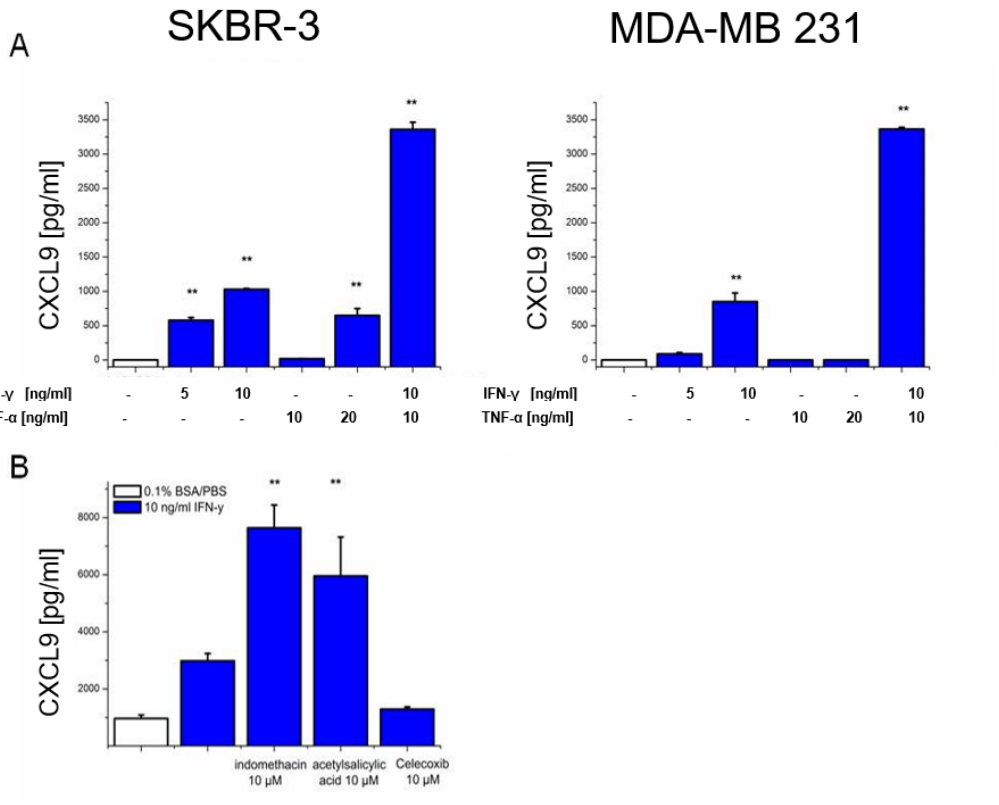

Figure 8: Induction of human CXCL9 expression in the human breast cancer cell lines SKBR3 and MDA-MB 231.

(A) ELISA measurement showed increased secretion of CXCL9 in SKBR3 and MDA-MB 231 cells after inflammatory cytokine stimulation (IFN-γ 5 and 10 ng/ml, n=3, and TNF-α 10 and 20 ng/ml, n=3). (B) Unselective COX inhibition by indomethacin 10 µM and ASS 10 µM augments IFN-γ-induced CXCL9 secretion, whereas selective COX-2 inhibition with celecoxib (10 µM) does not alter CXCL9 secretion in SKBR3 cells (n=3). **p<0.005.

BSA-treated SKBR3 cells showed no baseline CXCL9 secretion in the cell supernatant, whereas stimulation with IFN-γ significantly increased the

secretion of CXCL9 in a dose-dependent manner (Figure 8A, page 71). Stimulation with 5 ng/ml IFN-γ and 10 ng/ml IFN-γ enhanced the secretion of CXCL9 to 579 ± 39 pg/ml and 1030 ± 13 pg/ml, respectively, in SKBR3 cells ($p<0.001$). The stimulatory effect of IFN-γ in MDA-MB 231 cells was significantly elevated at concentrations of 10 ng/ml IFN-γ (Figure 8A, page 71). Expression levels were comparable to SKBR3 (849 ± 127 pg/ml). Similar effects were detected for TNF-α in SKBR3 cells. Stimulation with 20 ng/ml TNF-α significantly increased CXCL9 secretion to 649 ± 100 pg/ml ($p<0.001$). MDA-MB 231 cells showed no sensitivity towards TNF-α stimulation with respect to CXCL9 secretion. Combined stimulation with TNF-α and IFN-γ showed a synergistic effect on chemokine secretion in both cell lines with a concentration of 3360 ± 104 pg/ml ($p<0.001$) (Figure 8A, page 71).

The addition of indomethacin, a non-selective COX inhibitor, to IFN-γ-treated cells further increased the secretion of CXCL9 to a concentration of 7641 ± 799 pg/ml compared to IFN-γ treated alone in this experimental series 2985 ± 258 pg/ml ($p<0.001$, Figure 8B, page 71). Similar effects were achieved with the non-selective COX inhibitor acetylsalicylic acid (5954 ± 360 pg/ml, $p=0.009$). The addition of the selective COX-2 inhibitor celecoxib had no effect on the CXCL9 concentrations in the cell culture supernatant (Figure 8B, page 71).

8. CXCL9 and CXCL10 concentrations in the sera of breast cancer patients

The concentration of serum CXCL9 levels was measured in blood samples of 161 breast cancer patients (Table 6 page 25). The blood samples were taken before any therapy was started.

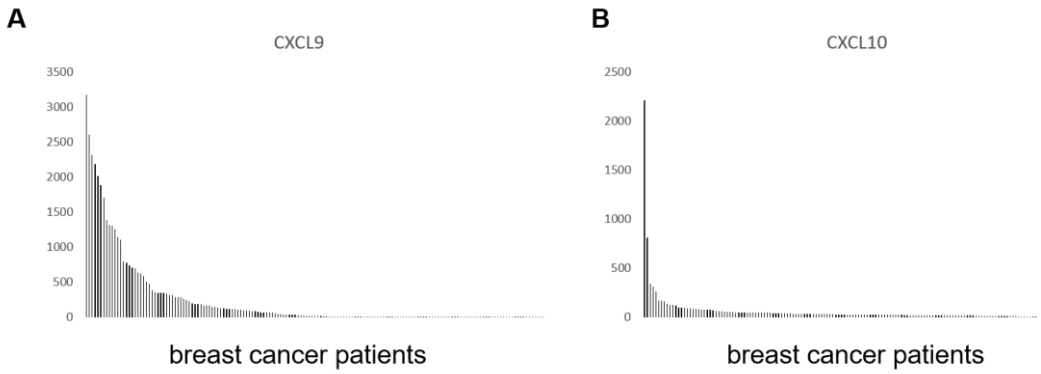

Figure 9: Serum levels of CXCL9 and CXCL10 in therapy-naïve breast cancer patients.

The serum levels of CXCL9 (A) and CXCL10 (B) were determined by ELISA in a group of 161 breast cancer patients**.**

Table 39: Distribution of CXCL9 and CXCL10 concentrations in the sera of breast cancer patients, classified according to the respective quartiles based on the maximal values.

	CXCL9	**CXCL10**
quartile	range	range
q1	0 pg/ml	<12.9 pg/ml
q2	0-11.7 pg/ml	12.9-25.7 pg/ml
q3	11.7-188 pg/ml	25.7-45.9 pg/ml
q4	188-3176.5 pg/ml	45.9-2209.5 pg/ml

There was no correlation of CXCL9 and CXCL10 serum concentrations detected in this cohort (Spearman-rho correlation R=0.166; p=0.036).

9. Stimulation of breast cancer cells with chemotherapeutics increased the IFN-γ-mediated CXCL9 secretion *in vitro*

SKBR3 and MDA-MB 231 cells were stimulated with IFN-γ and different concentrations and formulations of systemic therapeutic agents, including cyclophosphamide, paclitaxel, lapatinib, and epirubicin. All of these are well-established cornerstones of modern breast cancer therapy.

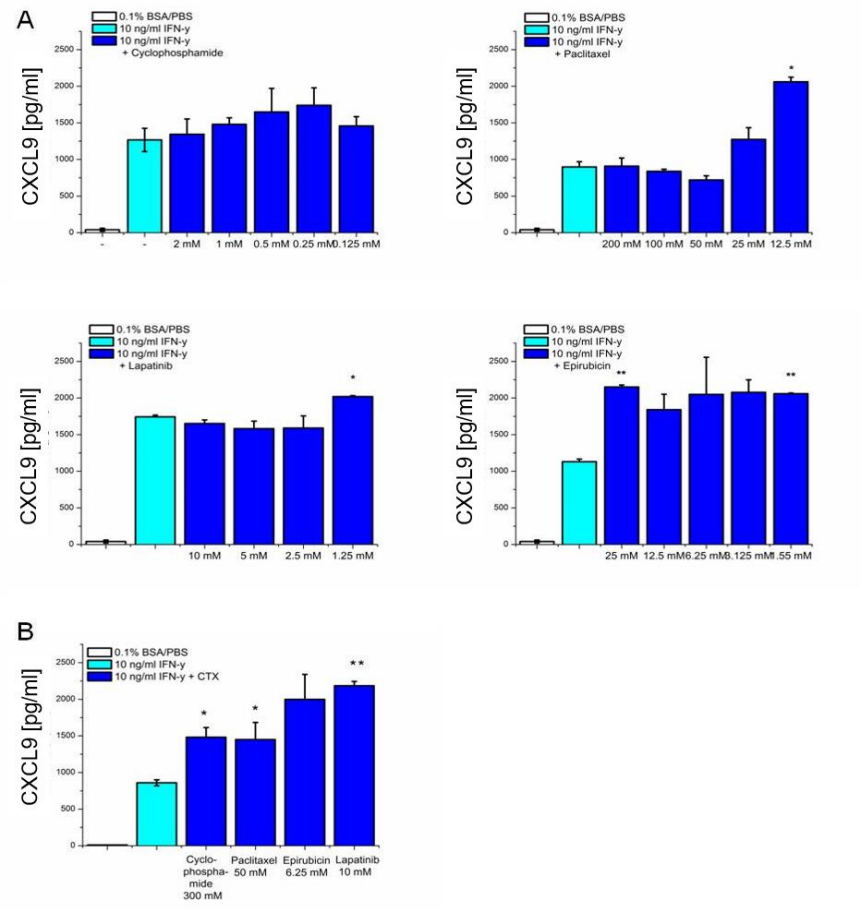

Figure 10: Co-stimulation with IFN-γ and chemotherapeutics of human breast cancer cells led to increased secretion of CXCL9.

(A) ELISA evaluation of CXCL9 showed increased chemokine secretion after treatment with different concentrations of cyclophosphamide, paclitaxel, lapatinib, and epirubicin in SKBR3 cells (n=3). (B) The most efficient concentrations of chemotherapy treatment (CTX), as seen in the SKBR3 cells, increased IFN-γ-induced CXCL9 secretion also in MDA-MB 231 cells (n=3). *$p < 0.05$; **$p < 0.005$.

As shown before, INF-γ induced a significant increase in CXCL9 expression in comparison to BSA-treated control cells (Figure 10, page 74). The treatment of SKBR3 cells with cyclophosphamide showed a trend towards increased chemokine concentrations. In contrast, paclitaxel altered the CXCL9 secretion only at low concentrations (25 mM and 12.5 mM), there, twice as much chemokine (1274 ± 160 pg/ml vs. 2060 ± 63 pg/ml, p=0.014) could be detected in the supernatant compared to IFN-γ only stimulated cells with 897 ± 72 pg/ml (Figure 10A, page 74). The addition of lapatinib to IFN-γ in SKBR3 cells enhanced CXCL9 secretion from 1742 ± 23 pg/ml to 2019 ± 13 pg/ml, respectively (p=0.002). Epirubicin treatment doubled the secretion of CXCL9 into the supernatant in comparison to IFN-γ-only treated samples (1130 ± 34 pg/ml vs. 2058 ± 10 pg/ml, p=0.001, Figure 10A, page 74).

The most efficient concentrations in terms of CXCL9 stimulation were validated in another cell line (MDA-MB 231 cells, Figure 10B, page 74). The chemotherapeutics cyclophosphamide (p=0.034) and paclitaxel (p=0.014) showed significantly increased CXCL9 secretion in this cell line by the factor of approx. two (1481 ± 132 pg/ml; 1450 ± 232 pg/ml, respectively vs IFN-γ 859 ± 40 pg/ml). For epirubicin treatment, there was an elevated chemokine secretion from 859 ± 40 pg/ml to 1998 ± 340 pg/ml (p=0.08) detected. Lapatinib treatment significantly increased CXCL9 expression in comparison to IFN-γ treated cells from 859 ± 40 pg/ml to 2183 ± 60 pg/ml (p=0.0018, Figure 10B, page 74).

10. *CXCL9* expression in human breast cancer samples

In order to analyze the distribution of CXCL9 expression in human breast cancer, 239 tissue samples of breast cancer patients were immunohistochemically analyzed (Table 40, page 77).

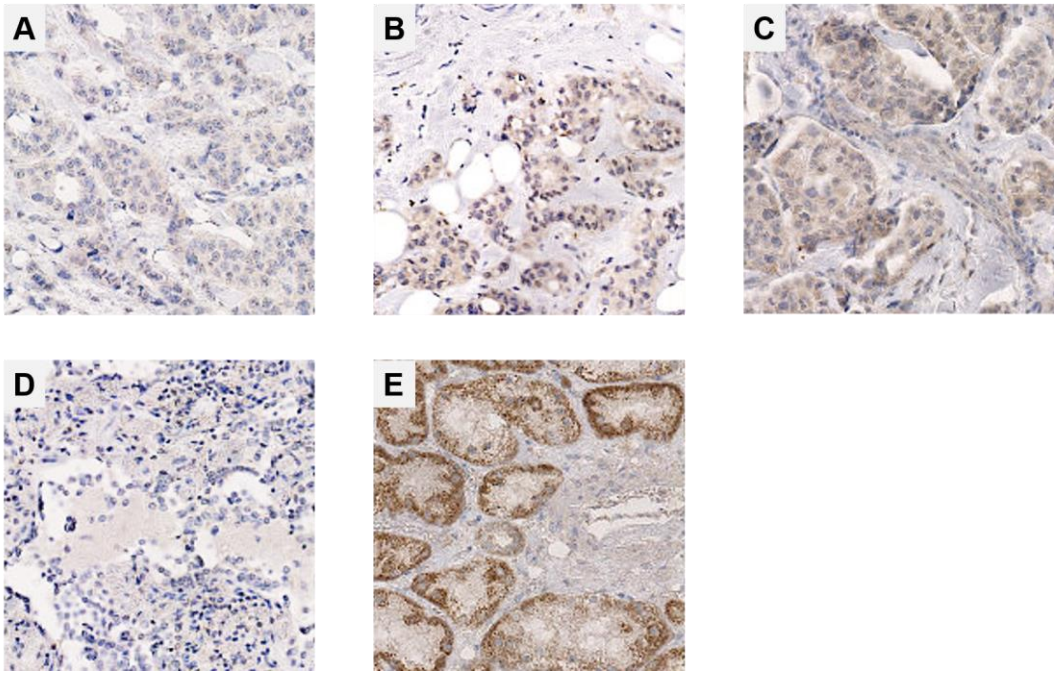

Figure 11: Immunohistochemical (IHC) analysis of CXCL9 expression in breast cancer tissues:

Immunohistochemical staining of CXCL9 showed low +1 (A), moderate +2 (B), or high +3 (C) expression in breast cancer tissue. (D) A negative control without primary antibody showed no background signals. (E) positive control: kidney.

CXCL9 is localized mainly to tumor cells, in particular to the cytoplasm, but also endothelial cells, whereas nuclei stay signal-free (Figure 11). There was no signal detected in stromal cells or fatty tissue. The expression is differentially distributed among samples of different patients and allowed to categorize the CXCL9 intensity into low expression (scores 0 and +1) and high expression (scores +2 and +3). A negative control without primary antibody showed no signal. CXCL9 detection in kidney samples was

localized to ductal structures. Other cell compartments like glomeruli, pericytes, and stromal cells showed no signal. Among 239 samples, 136 (56.9%) showed a high expression of CXCL9 in tumor tissue. There was an equal distribution of CXCL9 high and low cases among HR^+ and $HER2^+$ cases but a significant association of high CXCL9 expression and TNBC as well as HR^- cases (p=0.004 and p=0.015 respectively Table 40, page 77).

Table 40: Distribution of CXCL9 IHC scores in a cohort of 239 breast cancer patients.

Relative distribution among breast cancer subgroups divided into HER2 receptor (HER2), estrogen receptor (ER) and progesterone receptor (PR). Scores of 0 and 1+ were defined as low, and scores of 2+ and 3+ as high. High CXCL9 expression in the respective subgroups is indicated in bold.

scoring	percentage		
low	43%		
high	57%		
HER2		**CXCL9 high**	**CXCL9 low**
positive	25	15	10
negative	214	121	93
Chi-Quadrat	0.741		
HR		**CXCL9 high**	**CXCL9 low**
positive	189	100	89
negative	50	36	14
Chi-Quadrat	**0.015**		
TNBC		**CXCL9 high**	**CXCL9 low**
yes	25	21	4
no	214	115	99
Chi-Quadrat	**0.004**		

The analysis of the association of CXCL9 expression with clinical parameters and survival was performed with Kaplan-Meier analysis (Figure 12, page 78) as well as es univariate cox-regression analysis. The immunohistochemical data were further compared to publicly available Affymetrix datasets (Table 41, page 79)

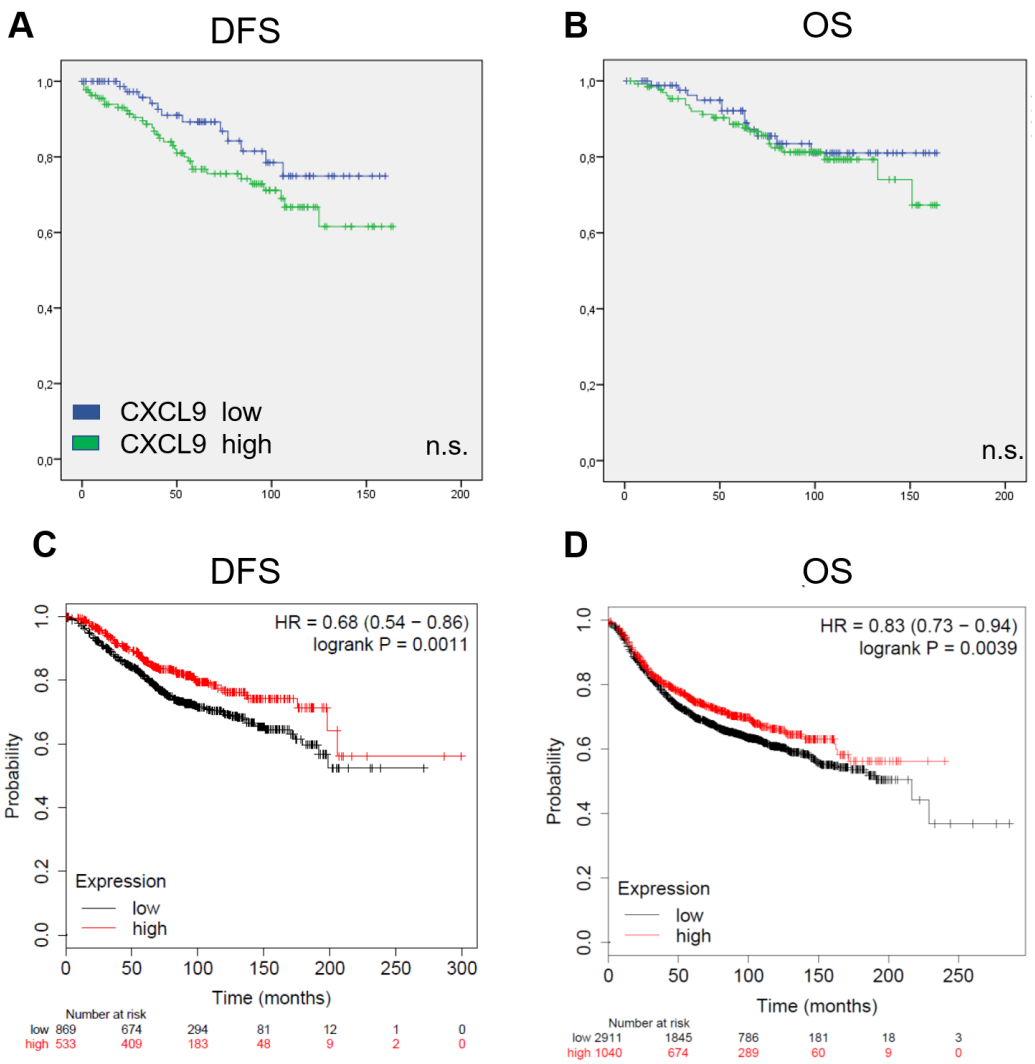

Figure 12: Association of CXCL9 expression with overall- and progression-free survival. Kaplan-Meier analysis of CXCL9 immunohistochemistry of 239 breast cancer patients reveals a trend towards significance for an association with (A) DFS (p=0.084) but not (B) OS (p=0.5). Kaplan Meier analysis of publicly available Affymetrix data shows a significant correlation of high CXCL9 expression and better (C) DFS (p=0.0011) as well as (D) OS (p=0.0039).

The analysis of *CXLC9* expression in 239 breast cancer specimens showed a borderline significant (p=0.084) association with an adverse prognosis for DFS and no association for OS (p=0.5, Figure 12A+B, page 78). However, the publicly available Affymetrix data (Győrffy et al. 2010) showed an association of high CXCL9 expression with better DFS (p=0.0011) and OS (p=0.0039, Figure 12C+D).

Table 41: Univariate cox regression analysis of CXCL9 expression

	DFS		**OS**	
	p	HR	p	HR
tumor≥20 mm	**0.019**	1.775 (1.098 - 2.869)	**0.002**	2.578 (1.399 - 4.753)
age≥60 y	0.831	0.950 (0.593 - 1.521)	0.083	1.704 (0.933 - 3.112)
pT≥2	**0.00047**	1.568 (1.219 - 2.017)	**0.000011**	1.864 (1.412 - 2.461)
pN positive	**0.01**	1.374 (1.079 - 1.749)	**0.003**	1.524 (1.154 - 2.014)
Grading≥3	0.125	1.341 (0.922 - 1.949)	**0.017**	1.78 (1.109 - 2.858)
TILs≥30%	0.89	0.953 (0.482 - 1.886)	0.931	0.960 (0.376 - 2.447)
CXCL9 low	0.088	1.777 (0.918 - 3.442)	0.499	1.270 (0.635 - 2.541)

Univariate cox-regression analysis of tumor-associated factors assessed within the breast cancer cohort showed that the clinical factors tumor size (p=0.019), tumor stage (p=0.00047), and nodal status (p=0.01) describe significant, prognostic factors for DFS and OS in this group of patients. In terms of OS, tumor grading also demonstrated prognostic impact in this cohort (Table 41).

11. Differential CXCR3 expression in human breast cancer patients

Detection of the CXCL9 receptor, CXCR3, in human breast cancer patients was performed in 287 samples by immunohistochemical analysis.

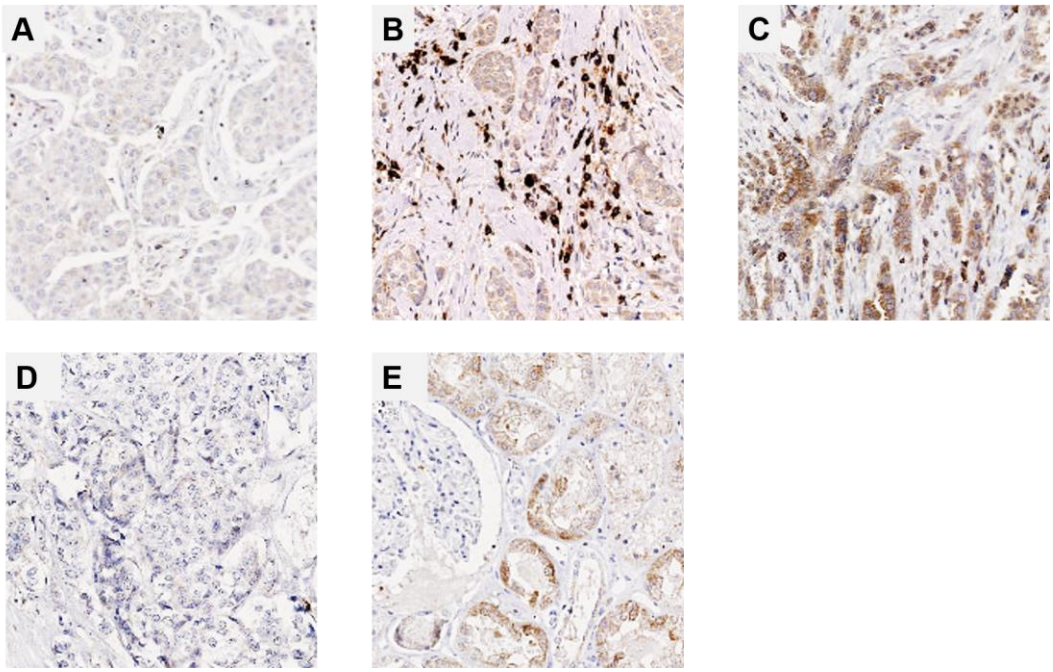

Figure 13: Immunohistochemistry (IHC) analysis of CXCR3 in breast cancer tissue: Scoring intensities of CXCR3 in IHC showed (A) low +1 (B) moderate +2 and (C) high +3 expression in breast cancer tissue. (D) A negative control without primary antibody showed no background signal. (E) Positive control: kidney.

CXCR3 was detected in tumor cells and lymphocytes located in tumor-surrounding tissue or blood vessels (Figure 13). Other tissue compartments like stroma and fatty tissue remained signal-free. The intensity was different in various samples, and a classification into low expressing (scores 0 +1) and high expressing (scores 2 +3) samples was done. Only the signal intensity in tumor cells was taken into account for scoring and the formation of the groups. A negative control without primary antibody showed no signal. Kidney samples were CXCR3-positive in ductal structures but not glomeruli,

stroma, or pericytes. 61.3% of all breast cancer cases showed high expression for CXCR3.

Among those cases, 50% of HER2-positive cases showed high expression of CXCR3 as well as 59% of HR^+ cases. Among the triple-negative cases, 88.9 % were stained positive for high CXCR3 expression and the correlation of CXC3 expression and the lack of HR and HER2 remained significant in the chi-Quadrat test. (p=0.033, Table , page 81)

Table 42: Distribution of CXCR3 IHC score in a cohort of 287 breast cancer patients.

Relative distribution among breast cancer subgroups divided into HER2 receptor (HER2), estrogen receptor (ER) and progesterone receptor (PR). Scores of 0 and 1+ were defined as low, and scores of 2+ and 3+ as high. High CXCR3 expression in the respective subgroups is indicated in bold.

scoring	percentage		
low	39%		
high	61%		
HER2		**CXCR3 high**	**CXCR3 low**
positive	25	11	14
negative	262	165	97
Chi-Quadrat	0.063		
HR		**CXCR3 high**	**CXCR3 low**
positive	236	144	92
negative	51	32	19
Chi-Quadrat	0.818		
TNBC		**CXCR3 high**	**CXCR3 low**
yes	26	21	5
no	261	155	106
Chi-Quadrat	**0.033**		

In the immunohistochemistry staining, this high expression of CXCR3 is associated with a worse prognosis for DFS and OS, though the effects did not reach significance (Figure 14, page 82). This association could not be verified by the univariate analysis (Table 43, page 82). Moreover, the analysis of the Affymetrix data supports a positive prognostic value of CXCR3 expression as well for OS as for DFS (p>0.001, Figure 14, page 82).

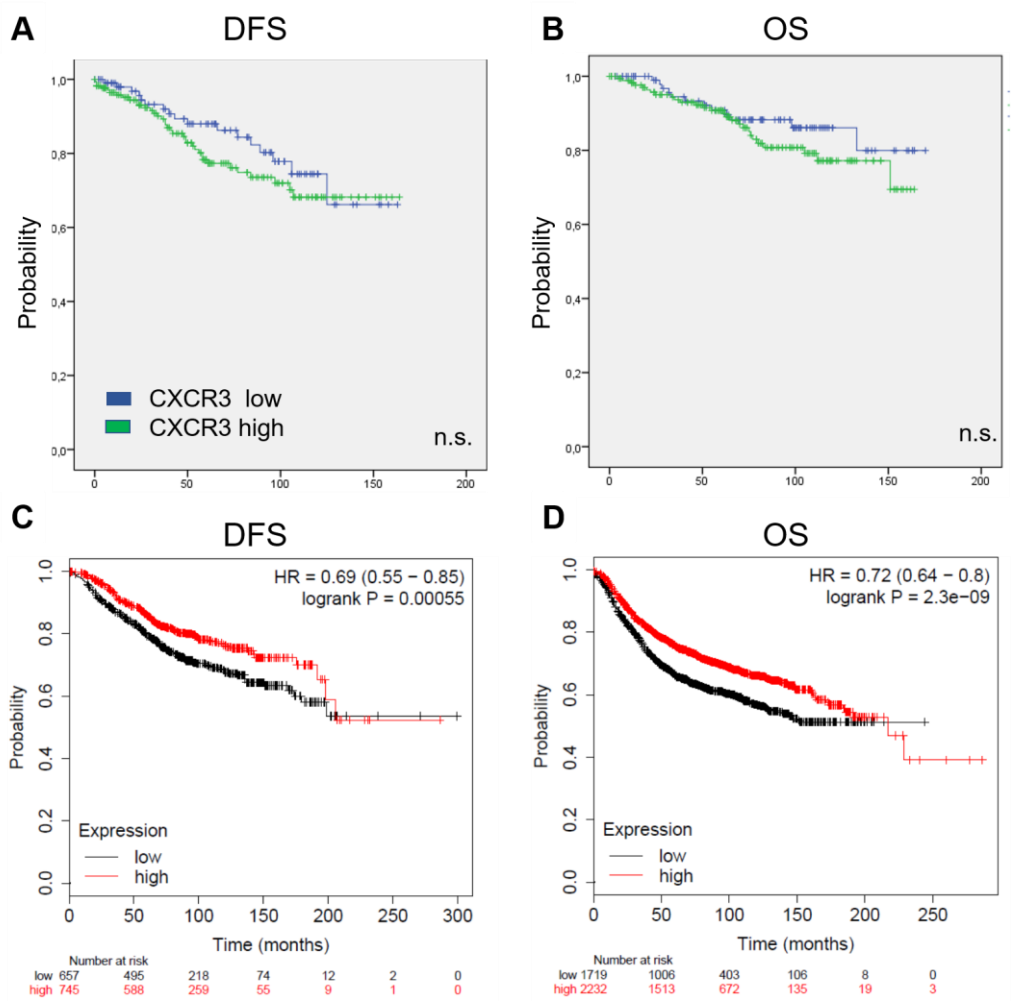

Figure 14: Association of CXCR3 expression in breast cancer specimens and patients' survival: Kaplan-Meier analysis of 287 breast cancer specimens stained for CXCR3 by immunohistochemistry showing (A) DFS p=0.264 and (B) OS p=0.263. Affymetrix based publicly available CXCR3 expression data correlated high expression of the receptor with better (C) OS (p=0.0005) and DFS ($p=2.3*10^{-9}$) in breast cancer patients.

Table 43: Univariate Cox regression analysis of the breast cancer cohort and CXCR3 expression.

	DFS		**OS**	
	p	HR	p	HR
tumor ≥20 mm	**0.019**	1775 (1.098 - 2.869)	**0.002**	2.578 (1.399 - 4.753)
age≥60 y	0.831	0.950 (0.593 - 1.521)	**0.083**	1.704 (0.933 - 3.112)
pT≥2	**0.00047**	1.568 (1.219 - 2.017)	**0.000011**	1.864 (1.412 - 2.461)
pN positive	**0.01**	1.374 (1.079 - 1.749)	**0.003**	1.524(1.154 - 2.014)
Grading≥3	0.125	1.341 (0.922 - 1.949)	**0.017**	1.78 (1.109 - 2.858)
TILs≥30%	0.89	0.953 (0.482 - 1.886)	0.931	0.960(0.376 - 2.447)
CXCR3 high	0.290	1.366 (0.767 - 2.432)	0.267	1.471(0.744 - 2.905)

12. CX3CL1 production is regulated by TNF-α stimulation and ADAM17 inhibition in human breast cancer cells *in vitro*

In order to investigate the role of CX3CL1 in human breast cancer, its expression and regulation were determined in three different HER2-positive human breast cancer cell lines (SKBR3, BT474, MDA-MB 453) and one low HER2-positive colon carcinoma cell line (HT29). The cells were stimulated *in vitro* with the inflammatory cytokine TNF-α (a known inducer of CX3CL1 in other cell types) as well as the ADAM17 inhibitor Tapi-2. Then, the CX3CL1 secretion of the soluble domain was measured via ELISA in the cell supernatants. CXCL10, a soluble chemokine, which is also induced by TNF-α, was measured in the cell supernatants as well to rule out unspecific effects. The membrane-bound compartment of CX3CL1 was determined by fluorescence-assisted cell sorting of living cells. Total protein concentration in the cells was measured by western blot, and membrane localization of CX3CL1 was also shown with immunofluorescence labeling of living cells (Figure 15, page 84).

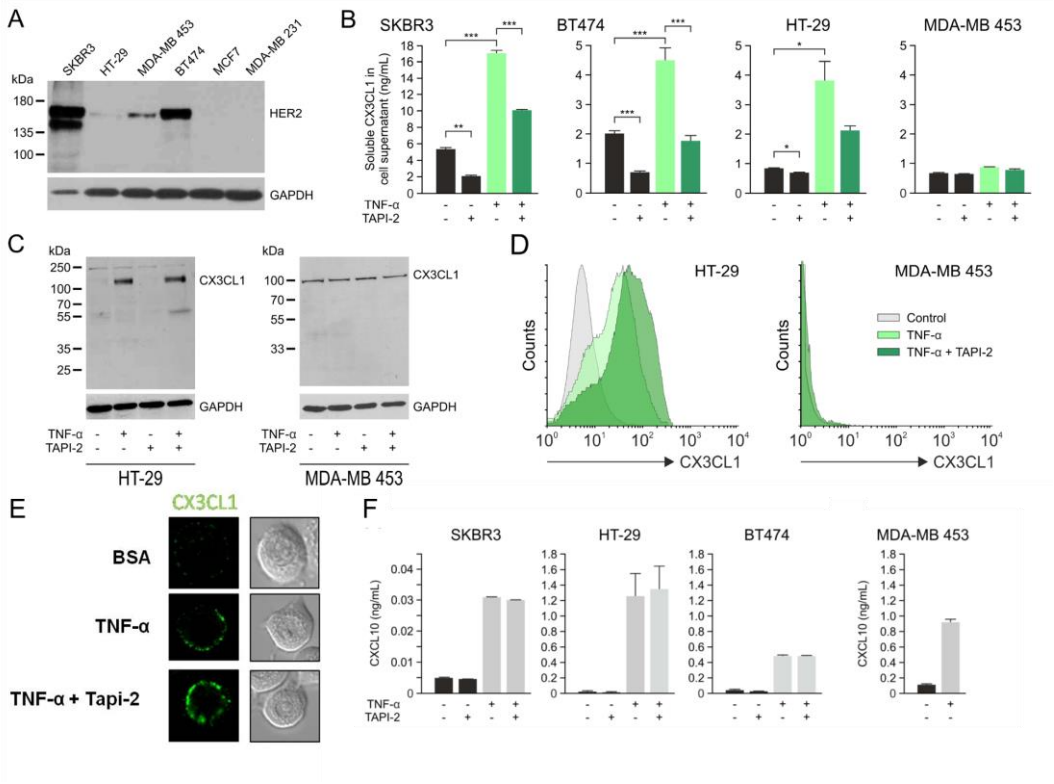

Figure 15: Regulation of CX3CL1 secretion and shedding in HER2-positive human breast cancer cell lines.

(A) HER2 expression in cell lines was confirmed by western blot. SKBR3, MDA-MB 453, and BT474 showed strong HER2 expression. HT29 cells had low HER2 expression. MCF7 and MDA-MB 231 served as negative controls. (B) Secretion of the soluble form of CX3CL1 is increased after treatment with the inflammatory cytokine TNF-α (10 ng/ml) in four human cancer cell lines SKBR3, BT474, MDA-MB 453 and HT29 measured by CX3CL1 ELISA of cell supernatant after 24 h (n=3). The shedding of soluble CX3CL1 could be decreased by the addition of ADAM17 inhibitor Tapi-2 (7.5 µM). (C) The regulation of CX3CL1 upon TNF-α and Tapi-2 treatment was assessed by western blot analysis in lysates of HT29 and MDA-MB 453 cells, GAPDH was used as the loading control. (D) The effects of shedding and stimulation on the membrane-bound CX3CL1 was shown with fluorescence assisted cell sorting (FACS) analysis of viable cells. (E) Localization of CX3CL1 in HT29 cells after TNF-α and Tapi-2 stimulation was visualized by immunofluorescence microscopy. (F) Functional response to TNF-α stimulation was shown by ELISA of CXCL10 in the corresponding cell supernatant (n=3) of HT29, SKBR3, BT474 and MDA-MB 453 cell lines, but this time Tapi-2 did not have any effect. *p < 0.05; **p < 0.005; ***p < 0.001.

All of the used cell lines (SKBR3, HT29, MDA-MB 453 and BT474) were tested for HER2 expression by western blot, including HER2 negative cell lines (MCF7 and MDA-MB 231) as controls (Figure 15A, page 84). The HER2 positive cell lines secreted CX3CL1 to various degrees, but SKBR3 and HT29 secreted significant amounts of chemokine without any

inflammatory stimulation. All of the cell lines but MDA-MB 453 showed increased CX3CL1 production upon stimulation with the inflammatory cytokine TNF-α. The amount of secreted CX3CL1 was significantly reduced by inhibition of ADAM17 by the Tapi-2 inhibitor (Figure 15B, page 84). ADAM17 inhibition did not affect CXCL10 release in the same cell lines, indicating a TNF-α independent effect on CX3CL1 secretion. The MDA-MB 453 cells lacking CX3CL1 secretion upon TNF-α stimulation also showed increased CXCL10 release under inflammatory cytokine treatment (Figure 15F, page 84).

Analysis of total protein using western blot showed no or weak bands for CX3CL1 in HT29. An induction was detected after stimulation with TNF-α (Figure 15C, page 84), as well as a prominent increase after ADAM17 inhibition. ADAM17 inhibition alone did not affect the whole-cell CX3CL1 expression in western blot analysis. In the MDA-MB 453 cell lysate western blots, constant bands for all stimuli were detected (Figure 15C, page 84). In line with these results, the quantification of the membrane-bound form of CX3CL1 with FACS analysis revealed a peak shift after TNF-α stimulation in HT29 cells, but not in MDA-MB 453 cells. This peak shift was further enhanced by ADAM17 inhibition in TNF-α stimulated HT29 cells (Figure 15D, page 84).

In addition, CX3CL1 was localized in the membrane as validated by confocal immunofluorescence microscopy of vital HT29 cells. The signal for CX3CL1 in the cell membrane increased after TNF-α stimulation and was further enhanced after the addition of ADAM17 inhibitor in HT29 cells (Figure 15E, page 84)

13. CX3CL1 is involved in TNF-α induced NK cell-mediated cell lysis of HER2-positive tumor cells

The effect of CX3CL1 on the specific NK cell-mediated cell lysis of different HER2-positive cancer cell lines (SKBR3, MDA-MB 453, BT474, and HT29) was measured using a europium release assay (EU assay). The cells were stimulated *in vitro* before the EU assay using TNF-α, ADAM17 inhibitor, and anti-CX3CL1 antibody (Figure 16). The observed effects remained stable throughout the different NK cell/tumor cell ratios. Therefore the focus for this work will be on the highest ratio of 1:10.

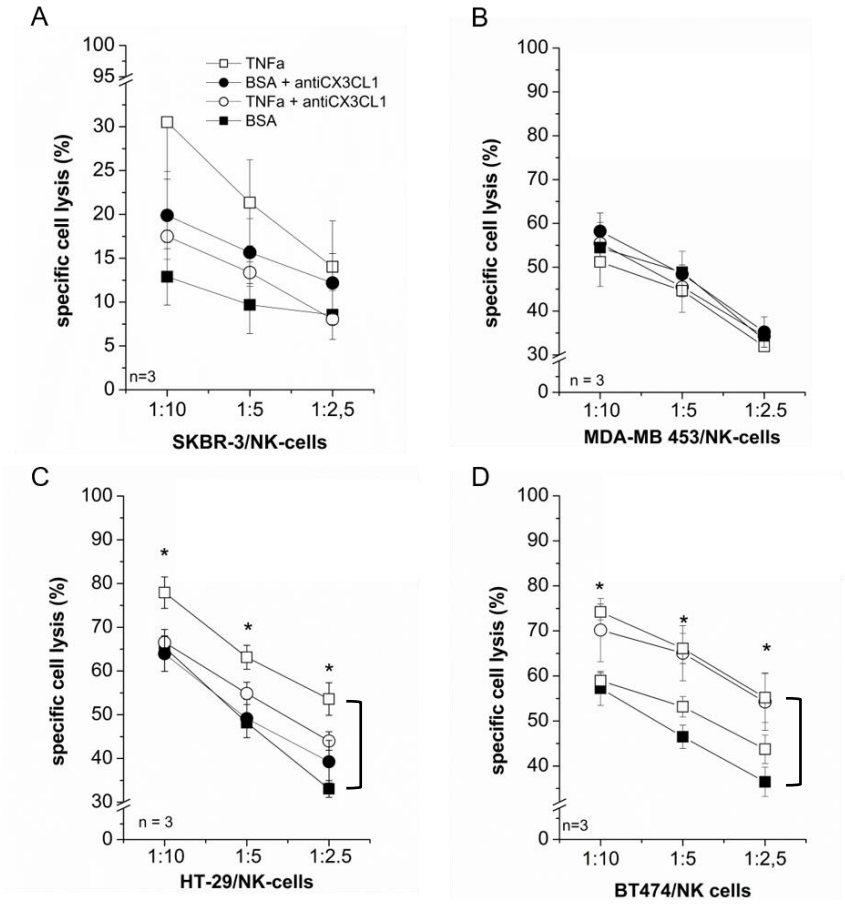

Figure 16: NK cell-mediated cell lysis of HER2-positive cancer cells can be increased by stimulation with TNF-α.

Europium-based cell lysis assay showed significantly increased NK cell-mediated cell lysis after treatment with TNF-α (10 ng/ml) in (A) SKBR3, (C) BT474 and (D) HT29 but not (B) MDA-MB 453 cells. The enhanced cell lysis was partially impaired by the addition of an anti-hCX3CL1 antibody in SKBR3 and HT29 cells but not in BT474 or MDA-MB 453

cells(n=3). *p < 0.05

The NK cell-mediated cell lysis of SKBR3 cells without any stimulation was at 12.9 ± 3.2%. This specific cell lysis was increased after the addition of TNF-α up to 30.5 ± 6.5% (p=0.015, Figure 16A, page 86). This increase in cell lysis was quenched after the addition of an anti-hCX3CL1 antibody. The effect was reduced to 17.4 ± 0.7% lysed cells (p=0.23). Antibody treatment without TNF-α stimulation increased the cell lysis to 19.9 ± 5.0% (p=0.23).

The cell lysis of MDA-MB 453 without further treatment was at 54.4 ± 4.0%. Neither TNF-α stimulation nor the anti-hCX3CL1 antibody affected the specific cell lysis of these cells (Figure 16B, page 86).

The blank NK cell-mediated cell lysis of both BT474 and HT29 cells was similar, with specific cell lysis of 57.2% ± 3.8% and 65.4 ± 2.7% (Figure 16C+D, page 86). The effect of TNF-α has significantly increased the specific cell lysis to 74.2 ± 1.7% and 78.0 ± 3.6%, respectively (p=0.004 and p=0.035). The addition of an anti-CX3CL1 antibody had no effect on the NK cell-dependent cell lysis with and without TNF-α stimulation in the BT474 cells but efficiently quenched the increased cell lysis in the HT29 cells (66.6 ± 2.9%, p=0.034). The anti CX3CL1 antibody alone did not have any effect on the NK-cell mediated cell lysis (Figure 16C+D, page 86).

14. ADAM17 inhibition increases the NK cell-mediated cell lysis *in vitro*

In order to estimate the effect of increased membrane-bound CX3CL1 on NK cell-mediated cell lysis, SKBR3, BT474, and HT29 cells treated with ADAM17 inhibitor (Tapi-2) and anti-hCX3CL1 antibody were analyzed using the europium assay (Figure 17, page 88).

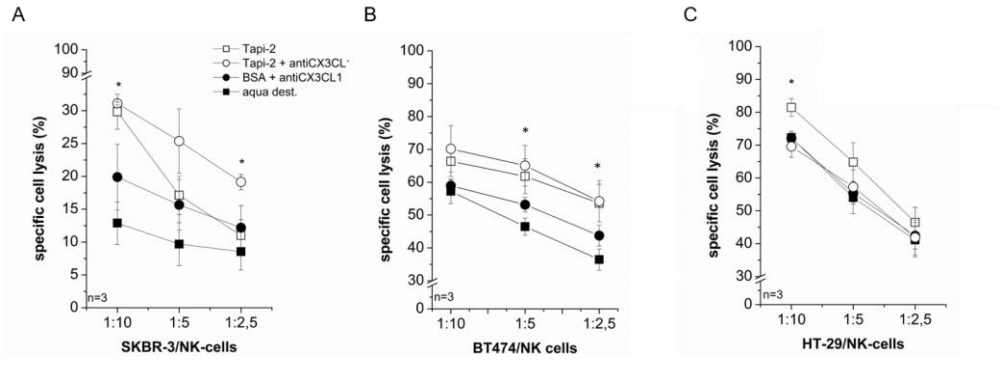

Figure 17: ADAM17 inhibition increases the NK cell-mediated cell lysis of HER2-positive human cancer cells *in vitro*.

The NK cell-mediated cell lysis was measured with a europium-based lysis assay (n=3). The inhibition of ADAM17 (Tapi-2) significantly increased the tumor cell lysis in (A) SKBR3, (B) BT474, and (C) HT29 cells compared to control (aqua dest.).The addition of an anti-hCX3CL1 antibody impaired the Tapi-2-induced cell lysis in SKBR3 and HT29 but not in BT474 cells compared to an isotype control (IgG).*$p<0.05$

The NK cell-mediated lysis of SKBR3 cells was 12.9 ± 3.3% with BSA treatment only. The inhibition of ADAM17 via Tapi-2 increased this effect to 31.1 ± 0.2% ($p=0.001$). Interestingly, the addition of an anti-CX3CL1 antibody did not show any alteration of the lysis capacity at a ratio of 1:10, but in the lower ratio of 1:2.5, the antibody was able to impair the Tapi-2 induced lysis increase back to the amount of BSA-treated samples (19.9% ± 5.0%, $p=0.08$, Figure 17A).

The positive effect of ADAM17 inhibition was also shown in BT474 cells.

The cell lysis was increased by more than 9% from 57.0 ± 3.7% to 66.4 ± 4.6% after the addition of Tapi-2 (p=0.012 for ratios 1:5 and 1:2.5, Figure 17B, page 88). An anti-hCX3CL1 antibody alone did not affect cell lysis in BT474 cells (58.0 ± 1.8%).

HT29 cells showed a target/ratio-dependent cell lysis without any stimulation of 72.3 ± 1.4%. An increase of 9% was detected after inhibition of ADAM17 (81.5% ± 2.7%; p=0.008). This effect was recovered after the addition of an anti-hCX3CL1 (69.6 ± 3.3%; p=0.013). The antibody alone did not affect the specific cell lysis of the HT29 cells (72.1 ± 2.1%, Figure 17C, page 88).

15. CX3CL1 increases the efficiency of trastuzumab therapy in vitro

In order to evaluate the impact of *CX3CL1* overexpression on the efficacy of an anti-HER2-treatment with the monoclonal trastuzumab antibody, SKBR3, HT29, and MDA-MB 453 cells were transiently transfected with *CX3CL1* or a control vector and treated with trastuzumab afterwards.

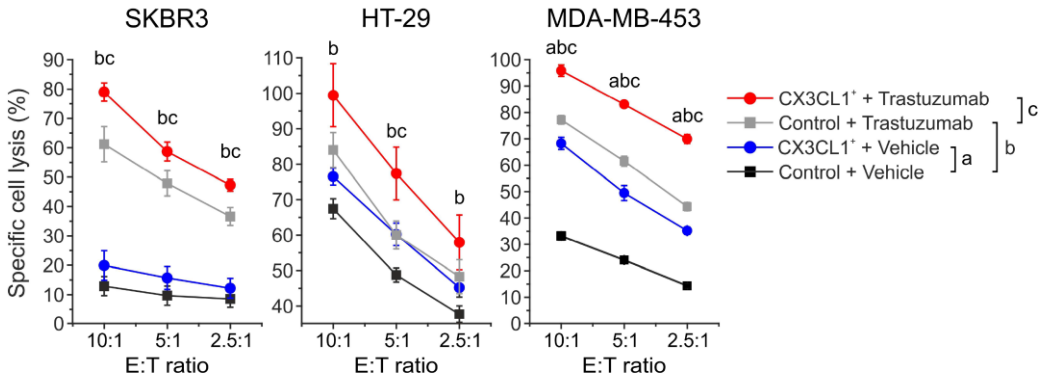

Figure 18: CX3CL1 enhances the efficacy of trastuzumab anti-HER2-therapy *in vitro*.

Europium-based cell lysis assay detected increased cell lysis for hCX3CL1-overexpressing SKBR3, HT29, and MDA-MB 453 cells ($CX3CL1^+$) and trastuzumab-treated cells (control + trastuzumab). These effects were additive for combined experiments ($CX3CL1^+$ + trastuzumab) compared to control cells (control + vehicle, n=3). Lower cases indicate statistical significance ($p<0.05$).

The specific lysis of SKBR3 cells without treatment was at 11.9 ± 3.0% ($p<0.001$). *CX3CL1* transfection alone was sufficient to increase the NK-cell efficiency to 19.9 ± 5.5%, although the effect was not significant ($p=0.23$). The treatment with trastuzumab enhanced the ADCC to a total of 61.2 ± 18.0% ($p<0.001$). A combined application of transient *CX3CL1* transfection and trastuzumab treatment could further improve the NK-cell mediated cell lysis to a total of 79.0 ± 3.1%, providing an additional 18% cytolytic capacity ($p<0.001$, Figure 18).

Similar effects were detected for the other cell lines. HT29 cells treated with lipofectin only showed an NK cell-specific cell lysis of 67.4 ± 2.8%. The cell lysis was significantly increased by either CX3CL1 overexpression or trastuzumab treatment to 76.4 ± 2.4% or 84.0 ± 4.9% (p=0.018 and p=0.036, respectively, Figure 18, page 90). Combined treatment significantly increased the cell lysis to 99.5 ± 8.9% compared to single treatment with trastuzumab or CX3CL1 overexpression (p=0.14 and p=0.002, Figure 18, page 90).

The most substantial effects were detected in the MDA-MB 453 cell line. The baseline cell lysis after BSA treatment was at 33.2 ± 1.6%. Both transient *CX3CL1* transfection or trastuzumab treatment increased the cell lysis (trastuzumab: 77.2 ± 1.6%; CX3CL1: 68.3 ± 2.3%, p<0.001 Figure 18, page 90). Joined treatment raised the NK cell-mediated cell lysis to 99,4 ± 8.9%, p>0.001.

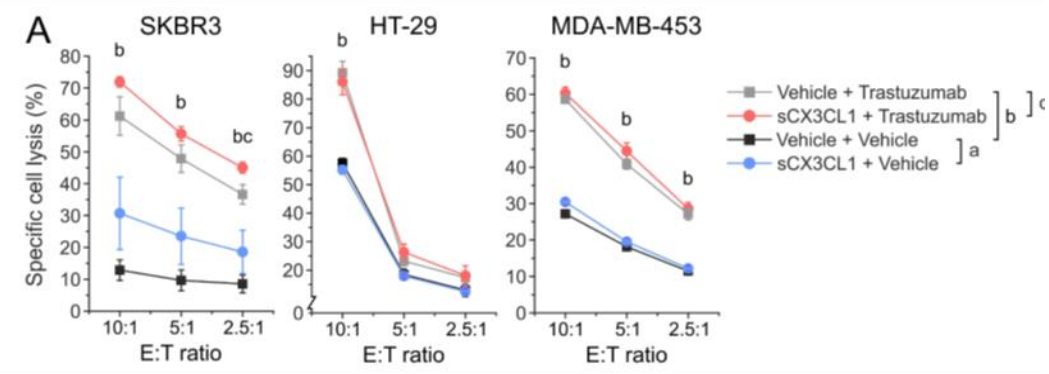

Figure 19: Soluble CX3CL1 does not increase the NK cell-mediated cell lysis.SKBR3, HT29, and MDA-MB 453 cells were treated with soluble CX3CL1 (100ng/ml) and trastuzumab antibody (40 µg/ml). Trastuzumab alone increased the NK-cell mediated cell lysis, but the addition of soluble CX3CL1 is not sufficient to further improve the trastuzumab effect. Lower cases indicate statistical significance. Data are presented as mean ± SEM, n=3.

Since the differential effect of the soluble and the membrane-bound form of

CX3CL1 is still unclear, the next experiment was set to investigate the distinct role of the soluble CX3CL1 in the mediation of increased ADCC upon addition of trastuzumab (Figure 19, page 91). The baseline cell lysis in this experimental setup was comparable to the stably transfected cell lines (13.0 ± 3.2% for SKBR3, 57.6 ± 1.1% for HT29, and 27.1 ± 0.9% for MDA-MB 453 at the 1:10 ratio). There was a significant effect of trastuzumab addition, which increased the NK-cell-mediated cell lysis to 61.2 ± 5.9%, 89.2 ± 4.0%, and 58.6 ± 0.8%, respectively (for all cases $p<0.001$ at the ratio 1:10, Figure 19, page 91). The combined treatment with trastuzumab and soluble CX3CL1 could not enhance the antibody effect in the HT29 and MDA-MB 453 cell lines (86.0 ± 7.8%; 60.3 ± 1.7%). Though there was an accumulating positive effect of the combined treatment in the SKBR3 cells (61.2 ± 5.9% trastuzumab vs. 71.9 ± 1.6% trastuzumab + soluble CX3CL1), however, this effect reached significance only at the lowest target/effector ratio of 1:2.5 (trastuzumab 36.6% vs. trastuzumab + soluble CX3CL1 45.0%, $p=0.03$, Figure 19, page 91).

16. *Cx3cl1* overexpression enhances anti-tumor response and promotes tumor-suppressive lymphocyte migration *in vivo*

Murine triple-negative 4T1 breast cancer cells were stably transfected with a murine *CX3CL1* (*Cx3cl1*)-overexpressing vector (pCMV6-Cx3cl1) or with empty control vector (pCMV6-Entry). The effects of *Cx3cl1* overexpression on tumor growth and lung metastasis were assessed, and effects on the lymphocyte influx into the tumor were quantified (Figure 20, page 93).

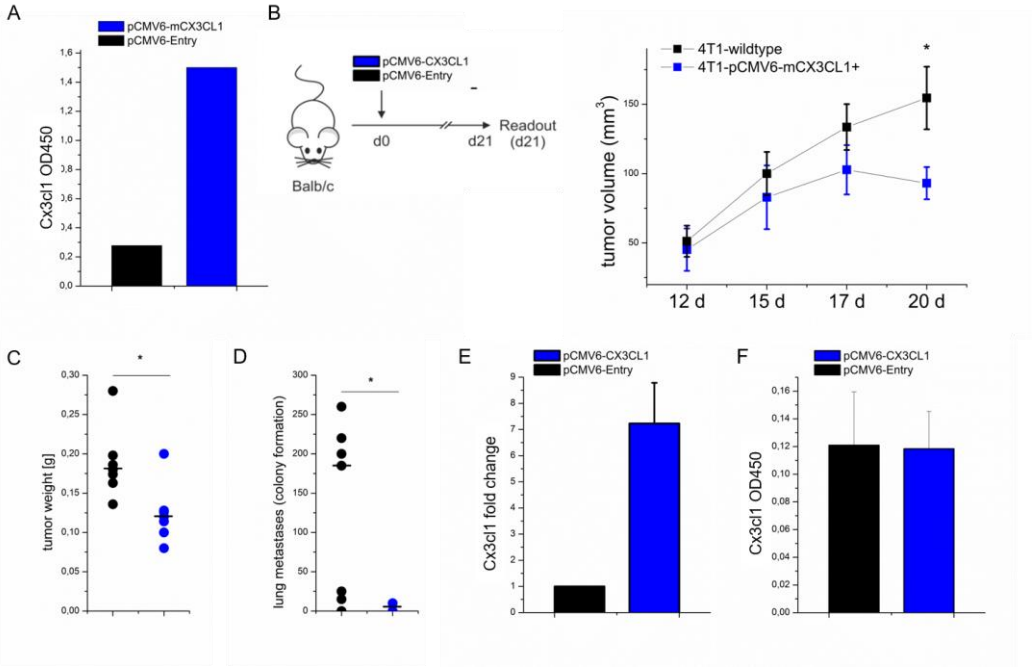

Figure 20: Murine CX3CL1 (Cx3cl1) promotes tumor-suppressive effects *in vivo*.

(A) Verification of transfection efficiency via ELISA showed that a *Cx3cl1* high expressing clone (pCMV6-Cx3cl1) was selected for *in vivo* experiments. (B) Eight weeks old female Balb/c mice were inoculated subcutaneously (s.c.) with 10^4 *Cx3cl1*-overexpressing 4T1 cells (4T1-pCMV6-Cx3cl1) or empty control vector cells (4T1-pCMV6-Entry, n=7). Tumor growth was significantly reduced in mice bearing *Cx3cl1*-overexpressing tumors compared to empty vector controls. (C) The tumor-suppressive effect was significant in total tumor mass of *Cx3cl1*-overexpressing mice compared to controls at the end of the experiment on day 21. (D) Formation of lung metastases was significantly decreased in mice bearing *Cx3c1*-overexpressing tumors compared to the control group. (E) Intratumoral *Cx3cl1* expression remained elevated during the experiment, as shown by RT-qPCR analysis of tumor tissue after 21 days (n=7). (F) Measured Cx3cl1 concentrations in murine plasma with ELISA showed no difference between *Cx3cl1*-overexpressing mice and the control group (n=7). *p<0.05.

Highly *Cx3cl1*-overexpressing clones were selected for *in vivo* experiments. The expression of *Cx3cl1* in overexpressing 4T1 cells was sevenfold higher than in empty vector control cells (Figure 19A, page 91). A difference in tumor volume was detected after 15 days with a mean tumor volume of 82 ± 22.9 mm^3 in mice bearing *Cx3cl1*-overexpressing tumors and 100 ± 15.6 mm^3 in the control group (Figure 19B, page 91). After 17 days, the mean tumor volume for the Cx3cl1 group was at 102 ± 17 mm^3 vs. 133 ± 16.5 mm^3 in the control group. Twenty days after tumor inoculation, mice bearing a *Cx3cl1*-overexpressing tumor showed a mean tumor volume of 93 ± 11.6 mm^3 compared to the control group with a mean tumor volume of 154 ± 22.6 mm^3 (p=0.049, Figure 19B, page 91). Total tumor weight was also significantly lower in the $Cx3cl1^+$ tumor-bearing group (0.124 ± 0.045 g) compared to the control group (0.181 ± 0.042 g; p=0.019, Figure 19C, page 91). The quantification of metastases in the lungs (4T1 colony formation assay) revealed a significantly reduced median colony count for *Cx3cl1*-overexpressing tumors compared to the control group (0 vs. 185; p=0.01, Figure 19D, page 91). After 21 days, there was still a sevenfold higher *Cx3cl1* mRNA expression detectable in the *Cx3cl1*-transfected tumors as compared to the control ones (p<0.001, Figure 19E, page 91), demonstrating the constant upregulation of Cx3cl1 in the transfected tumors during the whole *in vivo* experiment. However, this did not translate into elevated Cx3cl1 plasma levels of the mice at 21 days (Figure 19F, page 91).

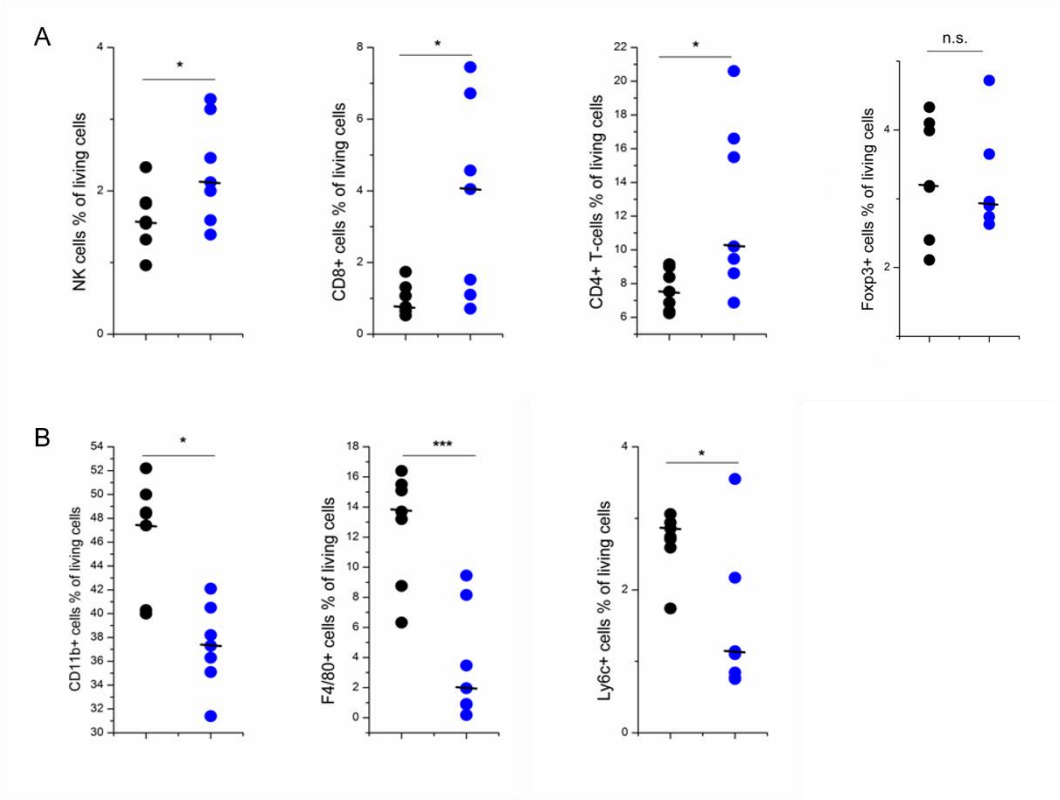

Figure 21: *Cx3cl1* overexpression modulates tumor immune infiltration *in vivo*.

(A) Increased populations of NK cells, $CD4^+$ T cells and $CD8^+$ T cells were detected in *Cx3cl1*-overexpressing tumors compared to the control group. There was no difference in the prevalence of $Foxp3^+$ T cells detected (n=7). (B) Analysis of myeloid cell populations showed decreased numbers of $CD11b^+$, $F4/80^+$ and $Ly6c^+$ cells in tumors of *Cx3cl1*-overexpressing mice compared to the control group (n=7). * $p<0.05$; ***$p< 0.001$.

The evaluation of different immune cell markers with FACS analysis showed significant changes in the immune milieu between *Cx3cl1*-overexpressing and control tumors. The influx of NK cells (0.41% vs. 0.94%, p=0.025), $CD8^+$ T cells (0.20% vs. 1.19%, p=0.02) and $CD4^+$ T-cells (1.95% vs. 3.39%, p=0.027) was increased, whereas no changes of $Foxp3^+$ T cells were detected (0.82% vs. 0.96%, p=0.8, Figure 21A, page 95). The analysis of myeloid cell populations also revealed major changes. There were decreased populations of $CD11b^+$ cells (47.5% vs. 37.8%, p=0.0012), $F4/80^+$ cells (13.9% vs. 2.1%, p=0.00066), and $Ly6c^+$ cells (2.9% vs. 1.2%, p=0.04, Figure 21B, page 95). The determination of immune cell

populations in the spleen showed no differences in any of the analyzed markers (data not shown).

17. CX3CL1 compensates for NK-cell depletion in a HER2-overexpressing xenograft model *in vivo*

The overexpression of *Cx3cl1* revealed a protective function in the syngeneic 4T1 mouse model, and the increased NK cell infiltration raised the possibility that Cx3cl1 might enhance the NK-cell dependent efficacy of an anti-HER2 treatment with trastuzumab, which was shown before *in vitro* (chapter 15). In the following experiment, the interaction of CX3CL1 and trastuzumab therapy should be evaluated in a HER2 highly expressing breast cancer xenograft model (Figure 22).

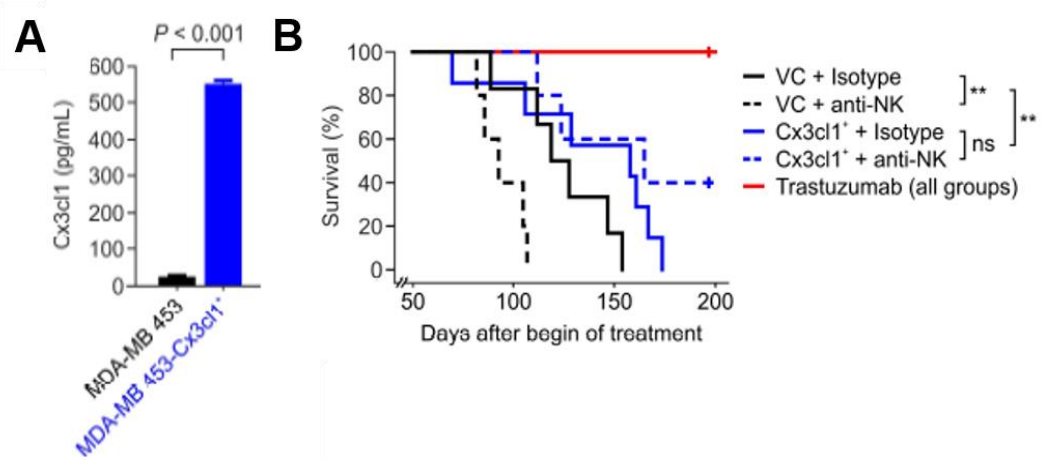

Figure 22: Cx3cl1 promotes tumor suppressive effects and compensates for NK cell depletion. (A) Efficient *Cx3cl1* transfection of MDA-MB 453 cells was verified with ELISA of cell culture supernatants (n=2). (B) Kaplan Meier survival analysis of Balb/c SCID mice inoculated with *Cx3cl1* expressing or empty vector control MDA-MB 453 cells. Mice were additionally treated with trastuzumab and/or NK cell depleting antibody GM-1 (n=7 per group). **p<0.01; ns=not significant.

The HER2 positive human breast cancer cell line MDA-MB 453 was stably transfected with a *Cx3cl1* plasmid (Figure 22A, page 96). Afterwards, the *Cx3cl1* overexpressing and empty vector control cells were inoculated in

Balb/c SCID mice. The animals were then randomized into eight groups, receiving trastuzumab or vehicle control treatment, and NK cell depletion by an anti-asialo GM1 antibody or a respective IgG control antibody.

The treatment was started after a tumor diameter of 0.5 cm had been reached. In this model, however, already small amounts of trastuzumab induced efficient tumor eradication after the first dose of antibody; thus, no further effects of *Cx3cl1* expression or NK cell depletion on tumor growth and survival could be observed. In the trastuzumab non-treated groups *Cx3cl1* overexpression prolonged survival of the animals compared to the not transfected control group (158 vs. 107 days, p=0.003, Figure 22B, page 96), although the initial tumor growth was slightly in favor of the Cx3cl1 group (time to therapy start 34 vs. 41 days; p=0.14). The depletion of NK cells reduced the survival of non-Cx3cl1 tumor-bearing mice (median survival 93 vs. 199 days; p= 0.009). These findings are in line with the as well accelerated tumor growth. The NK cell depletion in the *Cx3cl1* overexpressing group did not induce substantial survival differences (median survival 165 vs. 158 days, p=0.23, Figure 22B, page 96), indicating that the chemokine expression might compensate for the reduction in NK cell function.

18. *CX3CL1* overexpression impairs tumor growth and enables trastuzumab therapy in a low HER2-positive xenograft model *in vivo*

Human low HER2-positive colon cancer cells (HT29) were stably transfected with *Cx3cl1*-overexpressing vector (pCMV6-Cx3cl1) or empty control vector (pCMV6-Entry). $2*10^6$ cells were injected into the 4^{th} fat pad of 8 weeks old female Balb/c SCID mice, and mice were randomized into two groups (trastuzumab treatment or vehicle control treatment). After the tumor diameter reached 0.5 cm, the mice were treated with trastuzumab 5 mg/kg/day twice a week by intraperitoneal injection (Figure 23).

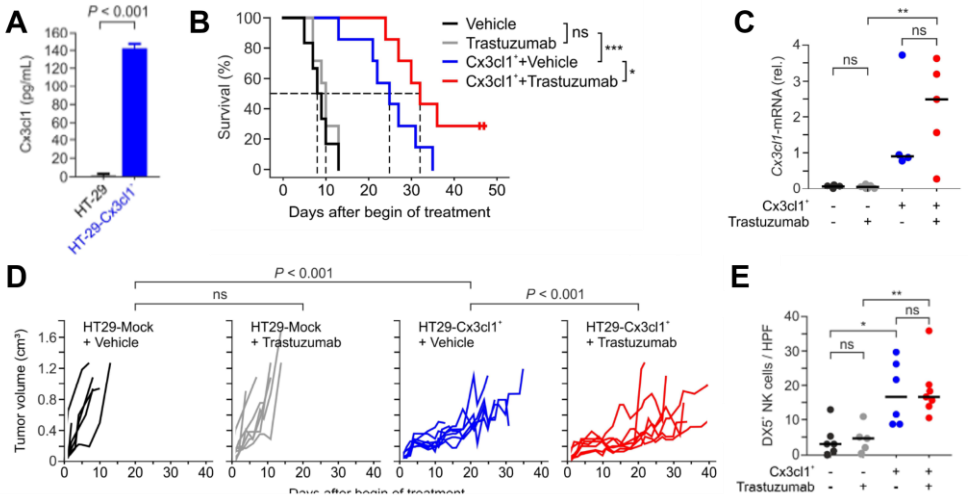

Figure 23: *Cx3cl1* overexpression promotes tumor-suppressive effects and enhances trastuzumab therapy *in vivo*.

$2*10^6$ human colon cancer cells (HT29) stably transfected with *Cx3cl1*-overexpressing vector (pCMV6-Cx3cl1) or empty vector control (pCMV6-Entry) were injected subcutaneously in the fat pad of female Balb/c SCID mice (n=7 per group). After a tumor diameter of 0.5 cm was reached, mice of each group were randomized and treated with trastuzumab (pCMV6-Entry + trastuzumab) or equivalent volumes of water (n=7). (A) ELISA readout of the efficient *Cx3cl1* transfection in HT29 cells (n=2). (B) Kaplan Meier analysis of HT29 inoculated Balb/c SCID mice. (C) Quantification of *Cx3cl1* mRNA expression in HT29 tumors, after completion of the experiment. (D) Tumor growth curves of the four groups (n=7). (E) Immunohistochemical determination of infiltrating $DX5^+$ NK cells into FFPE tumor tissue (n=7). *p < 0.05; ** p < 0.01; ***p < 0.001; ns=not significant.

The increased expression of *Cx3cl1* led to a threefold prolonged median

survival (25 vs. 8 days, p<0.001, Figure 23B, page 98). More importantly, mice bearing the HT29 control tumors did not respond to trastuzumab therapy in terms of survival (8 vs. 10 days, p=0.43). This therapy resistance was reversed in the *Cx3cl1* transfected tumor-group. Here the overall survival was increased from 25 to 32 days by the trastuzumab treatment (p=0.04, Figure 23B, page 98). Two out of seven tumor-bearing animals never reached any vital stop criteria, and the experiment was terminated after 50 days (Figure 23B, page 98). The expression of *Cx3cl1* in the transfected tumors was solidly detectable after dissection of the tumor tissue (Figure 23C, page 98). Trastuzumab treatment had no impact on Cx3cl1 mRNA transcription (Figure 23C, page 98). In this HER2 low-expressing xenograft model, the overexpression of *Cx3cl1* was sufficient to reduce tumor growth compared to the control group (Figure 23D, page 98). Tumor onset (9 vs. 12 days; p=0.0001) and time till therapy was started at a tumor size of 0.5 cm (12 vs. 15 days; p=0.03) were slowed down in the *Cx3cl1* overexpressing group.

Moreover, the determination of tumor-infiltrating NK cells via IHC revealed an about 5 fold increased influx of NK cells in the Cx3cl1 transfected HT29 tumors after the finalization of the *in vivo* experiment (Figure 23E, page 98).

19. Differential expression of *CX3CL1* in human breast cancer

The expression pattern of CX3CL1 was analyzed via immunohistochemistry (IHC) in 260 tissue samples of breast cancer patients (Table 5, page 24).

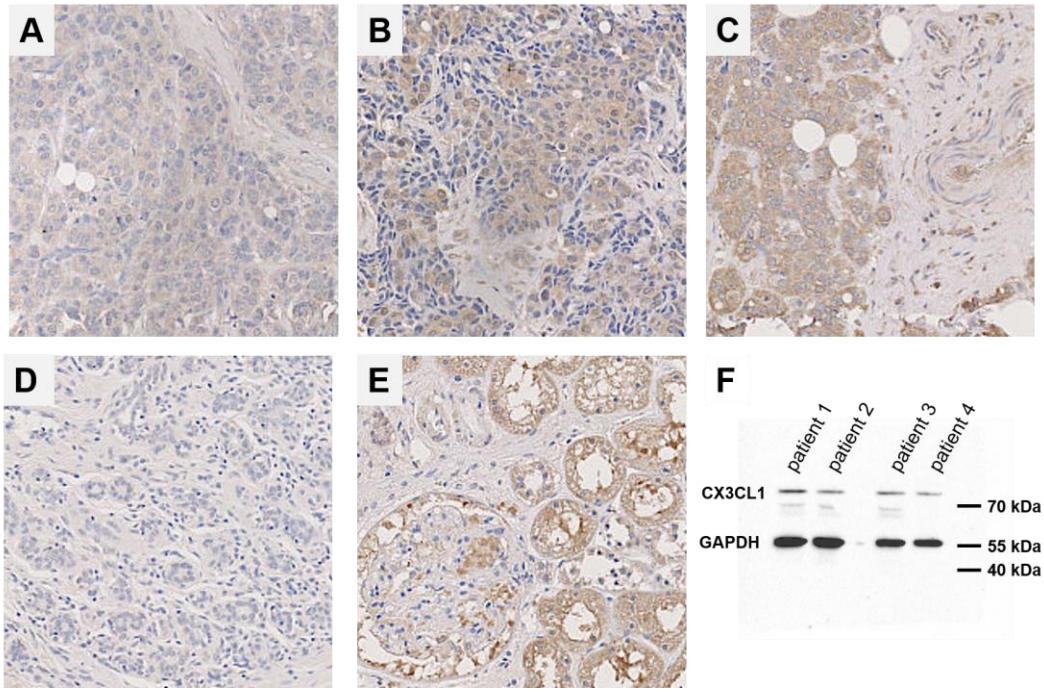

Figure 24: Immunohistochemical analysis of CX3CL1 in human breast cancer tissue.

Scoring intensities of CX3CL1 in IHC showed (A) low +1, (B) moderate +2, and (C) high +3 expression in mamma carcinoma tissue (n=260). (D) Negative control without primary antibody showed no background signals. (E) Kidney samples were used as a positive control. (F) The specificity of the anti-CX3CL1 antibody was further validated in western blot analysis of human breast cancer samples (n=4), GAPDH was used as a loading control.

The protein detection of CX3CL1 was located in tumor cells and endothelial cells. Surrounding tissue, and tumor stroma remained unstained in all samples (Figure 24A-D). A control sample without primary antibody showed no significant background signal, and positive detection in the kidney revealed clear *CX3CL1* expression in tubular structures but not in glomeruli, pericytes, or stromal tissue (Figure 24D+E). The samples were categorized

into low *CX3CL1* expression (scores 0 and +1) and high *CX3CL1* expression (scores +2 and +3). For the evaluation, only tumor cell expression was taken into account. Antibody specificity was further validated by western blot analysis of breast cancer tissue showing a distinct band at 90 kDa in each sample (Figure 24F, page 100).

Among the 260 breast cancer patients, 39% showed low CX3CL1 expression, and 61% showed moderate to high expression (Table 44, page 102). A subgroup analysis of the signal intensity was conducted based on the expression of HER2, progesterone receptor, and estrogen receptor. 92% of HER2-overexpressing tumors showed a high expression for CX3CL1, indicating an association of both factors (p=0.0001, Table 44, page 102). The opposite effect was detectable for TNBC cases, here 73% were determined for low *CX3CL1* expression (p<0.001, Table 44, page 102)

Table 44: Distribution of CX3CL1 IHC score in a cohort of 260 breast cancer patients.

Relative distribution among breast cancer subgroups, divided into HER2 receptor (HER2), hormone receptor (HR), and triple-negative breast cancer (TNBC). Scores of 0 and 1+ were displayed as low, and scores of 2+ and 3+ were displayed as high. High *CX3CL1* expression in the respective subgroups is indicated in bold.

CX3CL1			
scoring	percentage		
low	39%		
high	61%		
HER2		**CX3CL1 high**	**CX3CL1 low**
positive	24	22	2
negative	236	137	99
Chi-Quadrat	**0.001**		
HR		**CX3CL1 high**	**CX3CL1 low**
positive	210	130	80
negative	50	29	21
Chi-Quadrat	0.611		
TNBC		**CX3CL1 high**	**CX3CL1 low**
yes	26	7	19
no	234	152	82
Chi-Quadrat	**0.001**		

The Kaplan-Meier analysis of this cohort in terms of *CX3CL1* expression showed, among patients being positive for CX3CL1, a correlation of higher CX3CL1 scores with better DFS (p=0.043) and OS (p=ns) in a concentration-dependent manner (ranging from scores +1 to +3, Figure 25A+B, page 103). The analysis of publicly available Affymetrix data confirmed this observation in the IHC, providing substantial evidence that high CX3CL1 expression is associated with better DFS (p<0.001) and OS (p=0.015) in breast cancer patients (Figure 25C+D, page 103). The significant association for the immunohistochemical analysis can not be validated in the univariate Cox regression analysis (Table 45, page 103).

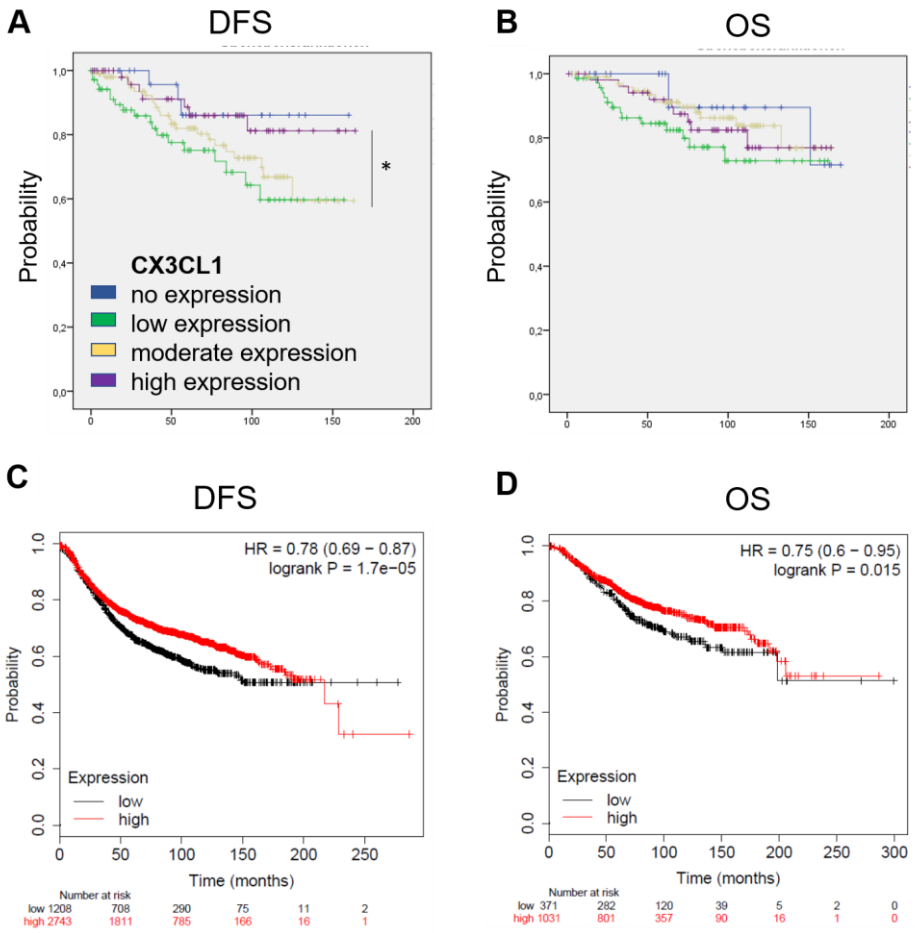

Figure 25: Association of CX3CL1 expression in breast cancer specimens and patients' survival. Kaplan-Meier analysis of 260 breast cancer specimens stained for CX3CL1 by immunohistochemistry showing (A) a correlation with good DFS among CX3CL1 positive cases p=0.041 but not for (B) OS (p=0.29). Affymetrix based public available CXCR3 expression data correlated high expression of the receptor with better (C) DFS ($p=1.7*10^{-5}$) and (D) OS (p=0.015) in breast cancer patients.

Table 45: univariate Cox regression analysis of the breast cancer cohort and *CX3CL1* expression.

	DFS		**OS**	
	p	HR	p	HR
tumor≥20 mm	**0.019**	1775 (1.098 - 2.869)	**0.002**	2.578 (1.399 - 4.753)
age≥60 y	0.831	0.950 (0.593 - 1.521)	**0.083**	1.704 (0.933 - 3.112)
pT≥2	**0.00047**	1.568 (1.219 - 2.017)	**0.000011**	1.864 (1.412 - 2.461)
pN positive	**0.01**	1.374 (1.079 - 1.749)	**0.003**	1.524(1.154 - 2.014)
Grading≥3	0.125	1.341 (0.922 - 1.949)	**0.017**	1.78 (1.109 - 2.858)
TILs≥30%	0.89	0.953 (0.482 - 1.886)	0.931	0.960(0.376 - 2.447)
CX3CL1 high	0.395	0.785 (0.449 - 1.372)	0.296	0.731 (0.378 - 1.344)

20. Expression of *CX3CR1* in human breast cancer

346 breast cancer cases (Table 5, page 24) were analyzed for CX3CR1, and differential signal intensity was detected throughout the samples. The signal distribution was limited to tumor cells, and the staining was located

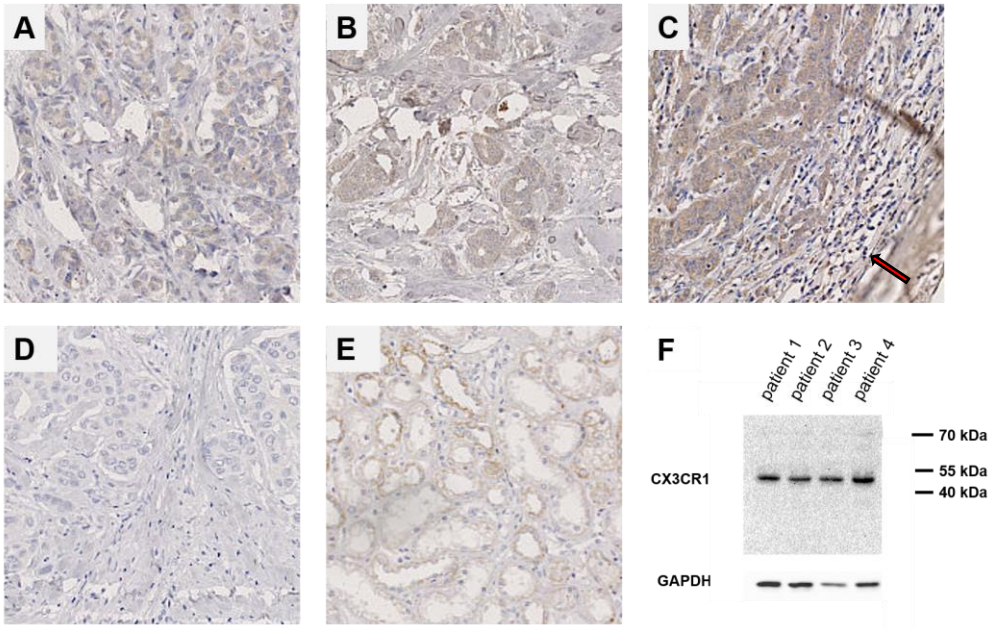

Figure 26: Immunohistochemistry (IHC) analysis of CX3CR1 in breast cancer tissue.

Scoring intensities of CX3CR1 in IHC showed (A) low 1+, (B) moderate 2+, and (C) high 3+ expression in breast cancer tissue (n=346). (D) Negative control without primary antibody showed no background signal. (E) Kidney samples were used as a positive control. (F) Specificity of the anti-hCX3CR1 antibody was shown in western blot analysis of human breast cancer samples (n=4), GAPDH was used as a loading control. Red arrow indicates area of immune cell staining.

cytoplasmically as well as membrane-bound (Figure 26). Other cells in the tumor microenvironment, including stroma, fatty tissue, and endothelial cells, remained signal-free (Figure 26A-C). Nevertheless, in some cases, robust detection of lymphocytes in the tumor-surrounding stroma was observed (Figure 26C, red arrow). The samples were categorized into low *CX3CR1* expression (scores 0 and +1) and high *CX3CR1* expression

(scores +2 and +3). Antibody specificity was evaluated by western blot analysis of breast cancer tissue showing single bands at 50 kDa for each patient (Figure 26F, page 104).

Among 346 breast cancer samples, 80% showed a weak signal for CX3CR1, and 20% were moderate to high. There was no significant association of *CX3CR1* expression and the subtype classification of breast cancer cases (Table 46).

Table 46: Distribution of tumor cell CX3CR1 IHC score in a cohort of 346 breast cancer patients:

Relative distribution among breast cancer subgroups, divided into HER2 receptor (HER2), hormone receptor (HR), and triple-negative breast cancer (TNBC). Scores of 0 and 1+ were displayed as low, and scores of 2+ and 3+ were displayed as high. High *CX3CR1* expression in the respective subgroups is indicated in bold.

scoring	percentage		
low	80%		
high	20%		
HER2		**CX3CR1 high**	**CX3CR1 low**
positive	36	4	32
negative	310	65	245
Chi-Quadrat	0.161		
HR		**CX3CR1 high**	**CX3CR1 low**
positive	283	59	224
negative	63	10	53
Chi-Quadrat	0.371		
TNBC		**CX3CR1 high**	**CX3CR1 low**
yes	27	6	21
no	319	63	265
Chi-Quadrat	0.757		

The analysis of an association between *CX3CR1* expression and survival by Kaplan-Meier log-rank test showed no correlation of this receptor expression on tumor cells with neither DFS (p=0.277) nor OS (p=0.906) in the immunohistochemistry data (Figure 27A+B, page 106). However, there was a strong association found in the Affymetrix data. Here *CX3CR1*

expression is a favorable prognostic factor both for DFS and OS (p<0.001, Figure 27C+D, page 106). Matching to the Kaplan-Meier curves, there was no prognostic value of CX3CR1 protein levels in univariate Cox regression analysis (Table 47, page 107).

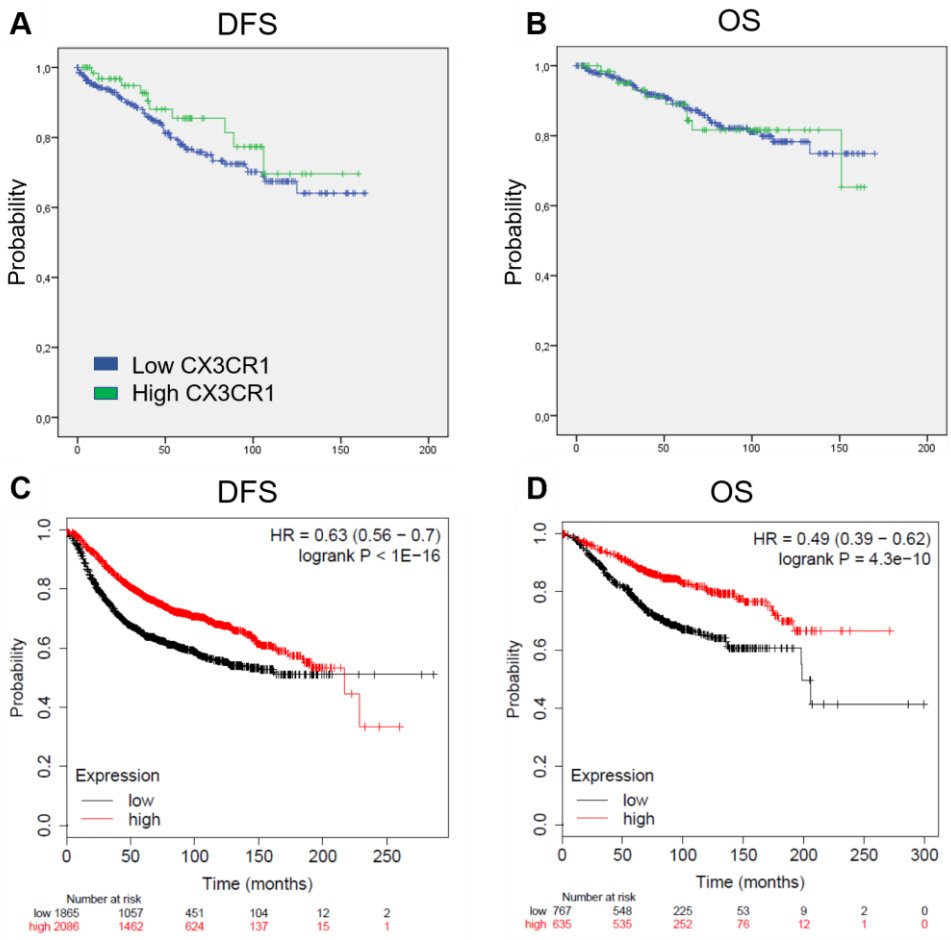

Figure 27: Association of *CX3CR1* expression in breast cancer specimens and patients' survival. Kaplan-Meier analysis of 346 breast cancer specimens stained for CX3CR1 by immunohistochemistry revealed no association with (A) DFS or (B) OS. Affymetrix based public available *CX3CR1* expression data correlated high expression of the receptor with better (C) DFS (p<0.001) and (D) OS (p<0.001) in breast cancer patients.

Table 47: Univariate Cox regression analysis of the breast cancer cohort and *CX3CR1* expression.

	DFS		**OS**	
	p	HR	p	HR
tumor≥20 mm	**0.019**	1775 (1.098 - 2.869)	**0.002**	2.578 (1.399 - 4.753)
age≥60 y	0.831	0.950 (0.593 - 1.521)	**0.083**	1.704 (0.933 - 3.112)
pT≥2	**0.00047**	1.568 (1.219 - 2.017)	**0.000011**	1.864 (1.412 - 2.461)
pN positive	**0.01**	1.374 (1.079 - 1.749)	**0.003**	1.524(1.154 - 2.014)
Grading≥3	0.125	1.341 (0.922 - 1.949)	**0.017**	1.78 (1.109 - 2.858)
TILs≥30%	0.89	0.953 (0.482 - 1.886)	0.931	0.960(0.376 - 2.447)
CX3CR1 high	0.280	0.691 (0.353 - 1.353)	0.906	1.043(0.519 - 2.094)

21. Differential expression of *ADAM10* in human breast cancer

Detection of ADAM10 was successfully performed on 276 breast cancer patients (Table 5, page 24) samples using IHC analysis. Expression was localized to tumor tissue, whereas other tissue compartments remained signal-free (Figure 28A-C, page 108). There was no background detection in primary antibody control samples, and a stable signal was detected in the kidney as a positive control (Figure 28D+E, page 108). A differential expression throughout the samples was detected. The cases were categorized in low expression (score 0 and +1) and high expression (score +2 and +3). Only expression in tumor tissue was taken into consideration.

Antibody specificity was evaluated by western blot analysis of breast cancer tissue showing single bands at 50 kDa for each patient (Figure 28F, page 108).

High signal intensity for ADAM10 was detected in 84% of 346 breast cancer patients (Table 48, page 109). There was a strong association of low *ADAM10* expression in the HR^+ cases (Table 48, page 109). The negative

correlation between *ADAM10* expression and the presence of the estrogen receptor was significant as compared by the Chi-square test (p=0.027).

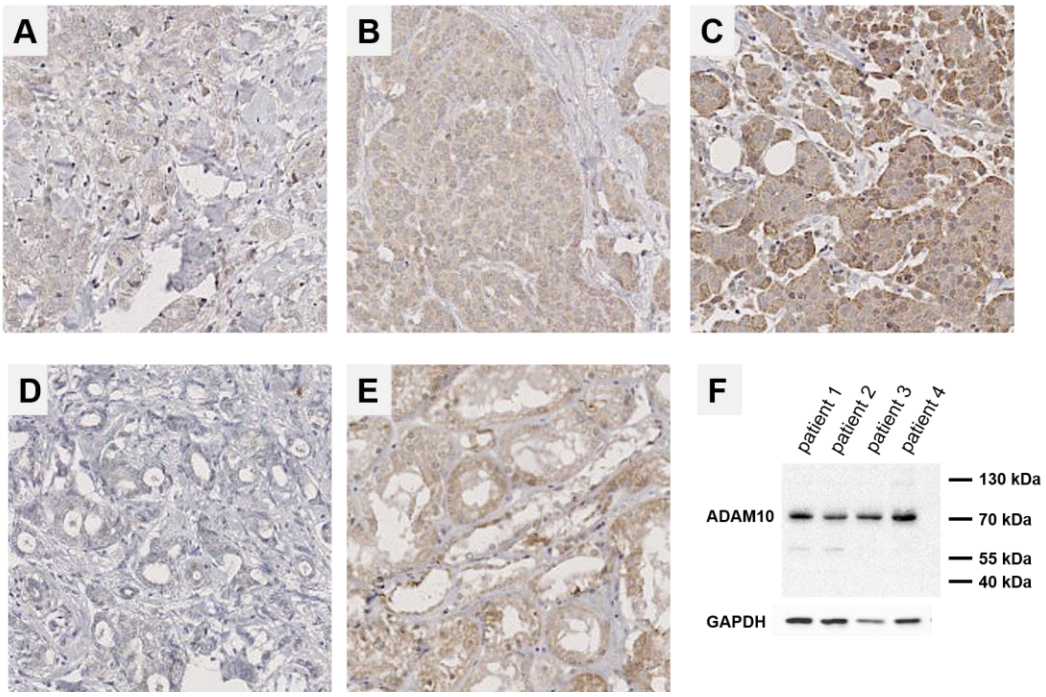

Figure 28: Immunohistochemistry (IHC) analysis of ADAM10 in breast cancer tissue.

Scoring intensities of ADAM10 in IHC showed (A) low +1, (B) moderate +2, and (C) high 3+ expression in breast cancer tissue. (D) Negative control without primary antibody showed no background detection. (E) Kidney samples were used as a positive control. (F) The specificity of the anti-ADAM10 antibody was shown in western blot analysis of human breast cancer samples (n=4), GAPDH was used as a loading control.

Table 48: Distribution of ADAM10 IHC score in a cohort of 276 breast cancer patients:

Relative distribution among breast cancer sub-groups, divided into HER2 receptor (HER2), hormone receptor (HR), and TNBC. Scores of 0 and 1+ were displayed as low, and scores of 2+ and 3+ were displayed as high.

scoring	percentage
low	16%
high	84%

HER2		**ADAM10 high**	**ADAM10 low**
positive	5	4	1
negative	262	221	41
Chi-Quadrat	0.791		
HR		**ADAM10 high**	**ADAM10 low**
positive	237	33	204
negative	30	21	9
Chi-Quadrat	**0.023**		
TNBC		**ADAM10 high**	**ADAM10 low**
yes	25	17	8
no	242	208	34
Chi-Quadrat	**0.019**		

With respect to survival, there was a trend suggesting ADAM10 as a favorable prognostic factor. This correlation was shown for DFS (p=0.204) and OS (p=0.42, Figure 29A+B, page 110). The favorable prognostic value of ADAM10 was further support by the Affymetrix data, which showed a highly significant correlation between high ADAM10 expression and better DFS (p=0.027, Figure 29C, page 110). Despite the consistent tendency from the KM analysis, ADAM10 does not prove as a prognostic factor in the univariate Cox regression analysis (Table 49, page 110).

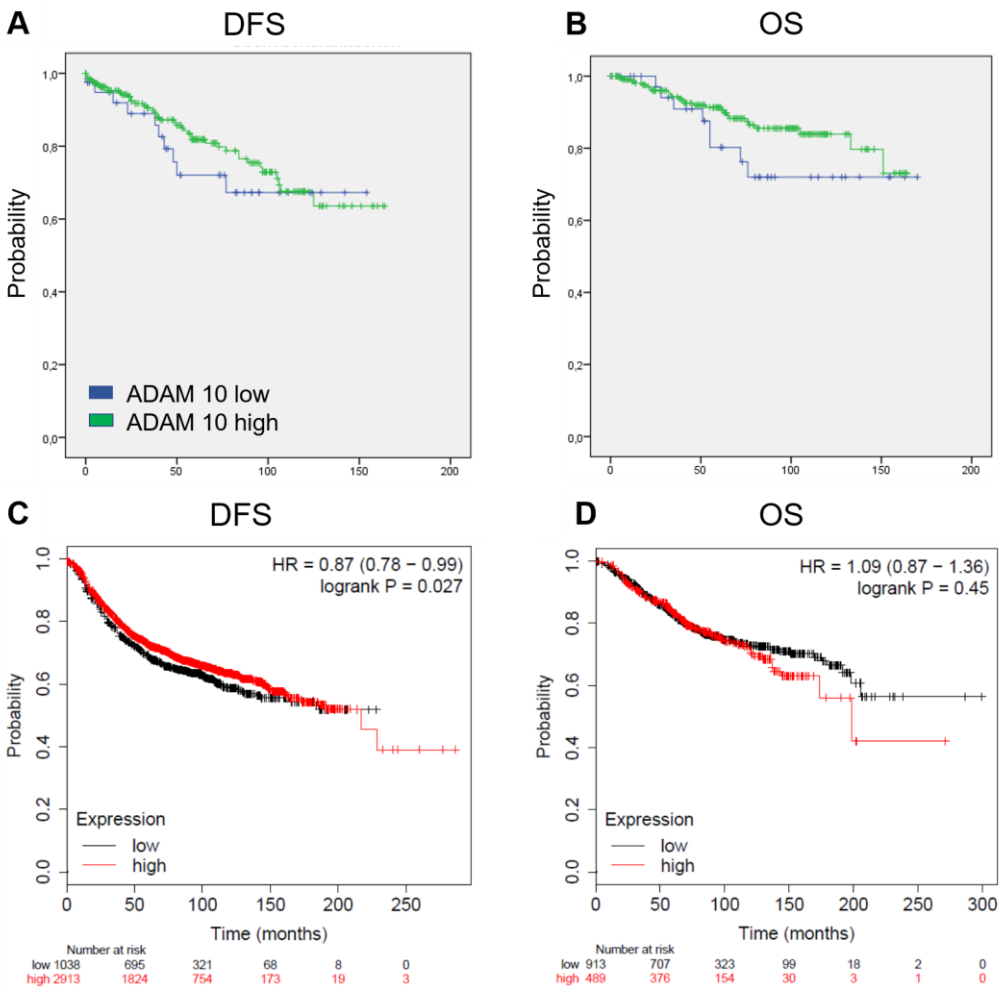

Figure 29: Association of ADAM10 expression in breast cancer specimens and patients' survival: Kaplan-Meier analysis of 276 breast cancer specimens stained for ADAM10 by immunohistochemistry and the association with (A) DFS and (B) OS. Affymetrix based public available ADAM10 expression data correlated high expression of the receptor with better(C) DFS (p=0.027) but not (D) OS (p=0.45) in breast cancer patients.

Table 49: Univariate Cox regression analysis of the breast cancer cohort and ADAM10 expression.

	DFS		**OS**	
	p	HR	p	HR
tumor≥20 mm	**0.019**	1775 (1.098 - 2.869)	**0.002**	2.578 (1.399 - 4.753)
age≥60 y	0.831	0.950 (0.593 - 1.521)	**0.083**	1.704 (0.933 - 3.112)
pT≥2	**0.00047**	1.568 (1.219 - 2.017)	**0.000011**	1.864 (1.412 - 2.461)
pN positive	**0.01**	1.374 (1.079 - 1.749)	**0.003**	1.524(1.154 - 2.014)
Grading≥3	0.125	1.341 (0.922 - 1.949)	**0.017**	1.78 (1.109 - 2.858)
TILs≥30%	0.89	0.953 (0.482 - 1.886)	0.931	0.960(0.376 - 2.447)
ADAM10	0.432	0.758 (0.380 - 1.512)	0.209	0.601(0.272 - 1.329)

22. Differential expression of *ADAM17* in human breast cancer

The analysis of ADAM17 with immunohistochemistry was performed in 322 breast cancer patient samples (Table 5, page 24).

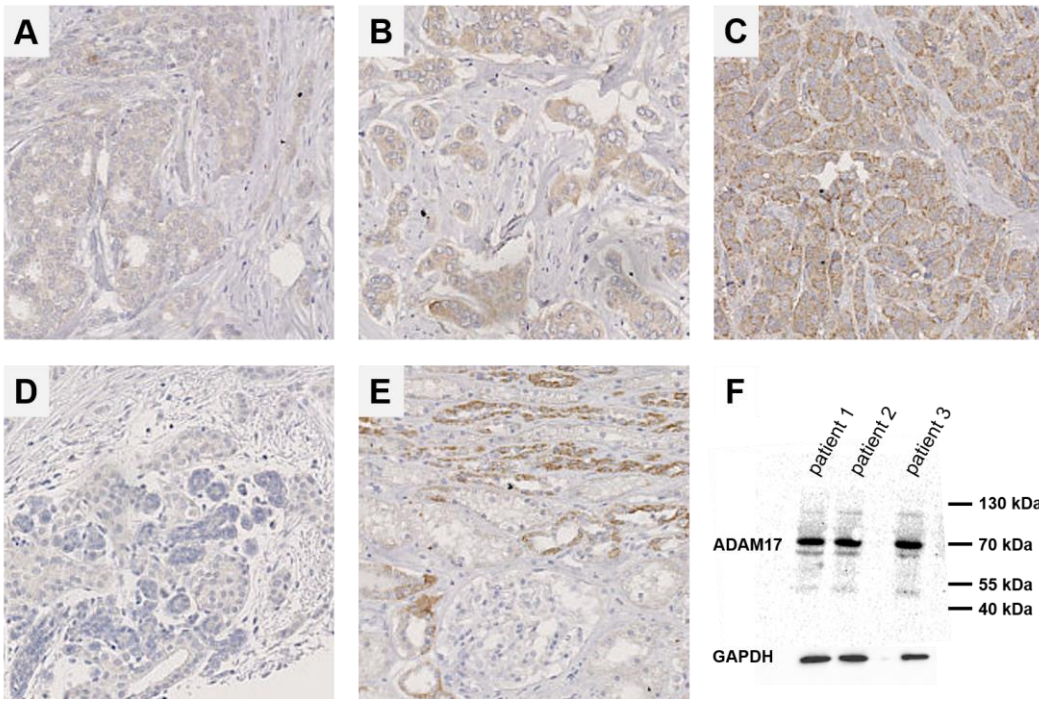

Figure 30: Immunohistochemistry (IHC) analysis of ADAM17 in breast cancer tissue.

Scoring intensities of ADAM17 in IHC showed (A) low +1, (B) moderate +2 and (C) high +3 expression in breast cancer tissue. (D) A negative control without primary antibody showed no background staining. (E) Kidney samples were used as a positive control. (F) The specificity of the anti-ADAM17 antibody was shown in the western-blot analysis of human breast cancer samples (n=3), GAPDH was used as a loading control.

The analysis of ADAM17 showed differential expression across the different samples with specific cytoplasmic expression located to tumor cells (Figure 30A-C). There was no signal detected in stroma cells or endothelial cells. The cases were categorized in low expression (score 0 and +1) and high expression (score +2 and +3). A negative control without primary antibody did not show any signal. The analysis of kidney samples showed cytoplasmic expression in ductal structures but no signal in glomeruli, pericytes, and stromal cells (Figure 30E).

Antibody specificity was evaluated by western blot analysis of breast cancer tissue showing bands at 70 and 130 kDa for each patient (Figure 30F, page 111).

The distribution showed that 41% of the analyzed samples had low ADAM17 expression, and 59% showed high expression (Table 50). Further analysis of ADAM17 expression in breast cancer subtypes revealed no further association.

Table 50: Distribution of ADAM17 IHC score in a cohort of 322 breast cancer patients:

Relative distribution among breast cancer sub-groups, divided into HER2 receptor (HER2), estrogen receptor (ER) and progesterone receptor (PR). Scores of 0 and 1+ were displayed as low, and scores of 2+ and 3+ were displayed as high. High ADAM17 levels are indicated in bold.

scoring	percentage
low	41%
high	59%

HER2		**ADAM17 high**	**ADAM17 low**
positive	15	7	8
negative	307	182	125
Chi-Quadrat	0.647		
HR		**ADAM17 high**	**ADAM17 low**
positive	280	168	112
negative	42	22	20
Chi-Quadrat	0.349		
TNBC		**ADAM17 high**	**ADAM17 low**
yes	27	14	13
no	295	176	119
Chi-Quadrat	0.430		

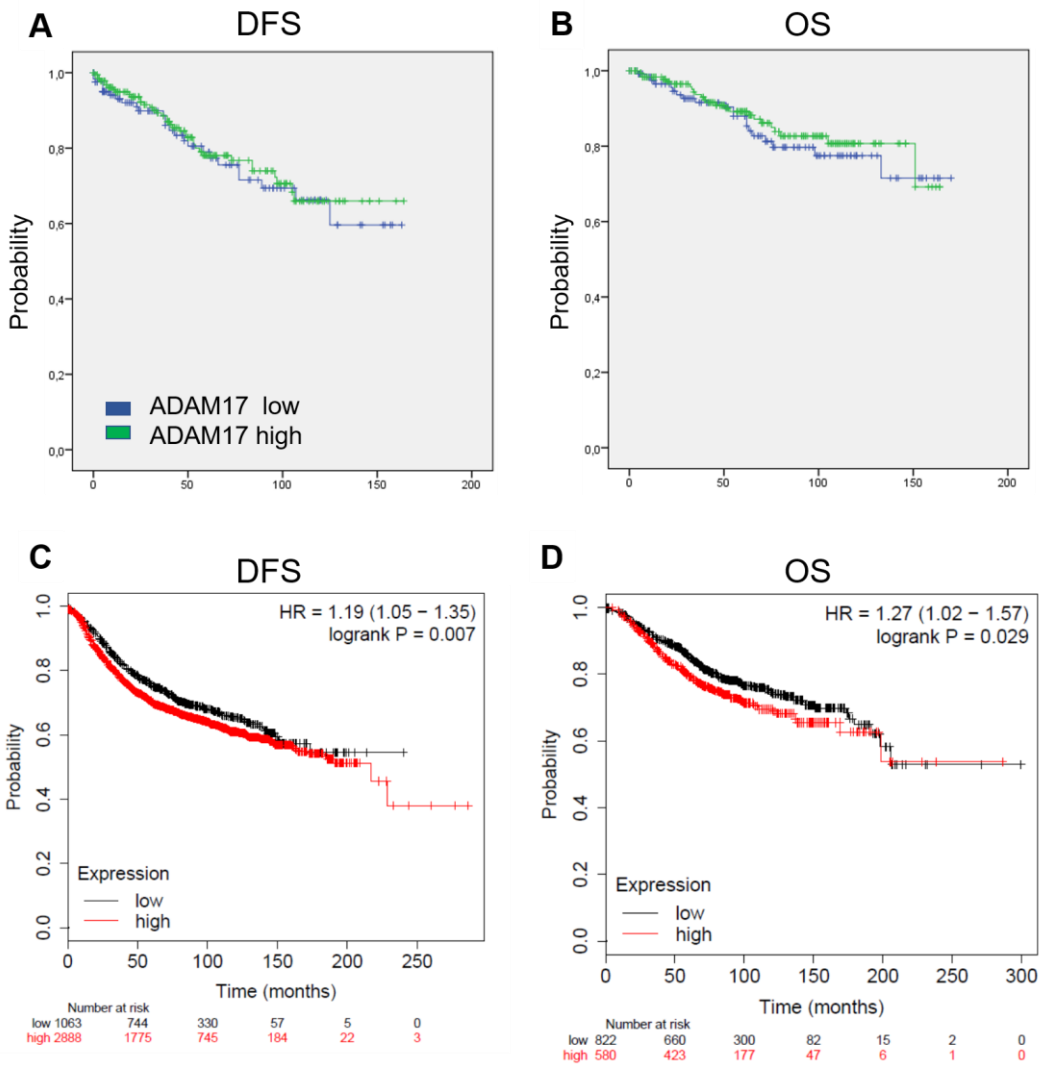

Figure 31: Association of ADAM17 expression in breast cancer specimens and patients' survival: Kaplan-Meier analysis of 322 breast cancer specimens stained for ADAM17 by immunohistochemistry and correlation with (A) DFS and (B) OS. Affymetrix based public available CXCR3 expression data correlated high expression of the receptor with better (C) DFS (p=0.007) and (D) OS (p=0.029) in breast cancer patients.

Survival data for ADAM17 showed no prognostic value for DFS or OS (Figure 31A+B). Nevertheless, the Affymetrix data showed that high ADAM17 expression is associated with a shorter DFS (p=0.007) and OS (p=0.029, Figure 31C+D). The univariate analysis of the prognostic value of *ADAM17* expression remained not significant.

	DFS		**OS**	
	p	HR	p	HR
tumor≥20 mm	**0.019**	1775 (1.098 - 2.869)	**0.002**	2.578 (1.399 - 4.753)
age≥60 y	0.831	0.950 (0.593 - 1.521)	**0.083**	1.704 (0.933 - 3.112)
pT≥2	**0.00047**	1.568 (1.219 - 2.017)	**0.000011**	1.864 (1.412 - 2.461)
pN positive	**0.01**	1.374 (1.079 - 1.749)	**0.003**	1.524(1.154 - 2.014)
Grading≥3	0.125	1.341 (0.922 - 1.949)	**0.017**	1.78 (1.109 - 2.858)
TILs≥30%	0.89	0.953 (0.482 - 1.886)	0.931	0.960(0.376 - 2.447)
ADAM17	0.660	0.894 (0.541 - 1.476)	0.530	0.827(0.456 - 1.498)

Thorough correlation analysis of all the immunohistochemically analyzed proteins above revealed some weak correlations. The most notable ones are listed in Table 51.

Table 51: Spearman correlation analysis of analyzed proteins in the immunohistochemistry cohort.

correlation	regression	p
ADAM10 vs. ADAM17	0.265	0.00002
ADAM10 vs. CX3CR1	0.150	0.014
ADAM17 vs.CX3CR1	0.330	0.0001
ADAM17 vs.CXCR3	0.243	0.0001
CX3CR1 vs. CXCR3	0.178	0.003
CX3CR1 vs. CX3CL1	-0.154	0.013

VI. DISCUSSION

1. CXCL9 shows anti-tumor activity in breast cancer

Breast cancer is the most common cause of cancer-related death among women in the western world. Though there are effective therapeutic strategies available, reaching from surgery to systemic therapy, the tumor-related mortality is still at about 20% (Akram et al. 2017). A major problem is the genetic diversity of breast cancer that is displayed in a wide variety of phenotypes. However, a feature that is shared among many breast cancer subtypes is a relatively high immunogenic potential, making it reasonable to aim for directed immuno-therapies, as it has been successfully demonstrated in the case of the anti-HER2 directed therapies already (Baselga et al. 2010). These therapies are highly dependent on functional and active host immunity. The main feature of efficient host immunity is the composition and amount of lymphocytes in the tumor (Solinas et al. 2017). Tumor-infiltrating lymphocytes are a strong prognostic marker of improved survival in different subsets of breast cancer patients (Denkert et al. 2017; Hellwig et al. 2019). This lymphocytic infiltration is directed into the tumor by chemokines, especially those binding and activating the CXCR3 receptor (Nagarsheth et al. 2017; Kuo et al. 2018). CXCL9 seems to play a crucial role in this process as it is highly associated with survival and the presence of tumor-infiltrating lymphocytes (Denkert et al. 2010, 2015; Specht et al. 2009).

The expression and secretion of CXCL9 are highly dependent on IFN-γ (Farber et al. 1997;Gorbachev et al. 2007; Wong et al. 1994). Moreover, this

secretion can be synergistically enhanced by simultaneous stimulation with TNF-α (Ohmori et al. 1993; Ohmori et al. 1997).

The experiments that are shown here demonstrate that these regulatory processes are also effective in the murine 4T1 breast cancer cell line as well as the human breast cancer cell lines SKBR3 and MDA-MB 231 *in vitro*. IFN-γ induces the secretion of CXCL9 in a dose-dependent manner, which can be further increased by the addition of TNF-α. As both cytokines are present in the tumor micro milieu, this sensitive regulation very likely also plays a vital role in inflammatory processes during cancer formation and progression.

Breast cancer is an inflammatory disease, and the amount of tumor-infiltrating lymphocytes (TILs) plays an important role in the progression and therapy of breast cancer (Dushyanthen et al. 2015). As mentioned above, the amount of TILs in the tumor is suggested as a feasible prognostic factor for all breast cancer subtypes (Roberto et al. 2017). The CXCR3 receptor is expressed on various, mainly tumor-suppressive, lymphocytes making them susceptible to CXCL9 recruitment. These lymphocytes include T-cells, NK cells, B-cells, dendritic cells (García-López et al. 2001; Qin et al. 1998; Loetscher et al. 1996; Hickman et al. 2015; Inngjerdingen et al. 2001; Muehlinghaus et al. 2005), but also regulatory T cells, eosinophils, and neutrophils (Hasegawa et al. 2008; Jinquan et al. 2000; Hartl et al. 2008). Especially NK cells and T cells have been shown to suppress tumor progression in a CXCL9-dependent manner (Andersson et al. 2011; Gorbachev et al. 2007; Wendel et al. 2008). This tumor-suppressive potential is not only due to the increase of total TILs but also to the

polarization of lymphocyte populations towards a tumor-suppressive phenotype. It has been shown that high concentrations of CXCL9 shift T cell populations towards T_H1 and T_H17 states, both showing anti-tumor activity (Groom and Luster 2012; J. K. Hu et al. 2011; Zohar et al. 2014a).

Beside the chemokine-immune cell interaction, CXCL9 shows a lymphocyte-independent tumor-suppressive mechanism: as a member of the ELR (Glu-Leu-Arg) chemokine family, there have been angiostatic functions reported, which additionally impair tumor progression (Arenberg et al. 2001; Pan et al. 2006) and even lead to the formation of necrotic intratumoral lesions (Sgadari et al. 1997). Taking all these mechanisms into consideration, the tumor-suppressive effects were successfully validated in xenograft mouse models using SCID mice (Addison et al. 2000; Arenberg et al. 2001). The same experimental setup was adequately performed in the syngenic 66.1 breast cancer mouse model in Balb/c mice (Walser et al. 2007). The authors found reduced tumor growth and metastasis together with increased T cell infiltration in the tumor transplants overexpressing CXCL9. Here, using the triple-negative 4T1 breast cancer mouse model with stably *CXCL9*-overexpressing 4T1 cells, we were able to confirm previous results. Mice bearing *CXCL9*-overexpressing tumors showed a 60% reduction in tumor growth and a significantly reduced tumor mass after 21 days. The chemokine concentration was re-evaluated after the experiment, and higher CXCL9 concentrations were detected in tumor tissue and blood samples of mice with *CXCL9*-overexpressing tumors. The elevated CXCL9 concentration in the sera of tumor-bearing mice corresponds to studies reporting that serum CXCL9 was elevated in breast cancer patients and might be a feasible biomarker for early detection (Ruiz-

Garcia et al. 2010). Moreover, as a proportion of breast cancer patients in the present study also exhibited elevated CXCL9 in their sera, CXCL9 might be a feasible liquid biopsy marker to assess the tumor immunologic micro milieu in breast cancer patients. The 4T1-Cxcl9 experiment demonstrates that systemic CXCL9 might be indeed tumor-derived. Further analyses are planned to determine the association of serum CXCL9 and the inflammatory tumor micro milieu.

Besides, in order to further support the role of CXCL9 in tumor progression, the experiment was extended using stably *CXCL9*-depleted 4T1 cells. However, the reduction of CXCL9 was not sufficient to have any impact on tumor growth. These results might be explained in different ways. Since CXCL9 is strongly regulated via inflammatory cytokines, which are present during tumor progression, the knockdown via RNA interference (60% compared to wildtype) might not have been sufficient to impair the various CXCL9 effects. It has also been shown that tumor cells not necessarily have to be the primary source of *CXCL9* expression. Dangaj and colleagues identified $CD11c^{+}$ dendritic cell populations as a significant chemokine producer (Dangaj et al. 2019). Those populations would not have been directly affected by a local, artificial knock out in the tumor cells. Similar effects have been detected for macrophage-derived *CXCL9* expression (House et al. 2020).

Furthermore, the compensation by the redundancy of the different CXCR3-ligands remains unclear till now, and it has been earlier discussed if missing CXCL9 functionality could be substituted by CXCL10 (Medoff et al. 2006) or leads to enhanced receptor internalization due to false regulation by

CXCL11 (Rajagopal et al. 2013; Sauty et al. 2001). The role of intratumoral receptor and ligand interaction needs to be further evaluated but was reported to have no impact on tumor growth *in vivo.* Stable knockout of *CXCR3* in 4T1 tumor cells in Balb/c mice showed no modulation of tumor growth (Zhu et al. 2015). Another reason for the lack of differential tumor growth might be that CXCL9 does not play a major role in the wild-type 4T1 model as only minor *CXCL9* mRNA expression was detected in the control tumors of the *CXCL9*-overexpression experiment.

Altogether, high CXCL9 concentrations show significant tumor-suppressive activity in triple-negative breast cancer *in vivo*. These findings provide substantial information that increasing intra-tumoral CXCL9 concentration is a potential therapeutic target for cancer therapy.

2. CXCL9 in cancer therapy

There have been different approaches performed using CXCL9 as a modulator of cancer therapy. High concentrations of CXCL9 show promoting effects in different antibody-based therapies, such as anti-PD1 therapy in melanoma and breast cancer (W. Peng et al. 2012; Chheda et al. 2016) and anti-CTLA4 therapy in colon cancer and melanoma (Ji et al. 2012). House and colleagues even suggest that CXCL9 modulation might be a good way to improve patients' response to checkpoint inhibition and that the modulation does not have to be tumor-derived but might be macrophage dependent (House et al. 2020). In terms of high intratumoral CXCL9 concentration, there have also been beneficial effects on other immuno-therapies suggested, including adoptive T cell transfer (Bedognetti et al. 2013). Since all these therapies benefit from high CXCL9 concentrations, there is a need for therapeutic options to induce intratumoral CXCL9 for use in a clinical setting. Recent data of our research group indicated that there is an impact of COX-2 and its major product PGE_2 on the regulation of CXCL9. PGE_2 impairs the IFN-γ mediated CXCL9 secretion from cancer cells (Bronger et al. 2016, 2012). The existence of this regulatory axis is also supported by the observation of an inverse correlation between CXCL9 and COX expression in a cohort of breast cancer patients (Bronger et al. 2012).

In the present work, it was demonstrated that both the murine 4T1 breast cancer cells, as well as human MDA-MB 231 and SKBR3 cells, show very low to no endogenous CXCL9 secretion. The inflammatory cytokine IFN-γ is capable of significantly increasing the chemokine secretion. After

combined treatment with IFN-γ and non-selective COX-inhibition by indomethacin, the chemokine secretion was significantly elevated compared to IFN-γ only treatment. More evidence for the connection of CXCL9 secretion and COX function came from the observation of increased secretion of CXCL9 after stable shRNA-mediated knockdown of COX-2 in 4T1 cells. Altogether, there is strong evidence that inhibition of COX leads to increased CXCL9 secretion.

Based on these data, indomethacin therapy was tested in our syngeneic 4T1 mouse model. Two weeks of treatment were sufficient to significantly reduce tumor growth by 75% and the formation of lung metastases by 70% compared with untreated mice. These findings support the results of Connolly and colleagues in the same experimental setting (Connolly et al. 2002). Additionally, the outcomes derived from the latter experiment in this thesis show that the treatment with indomethacin correlates with increased CXCL9 concentrations in mouse plasma. Furthermore, flow cytometry analysis of the tumor-infiltrating lymphocytes revealed higher concentrations of NK cells in tumor tissue. The higher immune cell influx contributes to a better anti-tumor response and agrees with previous data in lung cancer models (Andersson et al. 2009). Other lymphocyte subpopulations were also enriched by 2-10%, depending on the cell type, in indomethacin-treated mice, including inactive regulatory T cells, macrophages, and dendritic cells. All those cells have been shown to express the CXCL9 receptor CXCR3 indicating that the observed effects of indomethacin *in vivo* could indeed be dependent on CXCL9. Similar results were observed for flow cytometry analysis of spleen lymphocytes. Here, an increased accumulation of NK cells by a factor of 1.6, total $CD3^+$

lymphocytes by a factor of 1.3 including $CD4^+$ and $CD8^+$ T cells and regulatory T cells by a factor of 1.6 was detected. The enrichment of lymphocytes in the spleen is a strong indicator for immune response and systemic redistribution of immune-cells (Bronte and Pittet 2013). Summing up, treatment of mice with indomethacin in a syngenic breast cancer model displays significantly reduced tumor growth and metastasis. The microenvironment shifts towards a tumor-suppressive milieu by enrichment of NK cells in the tumor, together with strong inflammatory regulation. These effects are at least accompanied by an increase of CXCL9 concentrations in the sera of the corresponding mice. Nevertheless, although all these effects could be functionally linked to the induction of CXCL9 by COX inhibition, further experiments are now warranted to prove this link.

CXCL9 has also shown to be associated with a good response to standard chemotherapy. It was described that breast cancer patients with high *CXCL9* expression show a better response to CMF chemotherapy (Specht et al. 2009). Similar results were seen after combination therapy of cisplatin and plasmid-derived CXCL9 in colon and lung cancer (Zhang et al. 2006). The link between *CXCL9* expression and chemotherapy treatment was further underpinned by the treatment with lapatinib and doxorubicin, leading to increased *CXCL9* expression (Hannesdóttir et al. 2013). *In vitro* experiments performed in this thesis, with the two different human breast cancer cell lines, SKBR3 and MDA-MB 231, showed that major standard breast cancer chemotherapy agents were, at certain concentrations, sufficient to increase the CXCL9 secretion. This includes cyclophosphamide 0.25 mM (1.4 fold increased secretion), paclitaxel 12.5 mM (2.2 fold increases secretion), lapatinib 1.25 mM (1.2 fold increased secretion) and

epirubicin 25 mM (2 fold increased secretion). These findings further support the aspect of activation of the anti-tumoral immune response as a mechanism of action of standard chemotherapeutics. These hypothesis has been proposed earlier by Mattarollo et al. and Fridmann et al. (Mattarollo et al. 2011; Fridman et al. 2017). The mechanisms *in vivo* need to be further analyzed, but it seems reasonable to assume that CXCL9 plays a role in the tumor response to standard chemotherapy and might have predictive value in terms of chemotherapy response.

In order to validate the expression levels of CXCL9 in breast cancer patients, two cohorts of patients were compiled. On the one hand, the expression of CXCL9 and its receptor CXCR3 was evaluated in tumor tissue via immunohistochemical analysis in a cohort of 287 breast cancer patients including all subtypes (HR+, HER2+, triple-negative), on the other hand, the serum levels of CXCL9 and CXCL10 in breast cancer patients were tested before therapy. Most interestingly, 45% of all patients showed no expression of CXCL9. On the other hand, 50% of the patients showed a moderate to high expression based on the separation by quartiles. The CXCL10 expression was distributed equally among the quartiles. A correlation between CXCL9 and CXCL10 in the patient's sera was not detected. The idea of CXCL9 being a good prognostic marker has already been analyzed by other groups, including ER-negative breast cancer, lung cancer, and cervical cancer (Shiels et al. 2015; Ruiz-Garcia et al. 2010; Zhi et al. 2014).

Nevertheless, none of the studies mentioned above did also check for the correlation between serum CXCL9 concentration and expression in the corresponding tumor tissue. This correlation would be a crucial step to

understand better the prognostic value and underlying mechanism of action of this chemokine. It is the future perspective of this study once the follow up is long enough to have a sufficient number of survival events.

Besides the determination of the CXCL9 concentrations in the sera, the expression of *CXCL9* in breast cancer specimens was assessed and correlated with clinical parameters. In our cohort, high *CXCL9* expression was associated with a worse prognosis, although these results were not significant. The *CXCL9* expression was associated with the TNBC cases in our cohort, which has the worst prognosis among all breast cancer subtypes. This overall bad prognosis could be one explanation for the surprising outcome of this study. However, the general prognostic potential of CXCL9 is not fully understood until now. There is strong evidence that CXCL9 is a favorable prognostic marker for better survival, especially in breast cancer (Denkert et al. 2010), but also in other cancer entities like NSCLC, colorectal cancer, melanoma, and ovarian cancer. (Addison et al. 2000; Wu et al. 2016; Bedognetti et al. 2013; Kryczek et al. 2009). The protective nature is further underlined by the findings that CXCL9 can increase the amount of tumor-infiltrating lymphocytes into the tumor tissue, which is another strong marker for better prognosis and therapy response (Carsten Denkert et al. 2017; C. Denkert et al. 2014). On the other hand, several reports have associated high *CXCL9* expression with an adverse prognosis in several cancer entities, including hepatocellular carcinoma, lung cancer, melanoma, prostate cancer, glioblastoma, and oral cavity squamous carcinoma (Liu et al. 2015; Nakanishi and Rosenberg 2013; Amatschek et al. 2011; Hsin et al. 2013; Chang et al. 2013; Hu et al. 2015; Sreekanthreddy et al. 2010). These contradictory results demonstrate that

CXCL9 is a hallmark regulator of the immune response during cancer progression and treatment, but the exact mechanisms are not fully understood yet.

Even more important is the correlation between chemokine expression in the tissue, and the corresponding systemic effect in the bloodstream needs to be further evaluated since the promising results would suggest CXCL9 as a suitable predictive and prognostic biomarker with potential to become a biomarker even from a liquid biopsy.

3. Regulation of CX3CL1 in human cancer cell lines

CX3CL1 is a chemokine, which is translated as a transmembrane protein exposing its chemokine domain extracellularly (Bazan et al. 1997). It can be strongly induced by inflammatory cytokines such as TNF-α (Chandrasekar et al. 2003). The soluble isoform can be generated by proteolytic cleavage, still containing the chemokine domain. Proteases that can perform this shedding are, besides others, mainly ADAM10 and ADAM17 (Garton et al. 2001; Hundhausen et al. 2003). The soluble isoform shows chemotactic properties towards lymphocytes bearing the corresponding receptor CX3CR1 (Chen and Mellman 2013b). The membrane-bound CX3CL1 is additionally capable of providing tight adhesion to the cell populations mentioned above (Harrison et al. 2001). This dual character of CX3CL1 provides a broad spectrum of functional activity in inflammation and cancer disease. Herein, regulation and potential shedding of CX3CL1 were analyzed in four differentially HER2-expressing cancer cell lines (HT29, BT474, MDA-MB 453, SKBR3). The regulatory properties of these four cell

lines were quite different regarding up-regulation under inflammatory conditions and shedding. This individual adjustment indicates that CX3CL1 regulation is carefully adjusted and controlled. HT29 and SKBR3 cells showed expression of CX3CL1 under normal conditions, but respond strongly to stimulation with TNF-α and show increased CX3CL1 secretion. The shedding can be efficiently modulated by inhibition of ADAM17. The same was observed for the BT474 cells, but these showed increased CX3CL1 under normal conditions and no further up-regulation of membrane-bound CX3CL1 after the inhibition of ADAM17-mediated shedding.

Further analysis of the CX3CL1 turn-over has shown that CX3CL1 can be rapidly internalized and is stored in intracellular vesicles (Liu et al. 2005). The intrinsic storage indicates a fast regulatory mechanism to keep constant CX3CL1 concentration on the cell membrane. The MDA-MB 453 cells showed no regulation of CX3CL1 at all with deficient intrinsic concentrations. Altogether in this study, the thorough regulation of CX3CL1 was shown in four different HER2 positive cancer cell lines.

3.1. CX3CL1 improves the NK cell-mediated cell lysis of HER2-positive cancer cells.

NK cells are lymphocytes that are also known for their ability to kill tumor cells. Two different mechanisms have been identified for efficient killing: an unspecific killing, which is mainly based on missing MHC class antigens on the surface of the target cells, and a specific killing mediated via the Fc receptor on the NK cell membrane (Mota et al. 2003). The latter one is called antibody-dependent cellular toxicity (ADCC) and is an essential mechanism in many immunotherapies (Wu and Lanier 2003; Robertson and Ritz 1990).

A prominent example is the anti-HER2 therapy for HER2-positive breast cancer patients using trastuzumab. HER2 is a growth factor receptor, which is connected to oncogenic transformation and is correlated with poor patient survival, high recurrence rate, and metastasis formation (Slamon et al. 1987). Trastuzumab is a humanized anti-HER2 antibody for the treatment of human HER2-overexpressing tumor patients (Carter et al. 1992). This antibody binds to HER2 and has two modes of action. The first one is the intracellular blockade of the receptor tyrosine kinase activity, which also impairs the down-stream signaling and pathway activation. The second one is the improvement of ADCC by presenting the Fc fragment to the specific receptor of NK cells (Tokuda et al. 1996; Cooley et al. 1999). Arnould and colleagues have shown a strong dependency between NK cells and efficient anti-HER2 therapy (Arnould et al. 2006). Nevertheless, after a year of therapy, some patients show resistance to trastuzumab after successful treatment (Pohlmann et al. 2009), so more insight into the mechanism is needed, and alternative options are necessary.

CX3CL1 affects NK cell function *in vivo* (Robinson et al. 2003). Thereby, both isoforms seem to contribute to this regulation. The soluble form of CX3CL1 functions as a potent chemoattractant for NK cells, which leads to increased recruitment out of the bloodstream (Umehara et al. 2004) into the tumor (Guo et al. 2003). The membrane-bound form of CX3CL1 is capable of inducing strong adhesion (Harrison et al. 2001) and higher integrin affinity (Goda et al. 2000). Both mechanisms might contribute to an accumulation of NK cells in the tumor tissue. Furthermore, the chemokine domain itself, in both isoforms, stimulates IFN-γ secretion of NK cells, suggesting that CX3CL1 also acts as an NK cell activator (Yoneda et al. 2000).

In the present work, it was shown that NK cell-mediated killing of HER2-positive breast cancer cells could be increased by TNF-α *in vitro,* which is in agreement with previous data in MCF7 and MDA-MB 231 breast cancer cells (Branellec et al. 1992). Interestingly, in the present work, it could be demonstrated that this effect is partially dependent on CX3CL1 since the addition of an anti-CX3CL1 antibody quenched the killing efficiency. Additionally, the CX3CL1 low expressing cell line MDA-MB 453 showed no effect of TNF-α on cytotoxicity despite having a general TNF-α response that could be shown by the induction of CXCL10. The role of CX3CL1 in the NK cell-mediated killing could be further underpinned by effects in the wake of *CX3CL1* overexpression. The cell lysis of *CX3CL1*-overexpressing tumor cells was increased by 15% compared to control cells, and these cells also better responded to the treatment with trastuzumab. To date, this is the first study demonstrating additive effects of combined CX3CL1 and trastuzumab treatment of HER2-positive cancer cells *in vitro*.

In summary, CX3CL1 can enhance the NK cell-mediated cell lysis of breast cancer cells. Inhibition of ADAM17 and thereby the shedding and increase of the membrane-bound compartment was sufficient to increase the NK cell cytotoxicity further. Increased CX3CL1 concentrations could improve the trastuzumab efficiency in this model. Due to the structure of the Europium assay, which includes the incubation of NK cells and tumor cells in close proximity, the focus of this particular experiment was on the membrane-bound form of CX3CL1. The effects that have been described above are altogether signs for a tumor-suppressive function of this CX3CL1 isoform. The prognostic value for breast cancer is controversially discussed because CX3CL1 has been suggested as a marker for bad and good prognosis

(Tsang et al. 2013; Park et al. 2012). Since the two isoforms were not differentiated in these studies, this might be a potential explanation for the contradictory effects since the effects of the soluble forms have not been analyzed in detail yet.

4. CX3CL1 reduces tumor growth and metastasis *in vivo* and enhances trastuzumab therapy

Herein, *CX3CL1* overexpression in the syngenic 4T1 breast cancer mouse model showed a significant reduction of tumor growth and lung metastasis together with increased tumor-infiltrating NK cells, $CD4^+$, and $CD8^+$ T cells. These findings correspond to results reported in other cancer entities (Lavergne et al. 2003; Kee et al. 2013). However, in our experiments, no changes in regulatory T- cells were detected, which contribute to a tumor promotive environment (Plitas and Rudensky 2020). Moreover, there was no shift of myeloid cell populations, in particular dendritic cells and monocytes, detected. A lack of regulation of these cell populations might also contribute to a better outcome due to the tumor-promoting effects of these myeloid subpopulations (Chittezhath et al. 2014).

The tumor-suppressive effect of CX3CL1 was also shown in the two xenograft mouse models using human MDA-MB 453 and HT29 cells stably overexpressing murine CX3CL1. In both models, an accelerated initial tumor growth phase was detected in the mice bearing tumor with CX3CL1 overexpression. This accelerated tumor onset is in line with the observation in the 4T1 model, win which the separation of the growth curves occurred only at a very late stage. Nevertheless, in the end, CX3CL1 improved

survival and suppressed tumor growth in all three mouse models. In the MDA-MB 453 model, there was no improvement of trastuzumab therapy detectable, because small amounts of trastuzumab were already sufficient to eradicate the initially grown tumor. The powerful trastuzumab effect is in line with the clinical situation in which the immunoregulatory effects are not that important in HER2 overexpressing tumors. Tumor cells that show high expression of HER2 tend to be more sensitive to inhibition of the HER2 receptor activity, which is also a mode of action of the trastuzumab antibody (Pegram and Slamon 2000). In the low HER2 expressing HT29 mouse model, the overexpression of CX3CL1 was able to improve the survival of the animals together with increased infiltration of NK cells. The in this thesis acquired data further confirms what has been shown in previous studies that already have shown that intratumoral CX3CL1 is capable of recruiting NK and T cells and thereby suppress tumor growth in preclinical models of colon cancer, lung cancer, hepatocellular carcinoma and lymphoma (Vitale et al. 2007; Jun Guo et al. 2003; Tang et al. 2007; Kee et al. 2013; Xin et al. 2005). Moreover, CX3CL1 was sufficient to overcome trastuzumab resistance in this mouse model. Our study supports the protective role of CX3CL1 in breast cancer and suggests a potential therapeutic synergism with trastuzumab, which might enable this kind of therapy also for patients with HER2 low-expressing cancer entities.

5. CX3CL1 as a prognostic marker

The prognostic role of CX3CL1 and its receptor CX3CR1 was assessed in a cohort of breast cancer patients, including all subtypes. The immunohistochemical analysis revealed a favorable prognostic value for DSF among patients that have been positively tested for CX3CL1 expression. The positive association between *CX3CL1* expression and better survival was further validated in publicly available datasets for DFS as well as OS (Györffy et al. 2010). These findings might further underline the tumor-suppressive function of CX3LC1, which has been described earlier also in other entities (Zeng et al. 2007; Xin et al. 2005; Lavergne et al. 2003; J Guo et al. 2003; Yu et al. 2007). However, there are still contradictory data available, showing pro-tumorigenic effects, e.g., in pancreatic cancer (Xu et al. 2012). A major question that remains unanswered is the differential function of soluble and membrane-bound CX3CL1, which might contribute to the adverse effects observed in different studies and different cancer entities. Vitale and colleagues have shown that both forms have tumor-suppressive effects in colon cancer, but act via different mechanisms (Vitale et al. 2007).

Another aspect that can influence the effects of CX3CL1 is the interaction with its receptor CX3CR1. The receptor is predominantly expressed on various immune cell populations, leading to the efficient chemotactic effect of CX3CL1. This CX3CL1 induced chemotaxis mainly recruits tumor-suppressive immune cells into the solid tumor, including NK cells, $CD4^{+,}$ and $CD8^{+}$ T cells. (Hyakudomi et al. 2008; Ohta et al. 2005; Park et al. 2012; Blum et al. 2008; Erreni et al. 2016; Kehlen et al. 2014; Mlecnik et al. 2010;

J. Liu et al. 2019). However, the receptor is also expressed on tumor cells and might, therefore, interact with cells expressing the corresponding ligand. These might be the tumor cells themselves as well as epithelial cells in surrounding tissue or even distant organs. In this thesis, also the CX3CR1 receptor expression on tumor cells was analyzed, and differential expression among breast cancer samples could be observed. The expression on the protein level could not be associated with patients' survival. However, the Affymetrix data showed a clear correlation of high CX3CR1 expression and better disease-free and overall survival (Györffy et al. 2010). The expression of the CX3CR1 receptor can also be detected in other cancer entities listed in the TCGA database, including glioma, renal, and ovarian cancer, further supporting the tumor-associated role of this receptor. Most likely, the CX3CR1 receptor is an inducer of metastasis formation, as it has been described in other cancer entities such as colon or gastric cancer. However, a high tumoral CX3CL1 concentration might incorporate the CX3CR1 expressing tumor cells into the tumor and thereby keep them from moving into adjacent tissue. This mechanism has already been suggested for the CXCR3-system in ovarian cancer (Windmüller et al. 2017) and might be even more feasible for the CX3CR1/CX3CL1 axis as well since the membrane-bound form of the chemokine also mediates adhesive properties.

Another relevant aspect in terms of CX3CL1 regulation is the expression of proteases that can shed this chemokine into the soluble form. So far, the proteases ADAM10 and ADAM17 have been identified as the major shedding enzymes, although there are other proteases involved like Cathepsin S or MMP2. In this study, the expression of *ADAM10* and

ADAM17 in breast cancer tissue has been analyzed. The combined expression of ADAMs and CX3CL1 would allow a potential deductive effect on patients' survival and the distinct role of the soluble and membrane-bound form of CX3CL1.

The analysis of ADAM10 immunohistochemistry data suggested this protease as a favorable prognostic marker for DFS and OS. The IHC data for ADAM10 was in line with the Affymetrix data, which also associated high ADAM10 expression with better survival. A correlation with the CX3CL1 staining was not detected, so a possible interaction between both proteins is not derivable from the available data. This lack of correlation does not necessarily mean that there is no such interaction since it is very likely that the used CX3CL1 antibody detects both the soluble and the membrane-bound form, discriminating between both forms impossible. Nevertheless, the finding that *ADAM10* expression could be tumor suppressive is very controversial to the existing literature. The so-far common sense indicates that *ADAM10* expression is an unfavorable prognostic marker in several cancer entities and is associated with the promotion of tumor cell migration and growth, e.g., in cancers of the oral cavity, stomach, ovary, uterine, colon, prostate and leukemia. (Ko et al. 2007; Yoshimura et al. 2002; Fogel et al. 2003; McCulloch et al. 2004; Wu et al. 1997; Gavert et al. 2005).

Moreover, in triple-negative breast cancer, the tumor-promoting functions of ADAM10 have also been shown, including the increase of migration and invasion of TNBC cell lines BT20 and MDA-MB 231 (Mullooly et al. 2015). However, ADAM10 is a protease, and this gives the possibility to a wide range of cleavable substrates, so the effects have to be closely evaluated

in every entity individually. Especially the correlation of ADAM10 and a specific substrate needs to be carefully addressed (Atapattu et al. 2016). Besides, the activation of ADAM10 is probably even more important than the pure expression of this protein (Wozniak and Ludwig 2018). So in order to further elucidate the discrepancy, an activity base approach would be necessary for future research. The argumentation is, of course, also valid for the other CX3CL1 sheddase ADAM17.

The expression data in this cohort showed no association with adverse survival of the patients but the Affymetrix data suggest an association of ADAM17 expression with poor DFS and OS. Similar effects have also been detected in breast, kidney, and ovarian cancer (Lendeckel et al. 2005; Roemer et al. 2004; Tanaka et al. 2005). In terms of CX3CL1 shedding, these contrary effects of ADAM10 and ADAM17 are not very surprising. The gene regulation of both proteases is very different. ADAM10 is constitutively expressed, and ADAM17 is tightly regulated and only expressed upon distinct signaling.

Altogether, the expression of the CX3CL1/CX3CR1 axis has been shown to play a protective role in the progression of breast cancer, leading to overall better survival of those patients. The embedding in the context of ADAM10 and ADAM17 shedding remains difficult since both proteases themselves are part of a complex regulatory network. However, the whole system remains an important regulatory player and might influence future breast cancer therapies and the development of new therapeutic options.

VII. CONCLUSION

The chemokines CXCL9 and CX3CL1 exhibit tumor-suppressive capabilities that are associated with a higher lymphocytic infiltration and less metastatic spread in breast cancer. Moreover, for CX3CL1, a synergistic effect with trastuzumab in the therapy of HER2-positive tumors could be shown *in vitro* and *in vivo.* It is tempting to speculate that this feature of CX3CL1 might extend to other monoclonal therapeutic antibodies as well, whose mode of action involves antibody-dependent cellular cytotoxicity. Pharmacological upregulation of *CXCL9* or *CX3CL1* expression might, therefore, be a suitable target to enhance immune intervention in these cancers. Another conceivable mechanism would be to inhibit chemokine degradation pharmacologically. Future studies will have to validate this functional role in a more clinical setting. Besides, the role of both chemokines as prognostic or predictive biomarkers has to be further evaluated. It has to be explored if CXCL9 and CX3CL1 make useful biomarkers by themselves or if it might be reasonable to combine them with an “immunoscore”. Altogether, the implementation of the chemokines CXCL9 and CX3CL1 in translational medicine might lead to more personalized cancer treatment in the future.

VIII. REFERENCES

’t Veer, Laura J. van, Hongyue Dai, Marc J. van de Vijver, Yudong D. He, Augustinus A. M. Hart, Mao Mao, Hans L. Peterse, et al. 2002. “Gene Expression Profiling Predicts Clinical Outcome of Breast Cancer.” *Nature* 415 (6871): 530–36. https://doi.org/10.1038/415530a.

Addison, Christina L., Douglas A. Arenberg, Susan B. Morris, Ying-Ying Xue, Marie D. Burdick, Michael S. Mulligan, Mark D. Iannettoni, and Robert M. Strieter. 2000. “The CXC Chemokine, Monokine Induced by Interferon-Gamma, Inhibits Non-Small Cell Lung Carcinoma Tumor Growth and Metastasis.” *Human Gene Therapy* 11 (2): 247–61. https://doi.org/10.1089/10430340050015996.

Akram, Muhammad, Mehwish Iqbal, Muhammad Daniyal, and Asmat Ullah Khan. 2017. “Awareness and Current Knowledge of Breast Cancer.” *Biological Research* 50. https://doi.org/10.1186/s40659-017-0140-9.

Amatschek, S., R. Lucas, A. Eger, M. Pflueger, H. Hundsberger, C. Knoll, S. Grosse-Kracht, et al. 2011. “CXCL9 Induces Chemotaxis, Chemorepulsion and Endothelial Barrier Disruption through CXCR3-Mediated Activation of Melanoma Cells.” *British Journal of Cancer* 104 (3): 469–79. https://doi.org/10.1038/sj.bjc.6606056.

Andersson, A., S.-C. Yang, M. Huang, L. Zhu, U. K. Kar, R. K. Batra, D. Elashoff, R. M. Strieter, S. M. Dubinett, and S. Sharma. 2009. “IL-7 Promotes CXCR3 Ligand-Dependent T Cell Antitumor Reactivity in Lung Cancer.” *The Journal of Immunology* 182 (11): 6951–58. https://doi.org/10.4049/jimmunol.0803340.

Andersson, Asa, Minu K Srivastava, Marni Harris-White, Min Huang, Li Zhu, David Elashoff, Robert M Strieter, Steven M Dubinett, and Sherven Sharma. 2011. “Role of CXCR3 Ligands in IL-7/IL-7R Alpha-Fc-Mediated Antitumor Activity in Lung Cancer.” *Clinical Cancer Research : An Official Journal of the American Association for Cancer Research* 17 (11): 3660–72. https://doi.org/10.1158/1078-0432.CCR-10-3346.

Angelova, Mihaela, Pornpimol Charoentong, Hubert Hackl, Maria L Fischer, Rene Snajder, Anne M Krogsdam, Maximilian J Waldner, et al. 2015. “Characterization of the Immunophenotypes and Antigenomes of Colorectal Cancers Reveals Distinct Tumor Escape Mechanisms and Novel Targets for Immunotherapy.” *Genome Biology* 16 (1): 64. https://doi.org/10.1186/s13059-015-0620-6.

Arenberg, Douglas, Eric White, Marie Burdick, Scott Strom, and Robert Strieter. 2001. “Improved Survival in Tumor-Bearing SCID Mice Treated with Interferon-γ-Inducible Protein 10 (IP-10/CXCL10).” *Cancer Immunology, Immunotherapy* 50 (10): 533–38. https://doi.org/10.1007/s00262-001-0231-9.

Arnould, L, M Gelly, F Penault-Llorca, L Benoit, F Bonnetain, C Migeon, V Cabaret, et al. 2006. “Trastuzumab-Based Treatment of HER2-Positive

Breast Cancer: An Antibody-Dependent Cellular Cytotoxicity Mechanism?" *British Journal of Cancer* 94 (2): 259–67. https://doi.org/10.1038/sj.bjc.6602930.

Atapattu, Lakmali, Nayanendu Saha, Chanly Chheang, Moritz F. Eissman, Kai Xu, Mary E. Vail, Linda Hii, et al. 2016. "An Activated Form of ADAM10 Is Tumor Selective and Regulates Cancer Stem-like Cells and Tumor Growth." *Journal of Experimental Medicine* 213 (9): 1741–57. https://doi.org/10.1084/jem.20151095.

Barok, Mark, Heikki Joensuu, and Jorma Isola. 2014. "Trastuzumab Emtansine: Mechanisms of Action and Drug Resistance." *Breast Cancer Research*. https://doi.org/10.1186/bcr3621.

Barrett, Michael T., Elizabeth Lenkiewicz, Smriti Malasi, Anamika Basu, Jennifer Holmes Yearley, Lakshmanan Annamalai, Ann E. McCullough, et al. 2018. "The Association of Genomic Lesions and PD-1/PD-L1 Expression in Resected Triple-Negative Breast Cancers." *Breast Cancer Research* 20 (1): 71. https://doi.org/10.1186/s13058-018-1004-0.

Bartlett, John M.S., Jane Bayani, Andrea Marshall, Janet A. Dunn, Amy Campbell, Carrie Cunningham, Monika S. Sobol, et al. 2016. "Comparing Breast Cancer Multiparameter Tests in the OPTIMA Prelim Trial: No Test Is More Equal Than the Others." *Journal of the National Cancer Institute* 108 (9). https://doi.org/10.1093/jnci/djw050.

Baselga, J. 2010. "Treatment of HER2-Overexpressing Breast Cancer." *Annals of Oncology : Official Journal of the European Society for Medical Oncology* 21 Suppl 7 (October): vii36-40. https://doi.org/10.1093/annonc/mdq421.

Bazan, J. Fernando, Kevin B. Bacon, Gary Hardiman, Wei Wang, Ken Soo, Devora Rossi, David R. Greaves, Albert Zlotnik, and Thomas J. Schall. 1997. "A New Class of Membrane-Bound Chemokine with a CX3C Motif." *Nature* 385 (6617): 640–44. https://doi.org/10.1038/385640a0.

Bedognetti, D, T L Spivey, Y Zhao, L Uccellini, S Tomei, M E Dudley, M L Ascierto, et al. 2013. "CXCR3/CCR5 Pathways in Metastatic Melanoma Patients Treated with Adoptive Therapy and Interleukin-2." *British Journal of Cancer* 109 (9): 2412–23. https://doi.org/10.1038/bjc.2013.557.

Billottet, Clotilde, Cathy Quemener, and Andreas Bikfalvi. 2013. "CXCR3, a Double-Edged Sword in Tumor Progression and Angiogenesis." *Biochimica et Biophysica Acta* 1836 (2): 287–95. https://doi.org/10.1016/j.bbcan.2013.08.002.

Blum, D. L., T. Koyama, A. E. M'Koma, J. M. Iturregui, M. Martinez-Ferrer, C. Uwamariya, J. A. Smith, P. E. Clark, and N. A. Bhowmick. 2008. "Chemokine Markers Predict Biochemical Recurrence of Prostate Cancer Following Prostatectomy." *Clinical Cancer Research* 14 (23): 7790–97. https://doi.org/10.1158/1078-0432.CCR-08-1716.

Bourd-Boittin, Katia, Laetitia Basset, Dominique Bonnier, Annie

L'Helgoualc'h, Michel Samson, and Nathalie Théret. 2009. "CX3CL1/Fractalkine Shedding by Human Hepatic Stellate Cells: Contribution to Chronic Inflammation in the Liver." *Journal of Cellular and Molecular Medicine* 13 (8a): 1526–35. https://doi.org/10.1111/j.1582-4934.2009.00787.x.

Branellec, Didier, Patricia De Cremoux, Patricia Barreau, Fabien Calvo, and Salem Chouaib. 1992. "Tumor Necrosis Factor-Mediated Cell Lysisin Vitro: Relationship to CAMP Accumulation and Guanine Nucleotide-Binding Proteins." *European Journal of Immunology* 22 (4): 963–67. https://doi.org/10.1002/eji.1830220413.

Brierley, James, M. K. (Mary K.) Gospodarowicz, and Ch. (Christian) Wittekind. 2017. *TNM Classification of Malignant Tumours*. https://www.wiley.com/en-us/TNM+Classification+of+Malignant+Tumours%2C+8th+Edition-p-9781119263579.

Bronger, Holger, Sara Kraeft, Ulrike Schwarz-Boeger, Claudia Cerny, Alexandra Stöckel, Stefanie Avril, Marion Kiechle, and Manfred Schmitt. 2012. "Modulation of CXCR3 Ligand Secretion by Prostaglandin E2 and Cyclooxygenase Inhibitors in Human Breast Cancer." *Breast Cancer Research* 14 (1): R30. https://doi.org/10.1186/bcr3115.

Bronger, Holger, Viktor Magdolen, Peter Goettig, and Tobias Dreyer. 2019. "Proteolytic Chemokine Cleavage as a Regulator of Lymphocytic Infiltration in Solid Tumors." *Cancer Metastasis Reviews* 38 (3): 417–30. https://doi.org/10.1007/s10555-019-09807-3.

Bronger, Holger, Judith Singer, Claudia Windmüller, Ute Reuning, Daniela Zech, Claire Delbridge, Julia Dorn, et al. 2016. "CXCL9 and CXCL10 Predict Survival and Are Regulated by Cyclooxygenase Inhibition in Advanced Serous Ovarian Cancer." *British Journal of Cancer* 115 (5): 553–63. https://doi.org/10.1038/bjc.2016.172.

Bronte, Vincenzo, and Mikael J Pittet. 2013. "The Spleen in Local and Systemic Regulation of Immunity." *Immunity* 39 (5): 806–18. https://doi.org/10.1016/j.immuni.2013.10.010.

Bryant, Helen E., Niklas Schultz, Huw D. Thomas, Kayan M. Parker, Dan Flower, Elena Lopez, Suzanne Kyle, Mark Meuth, Nicola J. Curtin, and Thomas Helleday. 2005. "Specific Killing of BRCA2-Deficient Tumours with Inhibitors of Poly(ADP-Ribose) Polymerase." *Nature* 434 (7035): 913–17. https://doi.org/10.1038/nature03443.

Budczies, Jan, Michael Bockmayr, Carsten Denkert, Frederick Klauschen, Jochen K Lennerz, Balázs Györffy, Manfred Dietel, Sibylle Loibl, Wilko Weichert, and Albrecht Stenzinger. 2015. "Classical Pathology and Mutational Load of Breast Cancer - Integration of Two Worlds." *The Journal of Pathology. Clinical Research* 1 (4): 225–38. https://doi.org/10.1002/cjp2.25.

Burstein, Harold J., Kornelia Polyak, Julia S. Wong, Susan C. Lester, and Carolyn M. Kaelin. 2004. "Ductal Carcinoma in Situ of the Breast." *New*

England Journal of Medicine 350 (14): 1430–41. https://doi.org/10.1056/NEJMra031301.

Byler, Shannon, Sarah Goldgar, Sarah Heerboth, Meghan Leary, Genevieve Housman, Kimberly Moulton, and Sibaji Sarkar. 2014. “Genetic and Epigenetic Aspects of Breast Cancer Progression and Therapy.” *Anticancer Research*. International Institute of Anticancer Research.

Cairns, John. 1975. “Mutation Selection and the Natural History of Cancer.” *Nature* 255 (5505): 197–200. https://doi.org/10.1038/255197a0.

Carter, P, L Presta, C M Gorman, J B Ridgway, D Henner, W L Wong, A M Rowland, C Kotts, M E Carver, and H M Shepard. 1992. “Humanization of an Anti-P185HER2 Antibody for Human Cancer Therapy.” *Proceedings of the National Academy of Sciences of the United States of America* 89 (10): 4285–89. http://www.ncbi.nlm.nih.gov/pubmed/1350088.

Chandrasekar, Bysani, Srinivas Mummidi, Rao P. PERLA, Sailaja BYSANI, Nickolai O. DULIN, Feng LIU, and Peter C. MELBY. 2003. “Fractalkine (CX3CL1) Stimulated by Nuclear Factor KappaB (NF-KappaB)-Dependent Inflammatory Signals Induces Aortic Smooth Muscle Cell Proliferation through an Autocrine Pathway.” *Biochemical Journal* 373 (2): 547–58. https://doi.org/10.1042/bj20030207.

Chandrasekar, Bysani, Srinivas Mummidi, Rao P Perla, Sailaja Bysani, Nickolai O Dulin, Feng Liu, and Peter C Melby. 2003. “Fractalkine (CX3CL1) Stimulated by Nuclear Factor KappaB (NF-KappaB)-Dependent Inflammatory Signals Induces Aortic Smooth Muscle Cell Proliferation through an Autocrine Pathway.” *The Biochemical Journal* 373 (Pt 2): 547–58. https://doi.org/10.1042/BJ20030207.

Chang, Kai Ping, Chih Ching Wu, Ku Hao Fang, Chi Ying Tsai, Yu Liang Chang, Shiau Chin Liu, and Huang Kai Kao. 2013. “Serum Levels of Chemokine (C-X-C Motif) Ligand 9 (CXCL9) Are Associated with Tumor Progression and Treatment Outcome in Patients with Oral Cavity Squamous Cell Carcinoma.” *Oral Oncology* 49 (8): 802–7. https://doi.org/10.1016/j.oraloncology.2013.05.006.

Chen, Daniel S., and Ira Mellman. 2013a. “Oncology Meets Immunology: The Cancer-Immunity Cycle.” *Immunity*. https://doi.org/10.1016/j.immuni.2013.07.012.

Chen, Daniel S, and Ira Mellman. 2013b. “Oncology Meets Immunology: The Cancer-Immunity Cycle.” *Immunity* 39 (1): 1–10. https://doi.org/10.1016/j.immuni.2013.07.012.

Chheda, Zinal S, Rajesh K Sharma, Venkatakrishna R Jala, Andrew D Luster, and Bodduluri Haribabu. 2016. “Chemoattractant Receptors BLT1 and CXCR3 Regulate Antitumor Immunity by Facilitating CD8+ T Cell Migration into Tumors.” *Journal of Immunology (Baltimore, Md. : 1950)* 197 (5): 2016–26. https://doi.org/10.4049/jimmunol.1502376.

Chittezhath, Manesh, Manprit Kaur Dhillon, Jyue Yuan Lim, Damya Laoui,

Irina N. Shalova, Yi Ling Teo, Jinmiao Chen, et al. 2014. “Molecular Profiling Reveals a Tumor-Promoting Phenotype of Monocytes and Macrophages in Human Cancer Progression.” *Immunity* 41 (5): 815–29. https://doi.org/10.1016/j.immuni.2014.09.014.

Colvin, Richard A., Gabriele S.V. Campanella, Jieti Sun, and Andrew D. Luster. 2004. “Intracellular Domains of CXCR3 That Mediate CXCL9, CXCL10, and CXCL11 Function.” *Journal of Biological Chemistry* 279 (29): 30219–27. https://doi.org/10.1074/jbc.M403595200.

Connolly, E M, J H Harmey, T O’Grady, D Foley, G Roche-Nagle, E Kay, and D J Bouchier-Hayes. 2002. “Cyclo-Oxygenase Inhibition Reduces Tumour Growth and Metastasis in an Orthotopic Model of Breast Cancer.” *British Journal of Cancer* 87 (2): 231–37. https://doi.org/10.1038/sj.bjc.6600462.

Cooley, S, L J Burns, T Repka, and J S Miller. 1999. “Natural Killer Cell Cytotoxicity of Breast Cancer Targets Is Enhanced by Two Distinct Mechanisms of Antibody-Dependent Cellular Cytotoxicity against LFA-3 and HER2/Neu.” *Experimental Hematology* 27 (10): 1533–41. http://www.ncbi.nlm.nih.gov/pubmed/10517495.

Dangaj, Denarda, Marine Bruand, Alizée J. Grimm, Catherine Ronet, David Barras, Priyanka A. Duttagupta, Evripidis Lanitis, et al. 2019. “Cooperation between Constitutive and Inducible Chemokines Enables T Cell Engraftment and Immune Attack in Solid Tumors.” *Cancer Cell* 35 (6): 885-900.e10. https://doi.org/10.1016/j.ccell.2019.05.004.

Denkert, C., G. von Minckwitz, J. C. Brase, B. V. Sinn, S. Gade, R. Kronenwett, B. M. Pfitzner, et al. 2014. “Tumor-Infiltrating Lymphocytes and Response to Neoadjuvant Chemotherapy With or Without Carboplatin in Human Epidermal Growth Factor Receptor 2-Positive and Triple-Negative Primary Breast Cancers.” *Journal of Clinical Oncology*, December. https://doi.org/10.1200/JCO.2014.58.1967.

Denkert, Carsten, Sibylle Loibl, Aurelia Noske, Marc Roller, Berit Maria Müller, Martina Komor, Jan Budczies, et al. 2010. “Tumor-Associated Lymphocytes as an Independent Predictor of Response to Neoadjuvant Chemotherapy in Breast Cancer.” *Journal of Clinical Oncology : Official Journal of the American Society of Clinical Oncology* 28 (1): 105–13. https://doi.org/10.1200/JCO.2009.23.7370.

Denkert, Carsten, Gunter von Minckwitz, Jan C Brase, Bruno V Sinn, Stephan Gade, Ralf Kronenwett, Berit M Pfitzner, et al. 2015. “Tumor-Infiltrating Lymphocytes and Response to Neoadjuvant Chemotherapy with or without Carboplatin in Human Epidermal Growth Factor Receptor 2-Positive and Triple-Negative Primary Breast Cancers.” *Journal of Clinical Oncology : Official Journal of the American Society of Clinical Oncology* 33 (9): 983–91. https://doi.org/10.1200/JCO.2014.58.1967.

Denkert, Carsten, Gunter von Minckwitz, Silvia Darb-Esfahani, Bianca Lederer, Barbara I Heppner, Karsten E Weber, Jan Budczies, et al. 2017. “Tumour-Infiltrating Lymphocytes and Prognosis in Different Subtypes of Breast Cancer: A Pooled Analysis of 3771 Patients

Treated with Neoadjuvant Therapy." *The Lancet Oncology* 0 (0): 1–11. https://doi.org/10.1016/S1470-2045(17)30904-X.

———. 2018. "Tumour-Infiltrating Lymphocytes and Prognosis in Different Subtypes of Breast Cancer: A Pooled Analysis of 3771 Patients Treated with Neoadjuvant Therapy." *The Lancet. Oncology* 19 (1): 40–50. https://doi.org/10.1016/S1470-2045(17)30904-X.

Dieci, M V, N Radosevic-Robin, S Fineberg, G van den Eynden, N Ternes, F Penault-Llorca, G Pruneri, et al. 2018. "Update on Tumor-Infiltrating Lymphocytes (TILs) in Breast Cancer, Including Recommendations to Assess TILs in Residual Disease after Neoadjuvant Therapy and in Carcinoma in Situ: A Report of the International Immuno-Oncology Biomarker Working Group on Bre." *Semin Cancer Biol* 52 (Pt 2): 16–25. https://doi.org/10.1016/j.semcancer.2017.10.003.

Duffy, M. J., N. Harbeck, M. Nap, R. Molina, A. Nicolini, E. Senkus, and F. Cardoso. 2017. "Clinical Use of Biomarkers in Breast Cancer: Updated Guidelines from the European Group on Tumor Markers (EGTM)." *European Journal of Cancer*. Elsevier Ltd. https://doi.org/10.1016/j.ejca.2017.01.017.

Dushyanthen, Sathana, Paul A. Beavis, Peter Savas, Zhi Ling Teo, Chenhao Zhou, Mariam Mansour, Phillip K. Darcy, and Sherene Loi. 2015. "Relevance of Tumor-Infiltrating Lymphocytes in Breast Cancer." *BMC Medicine* 13 (1): 202. https://doi.org/10.1186/s12916-015-0431-3.

Early Breast Cancer Trialists' Collaborative Group (EBCTCG). 2005. "Effects of Chemotherapy and Hormonal Therapy for Early Breast Cancer on Recurrence and 15-Year Survival: An Overview of the Randomised Trials." *Lancet (London, England)* 365 (9472): 1687–1717. https://doi.org/10.1016/S0140-6736(05)66544-0.

Early Breast Cancer Trialists' Collaborative Group (EBCTCG), C Davies, J Godwin, R Gray, M Clarke, D Cutter, S Darby, et al. 2011. "Relevance of Breast Cancer Hormone Receptors and Other Factors to the Efficacy of Adjuvant Tamoxifen: Patient-Level Meta-Analysis of Randomised Trials." *The Lancet* 378 (9793): 771–84. https://doi.org/10.1016/S0140-6736(11)60993-8.

Easton, Douglas F., Karen A. Pooley, Alison M. Dunning, Paul D. P. Pharoah, Deborah Thompson, Dennis G. Ballinger, Jeffery P. Struewing, et al. 2007. "Genome-Wide Association Study Identifies Novel Breast Cancer Susceptibility Loci." *Nature* 447 (7148): 1087–93. https://doi.org/10.1038/nature05887.

Ehlert, Jan Erik, Christina A. Addison, Marie D. Burdick, Steven L. Kunkel, and Robert M. Strieter. 2004. "Identification and Partial Characterization of a Variant of Human CXCR3 Generated by Posttranscriptional Exon Skipping." *The Journal of Immunology* 173 (10): 6234–40. https://doi.org/10.4049/jimmunol.173.10.6234.

Ejaeidi, Ahmed A, Barbara S Craft, Louis V Puneky, Robert E Lewis, and Julius M Cruse. 2015. "Hormone Receptor-Independent CXCL10

Production Is Associated with the Regulation of Cellular Factors Linked to Breast Cancer Progression and Metastasis." *Experimental and Molecular Pathology* 99 (1): 163–72. https://doi.org/10.1016/j.yexmp.2015.06.002.

Elston, C W, and I O Ellis. 1991. "Pathological Prognostic Factors in Breast Cancer. I. The Value of Histological Grade in Breast Cancer: Experience from a Large Study with Long-Term Follow-Up." *Histopathology* 19 (5): 403–10. http://www.ncbi.nlm.nih.gov/pubmed/1757079.

Erreni, Marco, Imran Siddiqui, Giulia Marelli, Fabio Grizzi, Paolo Bianchi, Diego Morone, Federica Marchesi, et al. 2016. "The Fractalkine-Receptor Axis Improves Human Colorectal Cancer Prognosis by Limiting Tumor Metastatic Dissemination." *The Journal of Immunology* 196 (2): 902–14. https://doi.org/10.4049/jimmunol.1501335.

Farber, J M. 1997. "Mig and IP-10: CXC Chemokines That Target Lymphocytes." *Journal of Leukocyte Biology* 61 (3): 246–57. http://www.ncbi.nlm.nih.gov/pubmed/9060447.

Fogel, Mina, Paul Gutwein, Sabine Mechtersheimer, Svenja Riedle, Alexander Stoeck, Asya Smirnov, Lutz Edler, Alon Ben-Arie, Monica Huszar, and Peter Altevogt. 2003. "L1 Expression as a Predictor of Progression and Survival in Patients with Uterine and Ovarian Carcinomas." *Lancet* 362 (9387): 869–75. https://doi.org/10.1016/S0140-6736(03)14342-5.

Fonović, Urša Pečar, Zala Jevnikar, and Janko Kos. 2013. "Cathepsin S Generates Soluble CX3CL1 (Fractalkine) in Vascular Smooth Muscle Cells." *Biological Chemistry* 394 (10). https://doi.org/10.1515/hsz-2013-0189.

Fridman, W H, L Zitvogel, C Sautes-Fridman, and G Kroemer. 2017. "The Immune Contexture in Cancer Prognosis and Treatment." *Nat Rev Clin Oncol* 14 (12): 717–34. https://doi.org/10.1038/nrclinonc.2017.101.

García-López, M A, F Sánchez-Madrid, J M Rodríguez-Frade, M Mellado, A Acevedo, M I García, J P Albar, C Martínez, and M Marazuela. 2001. "CXCR3 Chemokine Receptor Distribution in Normal and Inflamed Tissues: Expression on Activated Lymphocytes, Endothelial Cells, and Dendritic Cells." *Laboratory Investigation; a Journal of Technical Methods and Pathology* 81 (3): 409–18. http://www.ncbi.nlm.nih.gov/pubmed/11310833.

García-Martínez, Elena, Ginés Luengo Gil, Asunción Chaves Benito, Enrique González-Billalabeitia, María Angeles Vicente Conesa, Teresa García García, Elisa García-Garre, Vicente Vicente, and Francisco Ayala de la Peña. 2014. "Tumor-Infiltrating Immune Cell Profiles and Their Change after Neoadjuvant Chemotherapy Predict Response and Prognosis of Breast Cancer." *Breast Cancer Research : BCR* 16 (6): 488. https://doi.org/10.1186/s13058-014-0488-5.

Garton, K J, P J Gough, C P Blobel, G Murphy, D R Greaves, P J Dempsey, and E W Raines. 2001. "Tumor Necrosis Factor-Alpha-Converting

Enzyme (ADAM17) Mediates the Cleavage and Shedding of Fractalkine (CX3CL1).” *The Journal of Biological Chemistry* 276 (41): 37993–1. https://doi.org/10.1074/jbc.M106434200.

Gavert, Nancy, Maralice Conacci-Sorrell, Daniela Gast, Annette Schneider, Peter Altevogt, Thomas Brabletz, and Avri Ben-Ze’Ev. 2005. “L1, a Novel Target of β-Catenin Signaling, Transforms Cells and Is Expressed at the Invasive Front of Colon Cancers.” *Journal of Cell Biology* 168 (4): 633–42. https://doi.org/10.1083/jcb.200408051.

Goda, S, T Imai, O Yoshie, O Yoneda, H Inoue, Y Nagano, T Okazaki, et al. 2000. “CX3C-Chemokine, Fractalkine-Enhanced Adhesion of THP-1 Cells to Endothelial Cells through Integrin-Dependent and -Independent Mechanisms.” *Journal of Immunology (Baltimore, Md. : 1950)* 164 (8): 4313–20. http://www.ncbi.nlm.nih.gov/pubmed/10754331.

Goldhirsch, A., W. C. Wood, A. S. Coates, R. D. Gelber, B. Thürlimann, and H. J. Senn. 2011. “Strategies for Subtypes-Dealing with the Diversity of Breast Cancer: Highlights of the St Gallen International Expert Consensus on the Primary Therapy of Early Breast Cancer 2011.” *Annals of Oncology* 22 (8): 1736–47. https://doi.org/10.1093/annonc/mdr304.

Gorbachev, a. V., H. Kobayashi, D. Kudo, C. S. Tannenbaum, J. H. Finke, S. Shu, J. M. Farber, and R. L. Fairchild. 2007. “CXC Chemokine Ligand 9/Monokine Induced by IFN- Production by Tumor Cells Is Critical for T Cell-Mediated Suppression of Cutaneous Tumors.” *The Journal of Immunology* 178 (4): 2278–86. https://doi.org/10.4049/jimmunol.178.4.2278.

Gorbachev, Anton V, Hirohito Kobayashi, Daisuke Kudo, Charles S Tannenbaum, James H Finke, Suyu Shu, Joshua M Farber, and Robert L Fairchild. 2007. “CXC Chemokine Ligand 9/Monokine Induced by IFN-Gamma Production by Tumor Cells Is Critical for T Cell-Mediated Suppression of Cutaneous Tumors.” *Journal of Immunology (Baltimore, Md.: 1950)* 178 (4): 2278–86. http://www.ncbi.nlm.nih.gov/pubmed/17277133.

Groom, Joanna R, and Andrew D Luster. 2011. “CXCR3 Ligands: Redundant, Collaborative and Antagonistic Functions.” *Immunology and Cell Biology* 89 (2): 207–15. https://doi.org/10.1038/icb.2010.158.

———. 2012. “CXCR3 in T Cell Function” 317 (5): 620–31. https://doi.org/10.1016/j.yexcr.2010.12.017.CXCR3.

Groom, Joanna R, Jillian Richmond, Thomas T Murooka, Elizabeth W Sorensen, Jung Hwan Sung, Katherine Bankert, Ulrich H von Andrian, James J Moon, Thorsten R Mempel, and Andrew D Luster. 2012. “CXCR3 Chemokine Receptor-Ligand Interactions in the Lymph Node Optimize CD4+ T Helper 1 Cell Differentiation.” *Immunity* 37 (6): 1091–1103. https://doi.org/10.1016/j.immuni.2012.08.016.

Guo, J, T Chen, B Wang, M Zhang, H An, Z Guo, Y Yu, Z Qin, and X Cao. 2003. “Chemoattraction, Adhesion and Activation of Natural Killer Cells

Are Involved in the Antitumor Immune Response Induced by Fractalkine/CX3CL1." *Immunology Letters* 89 (1): 1–7. http://www.ncbi.nlm.nih.gov/pubmed/12946858.

Guo, Jun, Taoyong Chen, Baocheng Wang, Minghui Zhang, Huazhang An, Zhenhong Guo, Yizhi Yu, Zhihai Qin, and Xuetao Cao. 2003. "Chemoattraction, Adhesion and Activation of Natural Killer Cells Are Involved in the Antitumor Immune Response Induced by Fractalkine/CX3CL1." *Immunology Letters* 89 (1): 1–7. https://doi.org/10.1016/S0165-2478(03)00101-9.

Győrffy, Balazs, Andras Lanczky, Aron C. Eklund, Carsten Denkert, Jan Budczies, Qiyuan Li, and Zoltan Szallasi. 2010. "An Online Survival Analysis Tool to Rapidly Assess the Effect of 22,277 Genes on Breast Cancer Prognosis Using Microarray Data of 1,809 Patients." *Breast Cancer Research and Treatment* 123 (3): 725–31. https://doi.org/10.1007/s10549-009-0674-9.

Hannesdóttir, Lára, Piotr Tymoszuk, Nirmala Parajuli, Marie-Helene Wasmer, Sonja Philipp, Nina Daschil, Sebak Datta, et al. 2013. "Lapatinib and Doxorubicin Enhance the Stat1-Dependent Antitumor Immune Response." *European Journal of Immunology* 43 (10): 2718–29. https://doi.org/10.1002/eji.201242505.

Harris, Gavin C, Helen E Denley, Sarah E Pinder, Andrew H S Lee, Ian O Ellis, Christopher W Elston, and Andrew Evans. 2003. "Correlation of Histologic Prognostic Factors in Core Biopsies and Therapeutic Excisions of Invasive Breast Carcinoma." *The American Journal of Surgical Pathology* 27 (1): 11–15. http://www.ncbi.nlm.nih.gov/pubmed/12502923.

Harrison, J K, A M Fong, P A Swain, S Chen, Y R Yu, M N Salafranca, W B Greenleaf, T Imai, and D D Patel. 2001. "Mutational Analysis of the Fractalkine Chemokine Domain. Basic Amino Acid Residues Differentially Contribute to CX3CR1 Binding, Signaling, and Cell Adhesion." *The Journal of Biological Chemistry* 276 (24): 21632–41. https://doi.org/10.1074/jbc.M010261200.

Hartl, Dominik, Susanne Krauss-Etschmann, Barbara Koller, Peter L Hordijk, Taco W Kuijpers, Florian Hoffmann, Andreas Hector, et al. 2008. "Infiltrated Neutrophils Acquire Novel Chemokine Receptor Expression and Chemokine Responsiveness in Chronic Inflammatory Lung Diseases." *Journal of Immunology (Baltimore, Md.: 1950)* 181 (11): 8053–67. http://www.ncbi.nlm.nih.gov/pubmed/19017998.

Hasegawa, H, A Inoue, M Kohno, J Lei, T Miyazaki, O Yoshie, M Nose, and M Yasukawa. 2008. "Therapeutic Effect of CXCR3-Expressing Regulatory T Cells on Liver, Lung and Intestinal Damages in a Murine Acute GVHD Model." *Gene Therapy* 15 (3): 171–82. https://doi.org/10.1038/sj.gt.3303051.

Haskell, C A, M D Cleary, and I F Charo. 2000. "Unique Role of the Chemokine Domain of Fractalkine in Cell Capture. Kinetics of Receptor Dissociation Correlate with Cell Adhesion." *The Journal of Biological Chemistry* 275 (44): 34183–89.

https://doi.org/10.1074/jbc.M005731200.

Hellwig, Birte. 2019. “Highlight Report: Tumor Infiltrating Lymphocytes in Breast Cancer.” *EXCLI Journal* 18: 129.

Hendrickx, Wouter, Ines Simeone, Samreen Anjum, Younes Mokrab, François Bertucci, Pascal Finetti, Giuseppe Curigliano, et al. 2017. “Identification of Genetic Determinants of Breast Cancer Immune Phenotypes by Integrative Genome-Scale Analysis.” *OncoImmunology* 6. https://doi.org/10.1080/2162402X.2016.1253654.

Hickman, Heather D., Glennys V. Reynoso, Barbara F. Ngudiankama, Stephanie S. Cush, James Gibbs, Jack R. Bennink, and Jonathan W. Yewdell. 2015. “CXCR3 Chemokine Receptor Enables Local CD8+ T Cell Migration for the Destruction of Virus-Infected Cells.” *Immunity* 42 (3): 524–37. https://doi.org/10.1016/j.immuni.2015.02.009.

Holbro, Thomas, Gianluca Civenni, and Nancy E Hynes. 2003. “The ErbB Receptors and Their Role in Cancer Progression.” *Experimental Cell Research* 284 (1): 99–110. http://www.ncbi.nlm.nih.gov/pubmed/12648469.

Hong, M., A.-L. Puaux, C. Huang, L. Loumagne, C. Tow, C. Mackay, M. Kato, et al. 2011. “Chemotherapy Induces Intratumoral Expression of Chemokines in Cutaneous Melanoma, Favoring T-Cell Infiltration and Tumor Control.” *Cancer Research* 71 (22): 6997–7009. https://doi.org/10.1158/0008-5472.CAN-11-1466.

House, Imran G., Peter Savas, Junyun Lai, Amanda X.Y. Chen, Amanda J. Oliver, Zhi L. Teo, Kirsten L. Todd, et al. 2020. “Macrophage-Derived CXCL9 and CXCL10 Are Required for Antitumor Immune Responses Following Immune Checkpoint Blockade.” *Clinical Cancer Research* 26 (2): 487–504. https://doi.org/10.1158/1078-0432.CCR-19-1868.

Howe, Louise R. 2007. “Inflammation and Breast Cancer. Cyclooxygenase/Prostaglandin Signaling and Breast Cancer.” *Breast Cancer Research : BCR* 9 (4): 210. https://doi.org/10.1186/bcr1678.

Hsin, Li-Jen, Huang-Kai Kao, I-How Chen, Ngan-Ming Tsang, Cheng-Lung Hsu, Shiau-Chin Liu, Yu-Sun Chang, and Kai-Ping Chang. 2013. “Serum CXCL9 Levels Are Associated with Tumor Progression and Treatment Outcome in Patients with Nasopharyngeal Carcinoma.” Edited by Maria G. Masucci. *PLoS ONE* 8 (11): e80052. https://doi.org/10.1371/journal.pone.0080052.

Hu, J. K., T. Kagari, J. M. Clingan, and M. Matloubian. 2011. “Expression of Chemokine Receptor CXCR3 on T Cells Affects the Balance between Effector and Memory CD8 T-Cell Generation.” *Proceedings of the National Academy of Sciences* 108 (21): E118–27. https://doi.org/10.1073/pnas.1101881108.

Hu, Shuai, Lei Li, Shuyuan Yeh, Yun Cui, Xin Li, Hong-Chiang Chang, Jie Jin, and Chawnshang Chang. 2015. “Infiltrating T Cells Promote Prostate Cancer Metastasis via Modulation of FGF11→miRNA-541→androgen Receptor (AR)→MMP9 Signaling.” *Molecular*

Oncology 9 (1): 44–57. https://doi.org/10.1016/j.molonc.2014.07.013.

Hundhausen, Christian, Dominika Misztela, Theo A Berkhout, Neil Broadway, Paul Saftig, Karina Reiss, Dieter Hartmann, et al. 2003. “The Disintegrin-like Metalloproteinase ADAM10 Is Involved in Constitutive Cleavage of CX3CL1 (Fractalkine) and Regulates CX3CL1-Mediated Cell-Cell Adhesion.” *Blood* 102 (4): 1186–95. https://doi.org/10.1182/blood-2002-12-3775.

Hunter, David J, Peter Kraft, Kevin B Jacobs, David G Cox, Meredith Yeager, Susan E Hankinson, Sholom Wacholder, et al. 2007. “A Genome-Wide Association Study Identifies Alleles in FGFR2 Associated with Risk of Sporadic Postmenopausal Breast Cancer.” *Nature Genetics* 39 (7): 870–74. https://doi.org/10.1038/ng2075.

Hussein, M R, and H I Hassan. 2006. “Analysis of the Mononuclear Inflammatory Cell Infiltrate in the Normal Breast, Benign Proliferative Breast Disease, in Situ and Infiltrating Ductal Breast Carcinomas: Preliminary Observations.” *Journal of Clinical Pathology* 59 (9): 972–77. https://doi.org/10.1136/jcp.2005.031252.

Hyakudomi, Miki, Takeshi Matsubara, Ryoji Hyakudomi, Tetsu Yamamoto, Shoichi Kinugasa, Akira Yamanoi, Riruke Maruyama, and Tsuneo Tanaka. 2008. “Increased Expression of Fractalkine Is Correlated with a Better Prognosis and an Increased Number of Both CD8+ T Cells and Natural Killer Cells in Gastric Adenocarcinoma.” *Annals of Surgical Oncology* 15 (6): 1775–82. https://doi.org/10.1245/s10434-008-9876-3.

Ikeda, Aki, Nobuhiro Aoki, Masahiro Kido, Satoru Iwamoto, Hisayo Nishiura, Ryutaro Maruoka, Tsutomu Chiba, and Norihiko Watanabe. 2014. “Progression of Autoimmune Hepatitis Is Mediated by IL-18-Producing Dendritic Cells and Hepatic CXCL9 Expression in Mice.” *Hepatology* 60 (1): 224–36. https://doi.org/10.1002/hep.27087.

Inngjerdingen, M, B Damaj, and A A Maghazachi. 2001. “Expression and Regulation of Chemokine Receptors in Human Natural Killer Cells.” *Blood* 97 (2): 367–75. http://www.ncbi.nlm.nih.gov/pubmed/11154210.

Ji, Rui-Ru, Scott D. Chasalow, Lisu Wang, Omid Hamid, Henrik Schmidt, John Cogswell, Suresh Alaparthy, et al. 2012. “An Immune-Active Tumor Microenvironment Favors Clinical Response to Ipilimumab.” *Cancer Immunology, Immunotherapy* 61 (7): 1019–31. https://doi.org/10.1007/s00262-011-1172-6.

Jinquan, T, C Jing, H H Jacobi, C M Reimert, A Millner, S Quan, J B Hansen, et al. 2000. “CXCR3 Expression and Activation of Eosinophils: Role of IFN-Gamma-Inducible Protein-10 and Monokine Induced by IFN-Gamma.” *Journal of Immunology (Baltimore, Md.: 1950)* 165 (3): 1548–56. http://www.ncbi.nlm.nih.gov/pubmed/10903763.

Junttila, Teemu T., Robert W. Akita, Kathryn Parsons, Carter Fields, Gail D. Lewis Phillips, Lori S. Friedman, Deepak Sampath, and Mark X. Sliwkowski. 2009. “Ligand-Independent HER2/HER3/PI3K Complex Is Disrupted by Trastuzumab and Is Effectively Inhibited by the PI3K

Inhibitor GDC-0941." *Cancer Cell* 15 (5): 429–40. https://doi.org/10.1016/j.ccr.2009.03.020.

Kanagawa, Naoko, Masakazu Niwa, Yutaka Hatanaka, Yoichi Tani, Shinsaku Nakagawa, Takuya Fujita, Akira Yamamoto, and Naoki Okada. 2007. "CC-Chemokine Ligand 17 Gene Therapy Induces Tumor Regression through Augmentation of Tumor-Infiltrating Immune Cells in a Murine Model of Preexisting CT26 Colon Carcinoma." *International Journal of Cancer* 121 (9): 2013–22. https://doi.org/10.1002/ijc.22908.

Karin, Nathan, and Gizi Wildbaum. 2015. "The Role of Chemokines in Shaping the Balance Between CD4(+) T Cell Subsets and Its Therapeutic Implications in Autoimmune and Cancer Diseases." *Frontiers in Immunology* 6: 609. https://doi.org/10.3389/fimmu.2015.00609.

Kee, Ji-Ye, Yoshihisa Arita, Kanna Shinohara, Yasukata Ohashi, Hiroaki Sakurai, Ikuo Saiki, and Keiichi Koizumi. 2013. "Antitumor Immune Activity by Chemokine CX3CL1 in an Orthotopic Implantation of Lung Cancer Model in Vivo." *Molecular and Clinical Oncology* 1 (1): 35–40. https://doi.org/10.3892/mco.2012.30.

Kehlen, Astrid, Thomas Greither, Sven Wach, Elke Nolte, Matthias Kappler, Matthias Bache, Hans Jürgen Holzhausen, et al. 2014. "High Coexpression of CCL2 and CX3CL1 Is Gender-Specifically Associated with Good Prognosis in Soft Tissue Sarcoma Patients." *International Journal of Cancer* 135 (9): 2096–2106. https://doi.org/10.1002/ijc.28867.

Kim, Sunghyun, Hyejon Lee, Hyunjung Kim, Yeun Kim, Jang-Eun Cho, Hyunwoo Jin, Dae Yeon Kim, et al. 2015. "Diagnostic Performance of a Cytokine and IFN-γ-Induced Chemokine MRNA Assay after Mycobacterium Tuberculosis-Specific Antigen Stimulation in Whole Blood from Infected Individuals." *The Journal of Molecular Diagnostics : JMD* 17 (1): 90–99. https://doi.org/10.1016/j.jmoldx.2014.08.005.

Klapper, L N, H Waterman, M Sela, and Y Yarden. 2000. "Tumor-Inhibitory Antibodies to HER-2/ErbB-2 May Act by Recruiting c-Cbl and Enhancing Ubiquitination of HER-2." *Cancer Research* 60 (13): 3384–88. http://www.ncbi.nlm.nih.gov/pubmed/10910043.

Ko, Shun-Yao, Shu-Chun Lin, Yong-Kie Wong, Chung-Ji Liu, Kuo-Wei Chang, and Tsung-Yun Liu. 2007. "Increase of Disintergin Metalloprotease 10 (ADAM10) Expression in Oral Squamous Cell Carcinoma." *Cancer Letters* 245 (1–2): 33–43. https://doi.org/10.1016/j.canlet.2005.10.019.

Kotoula, Vassiliki, Sotiris Lakis, Ioannis S. Vlachos, Eleni Giannoulatou, Flora Zagouri, Zoi Alexopoulou, Helen Gogas, et al. 2016. "Tumor Infiltrating Lymphocytes Affect the Outcome of Patients with Operable Triple-Negative Breast Cancer in Combination with Mutated Amino Acid Classes." Edited by Wei Xu. *PLOS ONE* 11 (9): e0163138. https://doi.org/10.1371/journal.pone.0163138.

Kryczek, I., M. Banerjee, P. Cheng, L. Vatan, W. Szeliga, S. Wei, E. Huang, et al. 2009. “Phenotype, Distribution, Generation, and Functional and Clinical Relevance of Th17 Cells in the Human Tumor Environments.” *Blood* 114 (6): 1141–49. https://doi.org/10.1182/blood-2009-03-208249.

Kundu, Namita, Xinrong Ma, Dawn Holt, Olga Goloubeva, Suzanne Ostrand-Rosenberg, and Amy M. Fulton. 2009. “Antagonism of the Prostaglandin E Receptor EP4 Inhibits Metastasis and Enhances NK Function.” *Breast Cancer Research and Treatment* 117 (2): 235–42. https://doi.org/10.1007/s10549-008-0180-5.

Kundu, Namita, Tonya C. Walser, Xinrong Ma, and Amy M. Fulton. 2005. “Cyclooxygenase Inhibitors Modulate NK Activities That Control Metastatic Disease.” *Cancer Immunology, Immunotherapy* 54 (10): 981–87. https://doi.org/10.1007/s00262-005-0669-2.

Kuo, Paula T., Zhen Zeng, Nazhifah Salim, Stephen Mattarollo, James W. Wells, and Graham R. Leggatt. 2018. “The Role of CXCR3 and Its Chemokine Ligands in Skin Disease and Cancer.” *Frontiers in Medicine*. Frontiers Media S.A. https://doi.org/10.3389/fmed.2018.00271.

Lavergne, Elise, Behazine Combadière, Olivia Bonduelle, Mutsunori Iga, Ji-Liang Gao, Maud Maho, Alexandre Boissonnas, Philip M Murphy, Patrice Debré, and Christophe Combadière. 2003. “Fractalkine Mediates Natural Killer-Dependent Antitumor Responses in Vivo.” *Cancer Research* 63 (21): 7468–74. http://www.ncbi.nlm.nih.gov/pubmed/14612547.

Lendeckel, Uwe, Jana Kohl, Marco Arndt, Stacy Carl-McGrath, Hans Donat, and Christoph Röcken. 2005. “Increased Expression of ADAM Family Members in Human Breast Cancer and Breast Cancer Cell Lines.” *Journal of Cancer Research and Clinical Oncology* 131 (1): 41–48. https://doi.org/10.1007/s00432-004-0619-y.

Liu, Guang-Ying, Vathany Kulasingam, R Todd Alexander, Nicolas Touret, Alan M Fong, Dhavalkumar D Patel, and Lisa A Robinson. 2005. “Recycling of the Membrane-Anchored Chemokine, CX3CL1.” *The Journal of Biological Chemistry* 280 (20): 19858–66. https://doi.org/10.1074/jbc.M413073200.

Liu, Jian, Yan Li, Xiaoqin Zhu, Qing Li, Xiaohong Liang, Jun Xie, Song Hu, Wanda Peng, and Chong Li. 2019. “Increased CX3CL1 MRNA Expression Level Is a Positive Prognostic Factor in Patients with Lung Adenocarcinoma.” *Oncology Letters* 17 (6): 4877–90. https://doi.org/10.3892/ol.2019.10211.

Liu, Rui-Xian, Yuan Wei, Qiu-Hui Zeng, Ka-Wo Chan, Xiao Xiao, Xiao-Yu Zhao, Min-Min Chen, et al. 2015. “Chemokine (C-X-C Motif) Receptor 3-Positive B Cells Link Interleukin-17 Inflammation to Protumorigenic Macrophage Polarization in Human Hepatocellular Carcinoma.” *Hepatology* 62 (6): 1779–90. https://doi.org/10.1002/hep.28020.

Loetscher, M, B Gerber, P Loetscher, S A Jones, L Piali, I Clark-Lewis, M

Baggiolini, and B Moser. 1996. “Chemokine Receptor Specific for IP10 and Mig: Structure, Function, and Expression in Activated T-Lymphocytes.” *The Journal of Experimental Medicine* 184 (3): 963–69. http://www.ncbi.nlm.nih.gov/pubmed/9064356.

Lu, Huili, Shunying Zhu, Lan Qian, Di Xiang, Wu Zhang, Aifang Nie, Jin Gao, et al. 2012. “Activated Expression of the Chemokine Mig after Chemotherapy Contributes to Chemotherapy-Induced Bone Marrow Suppression and Lethal Toxicity.” *Blood* 119 (21): 4868–77. https://doi.org/10.1182/blood-2011-07-367581.

Lucci, Anthony, Carolyn S Hall, Ashutosh K Lodhi, Anirban Bhattacharyya, Amber E Anderson, Lianchun Xiao, Isabelle Bedrosian, Henry M Kuerer, and Savitri Krishnamurthy. 2012. “Circulating Tumour Cells in Non-Metastatic Breast Cancer: A Prospective Study.” *The Lancet Oncology* 13 (7): 688–95. https://doi.org/10.1016/S1470-2045(12)70209-7.

Ludwig, Andreas, and Christian Weber. 2007. “Transmembrane Chemokines: Versatile ‘special Agents’ in Vascular Inflammation.” *Thrombosis and Haemostasis* 97 (5): 694–703. http://www.ncbi.nlm.nih.gov/pubmed/17479179.

Ma, Xinrong, Namita Kundu, Salah Rifat, Tonya Walser, and Amy M. Fulton. 2006. “Prostaglandin E Receptor EP4 Antagonism Inhibits Breast Cancer Metastasis.” *Cancer Research* 66 (6): 2923–27. https://doi.org/10.1158/0008-5472.CAN-05-4348.

Markosyan, Nune, Edward P Chen, Rebecca A Evans, Victoire Ndong, Robert H Vonderheide, and Emer M Smyth. 2013. “Mammary Carcinoma Cell Derived Cyclooxygenase 2 Suppresses Tumor Immune Surveillance by Enhancing Intratumoral Immune Checkpoint Activity.” *Breast Cancer Research : BCR* 15 (5): R75. https://doi.org/10.1186/bcr3469.

Martin, Miguel, Jan C. Brase, Lourdes Calvo, Kristin Krappmann, Manuel Ruiz-Borrego, Karin Fisch, Amparo Ruiz, et al. 2014. “Clinical Validation of the EndoPredict Test in Node-Positive, Chemotherapy-Treated ER+/HER2- Breast Cancer Patients: Results from the GEICAM 9906 Trial.” *Breast Cancer Research* 16 (2): R38. https://doi.org/10.1186/bcr3642.

Maruvka, Yosef E., Nicholas J. Haradhvala, and Gad Getz. 2019. “Analyzing Frequently Mutated Genes and the Association with Tumor Mutation Load.” *JAMA Oncology*. American Medical Association. https://doi.org/10.1001/jamaoncol.2019.0127.

Mattarollo, S. R., S. Loi, H. Duret, Y. Ma, L. Zitvogel, and M. J. Smyth. 2011. “Pivotal Role of Innate and Adaptive Immunity in Anthracycline Chemotherapy of Established Tumors.” *Cancer Research* 71 (14): 4809–20. https://doi.org/10.1158/0008-5472.CAN-11-0753.

Mayr, D. 2019. *Pathologie Der Mammakarzinome Und Der Intraepithelialen Proliferationen Der Mamma*.

McCulloch, Daniel R., Pascal Akl, Hemamali Samaratunga, Adrian C. Herington, and Dimitri M. Odorico. 2004. “Expression of the Disintegrin Metalloprotease, ADAM-10, in Prostate Cancer and Its Regulation by Dihydrotestosterone, Insulin-Like Growth Factor I, and Epidermal Growth Factor in the Prostate Cancer Cell Model LNCaP.” *Clinical Cancer Research* 10 (1 I): 314–23. https://doi.org/10.1158/1078-0432.CCR-0846-3.

Medoff, Benjamin D, John C Wain, Edward Seung, Ryan Jackobek, Terry K Means, Leo C Ginns, Joshua M Farber, and Andrew D Luster. 2006. “CXCR3 and Its Ligands in a Murine Model of Obliterative Bronchiolitis: Regulation and Function.” *Journal of Immunology (Baltimore, Md.: 1950)* 176 (11): 7087–95. http://www.ncbi.nlm.nih.gov/pubmed/16709871.

Meric-Bernstam, Funda, Amber M. Johnson, Ecaterina E. Ileana Dumbrava, Kanwal Raghav, Kavitha Balaji, Michelle Bhatt, Rashmi K. Murthy, Jordi Rodon, and Sarina A. Piha-Paul. 2019. “Advances in HER2-Targeted Therapy: Novel Agents and Opportunities beyond Breast and Gastric Cancer.” *Clinical Cancer Research*. American Association for Cancer Research Inc. https://doi.org/10.1158/1078-0432.CCR-18-2275.

Metzemaekers, Mieke, Vincent Vanheule, Rik Janssens, Sofie Struyf, and Paul Proost. 2018. “Overview of the Mechanisms That May Contribute to the Non-Redundant Activities of Interferon-Inducible CXC Chemokine Receptor 3 Ligands.” *Frontiers in Immunology* 8: 1970. https://doi.org/10.3389/fimmu.2017.01970.

Miyoshi, Yuichiro, Tadahiko Shien, Akiko Ogiya, Naoko Ishida, Kieko Yamazaki, R. I.E. Horii, Yoshiya Horimoto, et al. 2019. “Associations in Tumor Infiltrating Lymphocytes between Clinicopathological Factors and Clinical Outcomes in Estrogen Receptor-Positive/Human Epidermal Growth Factor Receptor Type 2 Negative Breast Cancer.” *Oncology Letters* 17 (2): 2177–86. https://doi.org/10.3892/ol.2018.9853.

Mlecnik, Bernhard, Marie Tosolini, Pornpimol Charoentong, Amos Kirilovsky, Gabriela Bindea, Anne Berger, Matthieu Camus, et al. 2010. “Biomolecular Network Reconstruction Identifies T-Cell Homing Factors Associated with Survival in Colorectal Cancer.” *Gastroenterology* 138 (4): 1429–40. https://doi.org/10.1053/j.gastro.2009.10.057.

Mohammed, Rabab AA, Stewart G Martin, Ali M Mahmmod, R. Douglas Macmillan, Andrew R Green, Emma C Paish, and Ian O Ellis. 2011. “Objective Assessment of Lymphatic and Blood Vascular Invasion in Lymph Node-Negative Breast Carcinoma: Findings from a Large Case Series with Long-Term Follow-Up.” *The Journal of Pathology* 223 (3): 358–65. https://doi.org/10.1002/path.2810.

Mota, Gabriela, Mioara Manciulea, Ecaterina Cosma, Iulia Popescu, Mirela Hirt, Erika Jensen-Jarolim, Ana Calugaru, et al. 2003. “Human NK Cells Express Fc Receptors for IgA Which Mediate Signal Transduction and Target Cell Killing.” *European Journal of Immunology* 33 (8): 2197–

2205. https://doi.org/10.1002/eji.200323534.

Moulis, Sharon, and Dennis C Sgroi. 2008. “Re-Evaluating Early Breast Neoplasia.” *Breast Cancer Research* 10 (1): 302. https://doi.org/10.1186/bcr1853.

Muehlinghaus, Gwendolin, Luisa Cigliano, Stephan Huehn, Anette Peddinghaus, Heike Leyendeckers, Anja E Hauser, Falk Hiepe, Andreas Radbruch, Sergio Arce, and Rudolf A Manz. 2005. “Regulation of CXCR3 and CXCR4 Expression during Terminal Differentiation of Memory B Cells into Plasma Cells.” *Blood* 105 (10): 3965–71. https://doi.org/10.1182/blood-2004-08-2992.

Mueller, A., A. Meiser, E. M. McDonagh, J. M. Fox, S. J. Petit, G. Xanthou, T. J. Williams, and J. E. Pease. 2008. “CXCL4-Induced Migration of Activated T Lymphocytes Is Mediated by the Chemokine Receptor CXCR3.” *Journal of Leukocyte Biology* 83 (4): 875–82. https://doi.org/10.1189/jlb.1006645.

Mullooly, Maeve, Patricia M. McGowan, Susan A. Kennedy, Stephen F. Madden, John Crown, Norma O’Donovan, and Michael J. Duffy. 2015. “ADAM10: A New Player in Breast Cancer Progression?” *British Journal of Cancer* 113 (6): 945–51. https://doi.org/10.1038/bjc.2015.288.

Murphy, P M, M Baggiolini, I F Charo, C A Hébert, R Horuk, K Matsushima, L H Miller, J J Oppenheim, and C A Power. 2000. “International Union of Pharmacology. XXII. Nomenclature for Chemokine Receptors.” *Pharmacological Reviews* 52 (1): 145–76. http://www.ncbi.nlm.nih.gov/pubmed/10699158.

Muthuswamy, R., J. Urban, J.-J. Lee, T. A. Reinhart, D. Bartlett, and P. Kalinski. 2008. “Ability of Mature Dendritic Cells to Interact with Regulatory T Cells Is Imprinted during Maturation.” *Cancer Research* 68 (14): 5972–78. https://doi.org/10.1158/0008-5472.CAN-07-6818.

Nagalla, Srikanth, Jeff W Chou, Mark C Willingham, Jimmy Ruiz, James P Vaughn, Purnima Dubey, Timothy L Lash, et al. 2013. “Interactions between Immunity, Proliferation and Molecular Subtype in Breast Cancer Prognosis.” *Genome Biology* 14 (4): R34. https://doi.org/10.1186/gb-2013-14-4-r34.

Nagarsheth, Nisha, Max S. Wicha, and Weiping Zou. 2017. “Chemokines in the Cancer Microenvironment and Their Relevance in Cancer Immunotherapy.” *Nature Reviews Immunology* 17 (9): 559–72. https://doi.org/10.1038/nri.2017.49.

Nakanishi, Masako, and Daniel W. Rosenberg. 2013. “Multifaceted Roles of PGE2 in Inflammation and Cancer.” *Seminars in Immunopathology* 35: 123–37. https://doi.org/10.1007/s00281-012-0342-8.

Ohmori, Y, R D Schreiber, and T A Hamilton. 1997. “Synergy between Interferon-Gamma and Tumor Necrosis Factor-Alpha in Transcriptional Activation Is Mediated by Cooperation between Signal Transducer and Activator of Transcription 1 and Nuclear Factor KappaB.” *The Journal*

of Biological Chemistry 272 (23): 14899–907. http://www.ncbi.nlm.nih.gov/pubmed/9169460.

Ohmori, Y, L Wyner, S Narumi, D Armstrong, M Stoler, and T A Hamilton. 1993. “Tumor Necrosis Factor-Alpha Induces Cell Type and Tissue-Specific Expression of Chemoattractant Cytokines in Vivo.” *The American Journal of Pathology* 142 (3): 861–70. http://www.ncbi.nlm.nih.gov/pubmed/8456945.

Ohta, Mitsuhiko, Fumiaki Tanaka, Hiroshi Yamaguchi, Noriaki Sadanaga, Hiroshi Inoue, and Masaki Mori. 2005. “The High Expression of Fractalkine Results in a Better Prognosis for Colorectal Cancer Patients.” *International Journal of Oncology* 26 (1): 41–47. http://www.ncbi.nlm.nih.gov/pubmed/15586223.

Pachmann, Katharina, Oumar Camara, Andreas Kavallaris, Sabine Krauspe, Nele Malarski, Mieczyslaw Gajda, Torsten Kroll, et al. 2008. “Monitoring the Response of Circulating Epithelial Tumor Cells to Adjuvant Chemotherapy in Breast Cancer Allows Detection of Patients at Risk of Early Relapse.” *Journal of Clinical Oncology* 26 (8): 1208–15. https://doi.org/10.1200/JCO.2007.13.6523.

Page, D L, W D Dupont, L W Rogers, and M S Rados. 1985. “Atypical Hyperplastic Lesions of the Female Breast. A Long-Term Follow-up Study.” *Cancer* 55 (11): 2698–2708. http://www.ncbi.nlm.nih.gov/pubmed/2986821.

Paik, Soonmyung, Steven Shak, Gong Tang, Chungyeul Kim, Joffre Baker, Maureen Cronin, Frederick L. Baehner, et al. 2004. “A Multigene Assay to Predict Recurrence of Tamoxifen-Treated, Node-Negative Breast Cancer.” *New England Journal of Medicine* 351 (27): 2817–26. https://doi.org/10.1056/NEJMoa041588.

Pan, Judong, Marie D Burdick, John A Belperio, Ying Ying Xue, Craig Gerard, Sherven Sharma, Steven M Dubinett, and Robert M Strieter. 2006. “CXCR3/CXCR3 Ligand Biological Axis Impairs RENCA Tumor Growth by a Mechanism of Immunoangiostasis.” *Journal of Immunology (Baltimore, Md.: 1950)* 176 (3): 1456–64. http://www.ncbi.nlm.nih.gov/pubmed/16424173.

Park, Min Ho, Ji Shin Lee, and Jung Han Yoon. 2012. “High Expression of CX3CL1 by Tumor Cells Correlates with a Good Prognosis and Increased Tumor-Infiltrating CD8+ T Cells, Natural Killer Cells, and Dendritic Cells in Breast Carcinoma.” *Journal of Surgical Oncology* 106 (4): 386–92. https://doi.org/10.1002/jso.23095.

Pegram, M., and D. Slamon. 2000. “Biological Rationale for HER2/Neu (c-ErbB2) as a Target for Monoclonal Antibody Therapy.” *Seminars in Oncology*.

Peng, Dongjun, Ilona Kryczek, Nisha Nagarsheth, Lili Zhao, Shuang Wei, Weimin Wang, Yuqing Sun, et al. 2015. “Epigenetic Silencing of TH1-Type Chemokines Shapes Tumour Immunity and Immunotherapy.” *Nature* 527 (7577): 249–53. https://doi.org/10.1038/nature15520.

Peng, W., C. Liu, C. Xu, Y. Lou, J. Chen, Y. Yang, H. Yagita, et al. 2012. “PD-1 Blockade Enhances T-Cell Migration to Tumors by Elevating IFN-Gamma Inducible Chemokines.” *Cancer Research* 72 (20): 5209–18. https://doi.org/10.1158/0008-5472.CAN-12-1187.

Perez, Edith A., Edward H. Romond, Vera J. Suman, Jong-Hyeon Jeong, Nancy E. Davidson, Charles E. Geyer, Silvana Martino, Eleftherios P. Mamounas, Peter A. Kaufman, and Norman Wolmark. 2011. “Four-Year Follow-Up of Trastuzumab Plus Adjuvant Chemotherapy for Operable Human Epidermal Growth Factor Receptor 2–Positive Breast Cancer: Joint Analysis of Data From NCCTG N9831 and NSABP B-31.” *Journal of Clinical Oncology* 29 (25): 3366–73. https://doi.org/10.1200/JCO.2011.35.0868.

Pierga, J.-Y., F.-C. Bidard, C. Mathiot, E. Brain, S. Delaloge, S. Giachetti, P. de Cremoux, R. Salmon, A. Vincent-Salomon, and M. Marty. 2008. “Circulating Tumor Cell Detection Predicts Early Metastatic Relapse After Neoadjuvant Chemotherapy in Large Operable and Locally Advanced Breast Cancer in a Phase II Randomized Trial.” *Clinical Cancer Research* 14 (21): 7004–10. https://doi.org/10.1158/1078-0432.CCR-08-0030.

Planes-Laine, Gabrielle, Philippe Rochigneux, François Bertucci, Anne Sophie Chrétien, Patrice Viens, Renaud Sabatier, and Anthony Gonçalves. 2019. “PD-1/PD-L1 Targeting in Breast Cancer: The First Clinical Evidences Are Emerging. a Literature Review.” *Cancers*. MDPI AG. https://doi.org/10.3390/cancers11071033.

Plitas, George, and Alexander Y. Rudensky. 2020. “Regulatory T Cells in Cancer.” *Annual Review of Cancer Biology* 4 (1): 459–77. https://doi.org/10.1146/annurev-cancerbio-030419-033428.

Pohlmann, Paula R, Ingrid A Mayer, and Ray Mernaugh. 2009. “Resistance to Trastuzumab in Breast Cancer.” *Clinical Cancer Research : An Official Journal of the American Association for Cancer Research* 15 (24): 7479–91. https://doi.org/10.1158/1078-0432.CCR-09-0636.

Polyak, Kornelia. 2007. “Breast Cancer: Origins and Evolution.” *The Journal of Clinical Investigation* 117 (11): 3155–63. https://doi.org/10.1172/JCI33295.

Pondé, Noam, Mariana Brandão, Georges El-Hachem, Emilie Werbrouck, and Martine Piccart. 2018. “Treatment of Advanced HER2-Positive Breast Cancer: 2018 and Beyond.” *Cancer Treatment Reviews*. W.B. Saunders Ltd. https://doi.org/10.1016/j.ctrv.2018.04.016.

Qin, S, J B Rottman, P Myers, N Kassam, M Weinblatt, M Loetscher, A E Koch, B Moser, and C R Mackay. 1998. “The Chemokine Receptors CXCR3 and CCR5 Mark Subsets of T Cells Associated with Certain Inflammatory Reactions.” *Journal of Clinical Investigation* 101 (4): 746–54. https://doi.org/10.1172/JCI1422.

Rack, B. K., C. Schindlbeck, U. Andergassen, A. Schneeweiss, T. Zwingers, W. Lichtenegger, M. Beckmann, et al. 2010. “Use of Circulating Tumor Cells (CTC) in Peripheral Blood of Breast Cancer Patients before and

after Adjuvant Chemotherapy to Predict Risk for Relapse: The SUCCESS Trial." *Journal of Clinical Oncology* 28 (15_suppl): 1003–1003. https://doi.org/10.1200/jco.2010.28.15_suppl.1003.

Rajagopal, Sudarshan, Daniel L Bassoni, James J Campbell, Norma P Gerard, Craig Gerard, and Tom S Wehrman. 2013. "Biased Agonism as a Mechanism for Differential Signaling by Chemokine Receptors." *The Journal of Biological Chemistry* 288 (49): 35039–48. https://doi.org/10.1074/jbc.M113.479113.

Richard-Fiardo, P, B Cambien, E Pradelli, F Beilvert, B Pitard, H Schmid-Antomarchi, and A Schmid-Alliana. 2011. "Effect of Fractalkine-Fc Delivery in Experimental Lung Metastasis Using DNA/704 Nanospheres." *Cancer Gene Therapy* 18 (11): 761–72. https://doi.org/10.1038/cgt.2011.42.

Ripperger, Tim, Dorothea Gadzicki, Alfons Meindl, and Brigitte Schlegelberger. 2009. "Breast Cancer Susceptibility: Current Knowledge and Implications for Genetic Counselling." *European Journal of Human Genetics : EJHG* 17 (6): 722–31. https://doi.org/10.1038/ejhg.2008.212.

Robert Koch-Institut. 2015. *Krebs in Deutschland*. *Http://Www.Rki.de/DE/Content/Service/ Presse/Pressemitteilungen/ 2012/01_2012.Html*. https://doi.org/10.17886/rkipubl-2015-004.

Robertson, M J, and J Ritz. 1990. "Biology and Clinical Relevance of Human Natural Killer Cells." *Blood* 76 (12): 2421–38. http://www.ncbi.nlm.nih.gov/pubmed/2265240.

Robinson, Lisa A., Chandra Nataraj, Dennis W. Thomas, Josette M. Cosby, Robert Griffiths, Victoria L. Bautch, Dhavalkumar D. Patel, and Thomas M. Coffman. 2003. "The Chemokine CX3CL1 Regulates NK Cell Activity in Vivo." *Cellular Immunology* 225 (2): 122–30. https://doi.org/10.1016/j.cellimm.2003.09.010.

Roemer, Andreas, Lutz Schwettmann, Monika Jung, J. A.N. Roigas, Glen Kristiansen, Dietmar Schnorr, Stefan A. Loening, Klaus Jung, and Ralf Lichtinghagen. 2004. "Increased MRNA Expression of ADAMs in Renal Cell Carcinoma and Their Association with Clinical Outcome." *Oncology Reports* 11 (2): 529–36. https://doi.org/10.3892/or.11.2.529.

Romagnani, P, F Annunziato, L Lasagni, E Lazzeri, C Beltrame, M Francalanci, M Uguccioni, et al. 2001. "Cell Cycle-Dependent Expression of CXC Chemokine Receptor 3 by Endothelial Cells Mediates Angiostatic Activity." *The Journal of Clinical Investigation* 107 (1): 53–63. https://doi.org/10.1172/JCI9775.

Ruiz-Garcia, E., V. Scott, C. MacHavoine, J. M. Bidart, L. Lacroix, S. Delaloge, and F. Andre. 2010. "Gene Expression Profiling Identifies Fibronectin 1 and CXCL9 as Candidate Biomarkers for Breast Cancer Screening." *British Journal of Cancer* 102 (3): 462–68. https://doi.org/10.1038/sj.bjc.6605511.

Salgado, R., C. Denkert, S. Demaria, N. Sirtaine, F. Klauschen, G. Pruneri,

S. Wienert, et al. 2015. “The Evaluation of Tumor-Infiltrating Lymphocytes (TILs) in Breast Cancer: Recommendations by an International TILs Working Group 2014.” *Annals of Oncology* 26 (2): 259–71. https://doi.org/10.1093/annonc/mdu450.

Salgado, Roberto, and Sherene Loi. 2017. “Tumour Infiltrating Lymphocytes in Breast Cancer: Increasing Clinical Relevance.” *The Lancet. Oncology* 2045 (17): 30904–5. https://doi.org/10.1016/S1470-2045(17)30905-1.

Sauty, A, R A Colvin, L Wagner, S Rochat, F Spertini, and A D Luster. 2001. “CXCR3 Internalization Following T Cell-Endothelial Cell Contact: Preferential Role of IFN-Inducible T Cell Alpha Chemoattractant (CXCL11).” *Journal of Immunology (Baltimore, Md. : 1950)* 167 (12): 7084–93. http://www.ncbi.nlm.nih.gov/pubmed/11739530.

Sciumè, Giuseppe, Alessandra Soriani, Mario Piccoli, Luigi Frati, Angela Santoni, and Giovanni Bernardini. 2010. “CX3CR1/CX3CL1 Axis Negatively Controls Glioma Cell Invasion and Is Modulated by Transforming Growth Factor-Beta1.” *Neuro-Oncology* 12 (7): 701–10. https://doi.org/10.1093/neuonc/nop076.

Sestak, Ivana, Jack Cuzick, Mitch Dowsett, Elena Lopez-Knowles, Martin Filipits, Peter Dubsky, John Wayne Cowens, et al. 2015. “Prediction of Late Distant Recurrence after 5 Years of Endocrine Treatment: A Combined Analysis of Patients from the Austrian Breast and Colorectal Cancer Study Group 8 and Arimidex, Tamoxifen Alone or in Combination Randomized Trials Using the PAM50 Risk of Recurrence Score.” *Journal of Clinical Oncology* 33 (8): 916–22. https://doi.org/10.1200/JCO.2014.55.6894.

Sgadari, C, J M Farber, A L Angiolillo, F Liao, J Teruya-Feldstein, P R Burd, L Yao, G Gupta, C Kanegane, and G Tosato. 1997. “Mig, the Monokine Induced by Interferon-Gamma, Promotes Tumor Necrosis in Vivo.” *Blood* 89 (8): 2635–43. http://www.ncbi.nlm.nih.gov/pubmed/9108380.

Sheikh, Asfandyar, Syed Ather Hussain, Quratulain Ghori, Nida Naeem, Abul Fazil, Smith Giri, Brijesh Sathian, Prajeena Mainali, and Dalal M Al Tamimi. 2015. “The Spectrum of Genetic Mutations in Breast Cancer.” *Asian Pacific Journal of Cancer Prevention : APJCP* 16 (6): 2177–85. http://www.ncbi.nlm.nih.gov/pubmed/25824734.

Shiels, Meredith S, Hormuzd A Katki, Allan Hildesheim, Ruth M Pfeiffer, Eric A Engels, Marcus Williams, Troy J Kemp, Neil E Caporaso, Ligia A Pinto, and Anil K Chaturvedi. 2015. “Circulating Inflammation Markers, Risk of Lung Cancer, and Utility for Risk Stratification.” *Journal of the National Cancer Institute* 107 (10). https://doi.org/10.1093/jnci/djv199.

Siddiqui, Imran, Marco Erreni, Mandy Van Brakel, Reno Debets, and Paola Allavena. 2016. “Enhanced Recruitment of Genetically Modified CX3CR1-Positive Human T Cells into Fractalkine:CX3CL1 Expressing Tumors- Importance of the Chemokine Gradient.” *Journal for ImmunoTherapy of Cancer*, 1–12. https://doi.org/10.1186/s40425-016-0125-1.

Slamon, D J, G M Clark, S G Wong, W J Levin, A Ullrich, and W L McGuire. 1987. “Human Breast Cancer: Correlation of Relapse and Survival with Amplification of the HER-2/Neu Oncogene.” *Science (New York, N.Y.)* 235 (4785): 177–82. http://www.ncbi.nlm.nih.gov/pubmed/3798106.

Smit, M. J., Pauline Verdijk, Elisabeth M H van der Raaij-Helmer, Marjon Navis, Paul J Hensbergen, Rob Leurs, and Cornelis P Tensen. 2003. “CXCR3-Mediated Chemotaxis of Human T Cells Is Regulated by a Gi- and Phospholipase C-Dependent Pathway and Not via Activation of MEK/P44/P42 MAPK nor Akt/PI-3 Kinase.” *Blood* 102 (6): 1959–65. https://doi.org/10.1182/blood-2002-12-3945.

Solinas, Cinzia, Luisa Carbognin, Pushpamali De Silva, Carmen Criscitiello, and Matteo Lambertini. 2017. “Tumor-Infiltrating Lymphocytes in Breast Cancer According to Tumor Subtype: Current State of the Art.” *Breast*. Churchill Livingstone. https://doi.org/10.1016/j.breast.2017.07.005.

Specht, Katja, Nadia Harbeck, Jan Smida, Katja Annecke, Ulrike Reich, Joerg Naehrig, Rupert Langer, et al. 2009. “Expression Profiling Identifies Genes That Predict Recurrence of Breast Cancer after Adjuvant CMF-Based Chemotherapy.” *Breast Cancer Research and Treatment* 118 (1): 45–56. https://doi.org/10.1007/s10549-008-0207-y.

Sreekanthreddy, P., H. Srinivasan, D. M. Kumar, M. B. Nijaguna, S. Sridevi, M. Vrinda, A. Arivazhagan, et al. 2010. “Identification of Potential Serum Biomarkers of Glioblastoma: Serum Osteopontin Levels Correlate with Poor Prognosis.” *Cancer Epidemiology Biomarkers & Prevention* 19 (6): 1409–22. https://doi.org/10.1158/1055-9965.EPI-09-1077.

Stewart, B W, and C P Wild. 2014. “World Cancer Report 2014.” *World Health Organization*, 1–2. https://doi.org/9283204298.

Sundling, Kaitlin E., and Alarice C. Lowe. 2019. “Circulating Tumor Cells: Overview and Opportunities in Cytology.” *Advances in Anatomic Pathology*. Lippincott Williams and Wilkins. https://doi.org/10.1097/PAP.0000000000000217.

T. Degenhardt, M. Braun, F. Ebner, J. Ettl, N. Harbeck, A . Hester. 2019. *Prognostische Und Prädiktive Faktoren*.

Tanaka, Yoshihiro, Shingo Miyamoto, Satoshi O. Suzuki, Eiji Oki, Hiroshi Yagi, Kenzo Sonoda, Ayano Yamazaki, et al. 2005. “Clinical Significance of Heparin-Binding Epidermal Growth Factor-like Growth Factor and A Disintegrin and Metalloprotease 17 Expression in Human Ovarian Cancer.” *Clinical Cancer Research* 11 (13): 4783–92. https://doi.org/10.1158/1078-0432.CCR-04-1426.

Tang, L, H-d Hu, P Hu, Y-h Lan, M-l Peng, M Chen, and H Ren. 2007. “Gene Therapy with CX3CL1/Fractalkine Induces Antitumor Immunity to Regress Effectively Mouse Hepatocellular Carcinoma.” *Gene Therapy* 14 (16): 1226–34. https://doi.org/10.1038/sj.gt.3302959.

Tokuda, Y, Y Ohnishi, K Shimamura, M Iwasawa, M Yoshimura, Y Ueyama,

N Tamaoki, T Tajima, and T Mitomi. 1996. “In Vitro and in Vivo Anti-Tumour Effects of a Humanised Monoclonal Antibody against c-ErbB-2 Product.” *British Journal of Cancer* 73 (11): 1362–65. http://www.ncbi.nlm.nih.gov/pubmed/8645580.

Tsang, Julia Y S, Yun-Bi Ni, Siu-Ki Chan, Mu-Min Shao, Ying-Kin Kwok, Kit-Wing Chan, Puay Hoon Tan, and Gary M Tse. 2013. “CX3CL1 Expression Is Associated with Poor Outcome in Breast Cancer Patients.” *Breast Cancer Research and Treatment* 140 (3): 495–504. https://doi.org/10.1007/s10549-013-2653-4.

Turnbull, Clare, and Nazneen Rahman. 2008. “Genetic Predisposition to Breast Cancer: Past, Present, and Future.” *Annual Review of Genomics and Human Genetics* 9 (1): 321–45. https://doi.org/10.1146/annurev.genom.9.081307.164339.

Umehara, H., Eda T Bloom, Toshiro Okazaki, Yutaka Nagano, Osamu Yoshie, and Toshio Imai. 2004. “Fractalkine in Vascular Biology: From Basic Research to Clinical Disease.” *Arteriosclerosis, Thrombosis, and Vascular Biology* 24 (1): 34–40. https://doi.org/10.1161/01.ATV.0000095360.62479.1F.

Vandercappellen, Jo, Jo Van Damme, and Sofie Struyf. 2008. “The Role of CXC Chemokines and Their Receptors in Cancer.” *Cancer Letters* 267 (2): 226–44. https://doi.org/10.1016/j.canlet.2008.04.050.

Vanguri, P, and J M Farber. 1990. “Identification of CRG-2. An Interferon-Inducible MRNA Predicted to Encode a Murine Monokine.” *The Journal of Biological Chemistry* 265 (25): 15049–57. http://www.ncbi.nlm.nih.gov/pubmed/2118520.

Verma, Chandan, Viriya Kaewkangsadan, Jennifer M Eremin, Gerard P Cowley, Mohammad Ilyas, Mohamed A El-Sheemy, and Oleg Eremin. 2015. “Natural Killer (NK) Cell Profiles in Blood and Tumour in Women with Large and Locally Advanced Breast Cancer (LLABC) and Their Contribution to a Pathological Complete Response (PCR) in the Tumour Following Neoadjuvant Chemotherapy (NAC): Differential Rest.” *Journal of Translational Medicine* 13 (1): 180. https://doi.org/10.1186/s12967-015-0535-8.

Vitale, S, B Cambien, B F Karimdjee, R Barthel, P Staccini, C Luci, V Breittmayer, F Anjuère, A Schmid-Alliana, and H Schmid-Antomarchi. 2007. “Tissue-specific Differential Antitumour Effect of Molecular Forms of Fractalkine in a Mouse Model of Metastatic Colon Cancer.” *Gut* 56 (3): 365. https://doi.org/10.1136/GUT.2005.088989.

Waks, Adrienne G., and Eric P. Winer. 2019. “Breast Cancer Treatment: A Review.” *JAMA - Journal of the American Medical Association*. American Medical Association. https://doi.org/10.1001/jama.2018.19323.

Walser, Tonya C., Xinrong Ma, Namita Kundu, Russell Dorsey, Olga Goloubeva, and Amy M. Fulton. 2007. “Immune-Mediated Modulation of Breast Cancer Growth and Metastasis by the Chemokine Mig (CXCL9) in a Murine Model.” *Journal of Immunotherapy* 30 (5): 490–

98. https://doi.org/10.1097/CJI.0b013e318031b551.

Wendel, M., I. E. Galani, E. Suri-Payer, and A. Cerwenka. 2008. “Natural Killer Cell Accumulation in Tumors Is Dependent on IFN-Gamma and CXCR3 Ligands.” *Cancer Research* 68 (20): 8437–45. https://doi.org/10.1158/0008-5472.CAN-08-1440.

WHO Classification of Tumours Editorial Board., International Agency for Research on Cancer., and World Health Organization. n.d. *WHO Classification of Tumours. Breast Tumours*.

Windmüller, Claudia, D Zech, S Avril, M Boxberg, T Dawidek, B Schmalfeldt, M Schmitt, M Kiechle, and H Bronger. 2017. “CXCR3 Mediates Ascites-Directed Tumor Cell Migration and Predicts Poor Outcome in Ovarian Cancer Patients.” *Oncogenesis* 6 (5): e331. https://doi.org/10.1038/oncsis.2017.29.

Wöckel, Achim, Dominic Varga, Ziad Atassi, Christian Kurzeder, Regine Wolters, Manfred Wischnewsky, Christine Wulff, and Rolf Kreienberg. 2010. “Impact of Guideline Conformity on Breast Cancer Therapy: Results of a 13-Year Retrospective Cohort Study.” *Onkologie* 33 (1–2): 9–9. https://doi.org/10.1159/000264617.

Wong, P, C W Severns, N B Guyer, and T M Wright. 1994. “A Unique Palindromic Element Mediates Gamma Interferon Induction of Mig Gene Expression.” *Molecular and Cellular Biology* 14 (2): 914–22. http://www.ncbi.nlm.nih.gov/pubmed/8289831.

Wozniak, Justyna, and Andreas Ludwig. 2018. “Novel Role of APP Cleavage by ADAM10 for Breast Cancer Metastasis.” https://doi.org/10.1016/j.ebiom.2018.11.012.

Wu, E., P. I. Croucher, and N. McKie. 1997. “Expression of Members of the Novel Membrane Linked Metalloproteinase Family ADAM in Cells Derived from a Range of Haematological Malignancies.” *Biochemical and Biophysical Research Communications* 235 (2): 437–42. https://doi.org/10.1006/bbrc.1997.6714.

Wu, Jun, and Lewis L Lanier. 2003. “Natural Killer Cells and Cancer.” *Advances in Cancer Research* 90: 127–56. http://www.ncbi.nlm.nih.gov/pubmed/14710949.

Wu, Zhenqian, Xiuyan Huang, Xiaodong Han, Zhongnan Li, Qinchao Zhu, Jun Yan, Song Yu, et al. 2016. “The Chemokine CXCL9 Expression Is Associated with Better Prognosis for Colorectal Carcinoma Patients.” *Biomedicine & Pharmacotherapy* 78 (March): 8–13. https://doi.org/10.1016/j.biopha.2015.12.021.

Xin, Hong, Toshiaki Kikuchi, Sita Andarini, Shinya Ohkouchi, Takuji Suzuki, Toshihiro Nukiwa, Huqun, Koichi Hagiwara, Tasuku Honjo, and Yasuo Saijo. 2005. “Antitumor Immune Response by CX3CL1 Fractalkine Gene Transfer Depends on Both NK and T Cells.” *European Journal of Immunology* 35 (5): 1371–80. https://doi.org/10.1002/eji.200526042.

Xu, Xianhui, Yang Wang, Jinshui Chen, Hongyun Ma, Zhuo Shao, Haitao Chen, and Gang Jin. 2012. “High Expression of CX3CL1/CX3CR1 Axis

Predicts a Poor Prognosis of Pancreatic Ductal Adenocarcinoma." *Journal of Gastrointestinal Surgery* 16 (8): 1493–98. https://doi.org/10.1007/s11605-012-1921-7.

Yoneda, O, T Imai, S Goda, H Inoue, a Yamauchi, T Okazaki, H Imai, et al. 2000. "Fractalkine-Mediated Endothelial Cell Injury by NK Cells." *Journal of Immunology (Baltimore, Md.: 1950)* 164 (8): 4055–62. https://doi.org/10.4049/jimmunol.164.8.4055.

Yoshimura, Tetsuro, Toshihiko Tomita, Michael F. Dixon, Anthony T. R. Axon, Philip A. Robinson, and Jean E. Crabtree. 2002. "ADAMs (A Disintegrin and Metalloproteinase) Messenger RNA Expression in Helicobacter Pylori –Infected, Normal, and Neoplastic Gastric Mucosa ." *The Journal of Infectious Diseases* 185 (3): 332–40. https://doi.org/10.1086/338191.

Yu, Y R, A M Fong, C Combadiere, J L Gao, P M Murphy, and D D Patel. 2007. "Defective Antitumor Responses in CX3CR1-Deficient Mice." *Int J Cancer* 121 (2): 316–22. http://www.ncbi.nlm.nih.gov/entrez/query.fcgi?cmd=Retrieve&db=PubMed&dopt=Citation&list_uids=17372897.

Zeng, Yan, Nicole Huebener, Stefan Fest, Silke Weixler, Ulrike Schroeder, Gerhard Gaedicke, Rong Xiang, et al. 2007. "Fractalkine (CX3CL1)- and Interleukin-2-Enriched Neuroblastoma Microenvironment Induces Eradication of Metastases Mediated by T Cells and Natural Killer Cells." *Cancer Research* 67 (5): 2331–38. https://doi.org/10.1158/0008-5472.CAN-06-3041.

Zhang, Chenlu, Zhi Li, Ling Xu, Xiaofang Che, Ti Wen, Yibo Fan, Ce Li, et al. 2018. "CXCL9/10/11, a Regulator of PD-L1 Expression in Gastric Cancer." *BMC Cancer* 18 (1): 462. https://doi.org/10.1186/s12885-018-4384-8.

Zhang, Lin, Jose R Conejo-Garcia, Dionyssios Katsaros, Phyllis A Gimotty, Marco Massobrio, Giorgia Regnani, Antonis Makrigiannakis, et al. 2003. "Intratumoral T Cells, Recurrence, and Survival in Epithelial Ovarian Cancer." *New England Journal of Medicine* 348 (3): 203–13. https://doi.org/10.1056/NEJMoa020177.

Zhang, R, L Tian, L-J Chen, F Xiao, J-M Hou, X Zhao, G Li, et al. 2006. "Combination of MIG (CXCL9) Chemokine Gene Therapy with Low-Dose Cisplatin Improves Therapeutic Efficacy against Murine Carcinoma." *Gene Therapy* 13 (17): 1263–71. https://doi.org/10.1038/sj.gt.3302756.

Zhi, Wenbo, Daron Ferris, Ashok Sharma, Sharad Purohit, Carlos Santos, Mingfang He, Sharad Ghamande, and Jin-Xiong She. 2014a. "Twelve Serum Proteins Progressively Increase With Disease Stage in Squamous Cell Cervical Cancer Patients." *International Journal of Gynecological Cancer* 24 (6): 1085–92. https://doi.org/10.1097/IGC.0000000000000153.

Zhi, Wenbo, Daron Ferris, Ashok Sharma, Sharad Purohit, Carlos Santos, Mingfang He, Sharad Ghamande, and Jin Xiong She. 2014b. "Twelve

Serum Proteins Progressively Increase with Disease Stage in Squamous Cell Cervical Cancer Patients." *International Journal of Gynecological Cancer* 24 (6): 1085–92. https://doi.org/10.1097/IGC.0000000000000153.

Zhu, Guiquan, H. Hannah Yan, Yanli Pang, Jiang Jian, Bhagelu R. Achyut, Xinhua Liang, Jonathan M. Weiss, Robert H. Wiltrout, M. Christine Hollander, and Li Yang. 2015. "CXCR3 as a Molecular Target in Breast Cancer Metastasis: Inhibition of Tumor Cell Migration and Promotion of Host Anti-Tumor Immunity." *Oncotarget* 6 (41): 43408–19. https://doi.org/10.18632/oncotarget.6125.

Zimmer, Alexandra S., Mitchell Gillard, Stanley Lipkowitz, and Jung Min Lee. 2018. "Update on PARP Inhibitors in Breast Cancer." *Current Treatment Options in Oncology*. Springer New York LLC. https://doi.org/10.1007/s11864-018-0540-2.

Zlotnik, Albert, and Osamu Yoshie. 2012. "The Chemokine Superfamily Revisited." *Immunity* 36 (5): 705–16. https://doi.org/10.1016/j.immuni.2012.05.008.

Zohar, Yaniv, Gizi Wildbaum, Rostislav Novak, Andrew L. Salzman, Marcus Thelen, Ronen Alon, Yiftah Barsheshet, Christopher L. Karp, and Nathan Karin. 2014a. "CXCL11-Dependent Induction of FOXP3-Negative Regulatory T Cells Suppresses Autoimmune Encephalomyelitis." *Journal of Clinical Investigation* 124 (5): 2009–22. https://doi.org/10.1172/JCI71951.

Zohar, Yaniv, Gizi Wildbaum, Rostislav Novak, Andrew L Salzman, Marcus Thelen, Ronen Alon, Yiftah Barsheshet, Christopher L Karp, and Nathan Karin. 2014b. "CXCL11-Dependent Induction of FOXP3-Negative Regulatory T Cells Suppresses Autoimmune Encephalomyelitis." *The Journal of Clinical Investigation.* 124 (5). https://doi.org/10.1172/JCI71951.and.

Zou, Weiping, Jedd D Wolchok, and Lieping Chen. 2016. "PD-L1 (B7-H1) and PD-1 Pathway Blockade for Cancer Therapy: Mechanisms, Response Biomarkers, and Combinations." *Science Translational Medicine* 8 (328): 328rv4. https://doi.org/10.1126/scitranslmed.aad7118.

VIV ACKNOWLEDGEMENTS

First and foremost, I want to thank my supervisor, mentor, and spiritual leader PD Dr. Holger Bronger, for giving me the opportunity to do my PhD thesis in his AG GTI. He was supportive and well organized from the very beginning and always gave me the chance to improve myself and follow my own ideas. Thank you also for the intense lab talks, encouraging discussions, guidance, for all your ideas and of course for the “teambuilding” activities.

I also want to thank Prof. Dr. Manfred Schmitt who supervised my thesis and was always keen to sprout some more ideas into the project. It is very sad that he cannot see this work to be finished.

I also want to thank Prof. Dr. Michael Groll who supervised this thesis and kept the meetings efficient and purposeful. He always offered help when there was need for it.

A special thanks goes to Prof. Viktor Magdolen who helped me a lot to get along in the word of science. Be it molecular biology background training, possibility to attend international conferences or enjoy the delight of writing paper, reviews and grant applications. Here I also want to thank Sabine Creutzburg for endless lab experience and knowledge which she was always willing to share in addition to best groomed lab journal I have ever seen.

I also want to thank the AG Reuning including Ute Reuning and Anke Benge. Both have been very supportive throughout my whole PhD. Ute in terms of input on methodology (SONY) and deep knowledge of intergrins and microscopy. Anke always helped to keep the motor running by last minute checking goods from the warehouse, technical assistant wisdom or political motivation on various topics.

Huge thanks go to all my former and present colleagues for creating this supportive and friendly atmosphere.I want to thank the AG GTI team 1.0 (Claudia, Joachim, Daniela) for making my start smooth and inspiring. It was my pleasure working in this group since all of them were helpful and created a team atmosphere also together with Thy-An, Raphael and Jil.
I also want to thank the actual AG GTI team (Steffi, Chris, Giulia, Kathi, Sina, Dorine) for making it fun to go to work everyday. The team spirit is great and everyone is working together and taking care of each other. I am very happy to be a part of this team especially when the annual retreat is ongoing..I also want to thank Nathalie, Elisabeth, Rosi and Daniela for fruitful discussions and support whenever needed.
In the end I want to thank my family and friends who always encouraged me and had indulgence for a lack of quality time every once in a while.